A Sustainable Air-Entraining and Internal Curing Agent

Final Report | February 2025

IOWA | DOT

IHRB celebrating 75 years

Disclaimer Notice

The contents of this report reflect the views of the authors, who are responsible for the facts and the accuracy of the information presented herein. The opinions, findings, and conclusions expressed in this publication are those of the authors and not necessarily those of the sponsors.

The sponsors assume no liability for the contents or use of the information contained in this document. This report does not constitute a standard, specification, or regulation. The sponsors do not endorse products or manufacturers. Trademarks or manufacturers' names appear in this report only because they are considered essential to the objectives of the document.

Statement of Non-Discrimination

The Iowa Department of Transportation (DOT) ensures non-discrimination in all programs and activities in accordance with Title VI of the Civil Rights Act of 1964. Any person who believes that they are being denied participation in a project, being denied benefits of a program, or otherwise being discriminated against because of race, color, national origin, gender, age, or disability, low income, and limited English proficiency, or needs more information or special assistance for persons with disabilities or limited English proficiency, please contact Iowa DOT Civil Rights at 515-239-7970 or by email at civil.rights@iowadot.us.

TECHNICAL REPORT DOCUMENTATION PAGE

TECHNICAL REPORT DOCUMENTATION PAGE

1. Report No. IHRB Project TR-808	**2. Government Accession No.**	**3. Recipient's Catalog No.**
4. Title and Subtitle TR-808: A sustainable air-entraining and internal curing agent		**5. Report Date** February 2025 **6. Performing Organization Code**
7. Author(s) Ravi Kiran Yellavajjala, Ph.D., P.E. https://orcid.org/0000-0001-8300-0767 Asif Jalal, https://orcid.org/0000-0002-8649-0121		**8. Performing Organization Report No.**
9. Performing Organization Name and Address North Dakota State University, 1340 Administration Ave, Fargo, ND-58105		**10. Work Unit No.** **11. Contract or Grant No.**
12. Sponsoring Agency Name and Address Iowa Highway Research Board Iowa Department of Transportation 800 Lincoln Way Ames, IA 50010.		**13. Type of Report and Period Covered** 6/1/2022-2/27/2025 **14. Sponsoring Agency Code**
15. Supplementary Notes		

16. Abstract

Air entrainment of concrete is crucial to dissipate the tensile stresses introduced by the volume expansion of frozen water in the capillary pores of the concrete. The air void system achieved using popular surfactants is sensitive to the properties of cementitious materials, water content, admixtures, aggregate, etc. Furthermore, vibration, compaction, and mechanical paving can lower the efficiency of surfactants. Every 1% increase in the air volume reduces strength by 5% which could be partially compensated by higher binder content. Achieving a stable air void system without compromising the strength of concrete is the goal of this study. A bio-based hydrogel synthesized from cornstarch was investigated alongside commercially available superabsorbent polymers (SAPs) and air-entraining agents. Firstly, hydrogels and SAPs were embedded in cement mortar, and their performance was assessed through hydration enhancement, void structure development, and durability improvements. The internal curing ability of hydrogels was quantified using a hydrogel capsule method, revealing cyclic water release governed by humidity gradients. Additionally, microcomputed tomography (micro-CT) scanning demonstrated that cornstarch hydrogels at 3% mixing water content produced a robust void structure with high porosity and small voids, without significant strength reduction. The influence of hydrogels on F-T resistance was evaluated through compression strength, mass change, scaling resistance, and chloride penetration after prolonged exposure to brine solution. While traditional air-entraining agents provided superior F-T resistance by creating small, uniformly distributed voids, they also reduced strength. Conversely, SAPs and cornstarch hydrogels improved hydration and strength retention while offering moderate scaling resistance. The microstructural analysis confirmed that bio-based hydrogels enhance both internal curing and durability, positioning them as sustainable alternatives to conventional admixtures. Overall, this research highlights the potential of bio-based hydrogels for enhancing hydration, mitigating shrinkage, and improving cementitious matrix durability under harsh environmental conditions.

17. Key Words Freeze thaw durability; Air entraining agents; Curing agents; Concrete pavements; and Porosity	**18. Distribution Statement** No restrictions.

19. Security Classif. (of this report) Unclassified	**20. Security Classif. (of this page)** Unclassified	**21. No. of Pages** 87	**22. Price**

Form DOT F 1700.7 (8-72) Reproduction of completed page authorized

TR-808: A SUSTAINABLE AIR-ENTRAINING AND INTERNAL CURING AGENT

Final Report
February 2025

Principal Investigator

Ravi Kiran Yellavajjala, Ph.D., P.E.
Associate Professor
School of Sustainable Engineering and the Built Environment
Arizona State University

Co-author

Asif Jalal*
*Graduate Research Assistant
Department of Civil and Environmental Engineering
North Dakota State University

Sponsored by

the Iowa Highway Research Board
(IHRB Project TR-808)
A Report from

Damage in Materials and Structures Laboratory
School of Sustainable Engineering and the Built Environment
Arizona State University
ISTB-5, 174
Tempe, AZ 58105-5285
Phone: 480-965-2790
https://labs.engineering.asu.edu/dams/

Acknowledgements

We sincerely appreciate the financial support from the Iowa Department of Transportation. We are especially grateful to Vanessa Goetz for her leadership and commitment to this project, which played a crucial role in its successful execution. The guidance and feedback from the Technical Assistance Committee have been instrumental in shaping our work, and we extend our heartfelt thanks to Todd Hanson, Elijah Gansen, Curtis Carter, Jesse Peterson, and Wayne Sunday for their valuable contributions. A special thanks to Prof. Mijia Yang for administering the project during its later stages and ensuring its smooth completion. Additionally, we acknowledge the support of the Civil, Construction and Environmental Engineering Department staff at North Dakota State University (NDSU) and the team at the Electron Microscopy Center at NDSU for their essential assistance in the experimental phase of this project.

Contents

List of figures

List of Tables

Chapter 1. INTRODUCTION

1.1 Background

Concrete, the second most utilized material after water, plays a vital role in human development and in shaping the global environment. However, modern architectural advancements, such as large-span bridges, skyscrapers, and severe weather conditions, demand higher-strength concrete to meet increased load requirements. Consequently, the market for high-strength concrete is expanding rapidly. In 2022, the High-Strength Concrete Market Size was valued at $19.3 billion and is projected to grow to $33.9 billion by 2032 [1].

High-strength concrete typically requires more cement but reduces the overall volume of concrete needed. It's also contributes to energy savings and a reduction in the carbon footprint by more than 50% [2],[3]. Additionally, high-strength concrete consumes less water, creating a denser pore structure that limits water availability for further hydration [4], [5]. While external curing methods can supply hydration water near the curing surface, they often fail to hydrate cement particles located away from the water source [6]. According to Powers' studies [7], external curing alone is insufficient to fully hydrate cement when the water-to-cement (W/C) ratio is below 0.36. In such cases, internal curing becomes essential to maximize cement utilization. Furthermore, insufficient pore water in high-strength concrete can lead to autogenous shrinkage, resulting in volumetric contraction and early-age cracking [8].

Extreme weather, particularly in cold regions, significantly impacts concrete durability. This has led to deterioration of road infrastructure, imposing a substantial economic burden in the United States. Estimates suggest that maintaining and repairing national road infrastructure requires an annual investment of $231.4 billion [9]. Notably, approximately 70% of these roads are located in areas with harsh winter conditions, where freezing temperatures are a primary contributor to concrete degradation.

A critical challenge in such climates is concrete's resistance to the freezing of water in concrete pores, which expands and exerts hydrostatic tension stresses, potentially leading to cracking [10]. These cracks facilitate atmospheric interaction with reinforcing steel, accelerating corrosion and structural failure. To mitigate the expansion of freezing water and the resulting tensile stresses, improving the void structure in the concrete is a common strategy. However, in high-strength concrete with low W/C ratios, the volume of capillary voids is minimal, which exacerbates durability challenges, particularly at freezing temperatures [11].

1.2 Internal Curing Agents

High-strength concrete prepared with a low W/C ratio exhibits exceptional mechanical properties and durability [12]. A lower water content reduces the surplus water available for evaporation, which minimizes void formation. Consequently, concrete with a low W/C ratio has lower porosity and permeability. Typically, external curing methods—such as water spraying, wet burlap coverings, or chemical sealant applications—are employed to prevent water evaporation from the specimen or to supply water consistently to sustain the hydration process, enabling the concrete to develop its strength. However, the low porosity of high-strength concrete restricts the

effectiveness of conventional external curing methods from penetrating deep enough to supply sufficient moisture internally. This limitation leads to incomplete hydration of the cement, resulting in autogenous shrinkage, and micro-cracking at an early age [7], [8].

As per Powers' studies [7], external curing alone is insufficient to fully hydrate cement when the W/C ratio is below 0.36. This underscores the necessity of an internal curing mechanism to fully utilize the available cement and mitigate moisture deficits. Internal curing techniques address water shortages, enabling continuous cement hydration and enhancing volumetric stability (illustrated in Figure 1.1). Two widely used approaches for internal curing include:

- Introducing porous materials.
- Incorporating water-absorbing materials.

These methods are explained below.

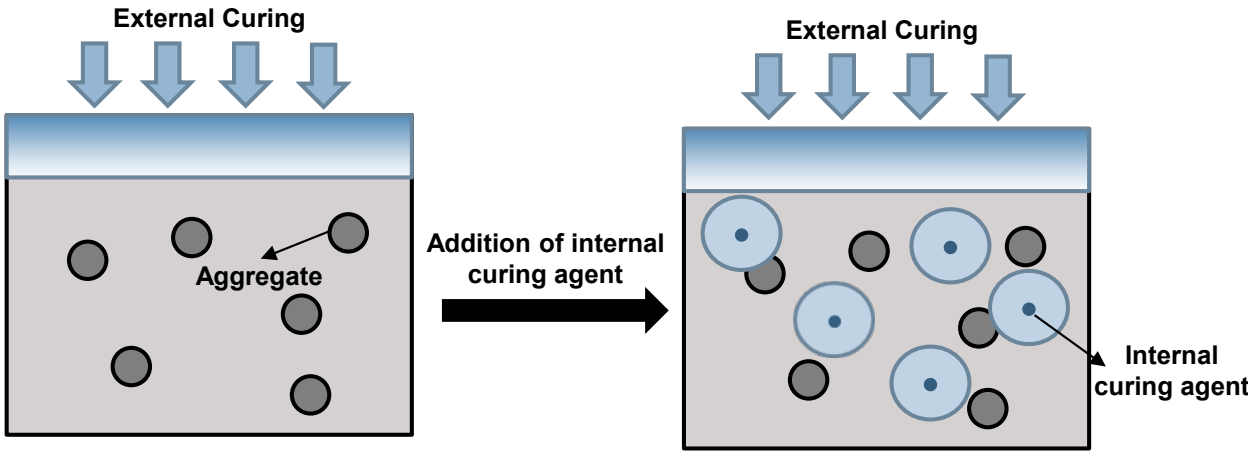

Figure 1.1 External and internal curing mechanisms in concrete.

1.2.1 Porous Material

Porous materials store water within their continuous internal porosity and gradually release it into the cementitious matrix. Internal curing with porous materials is typically achieved by replacing coarse aggregates with wet lightweight aggregates (LWAs) such as ceramic aggregates and recycled concrete aggregates or fine aggregates with superfine powders like bottom ash [13] and rice husk ash [14]. Various pre-wetted LWAs, including expanded clay [15], zeolite [16], limestone [17], and wood fibers [18], have been successfully utilized for internal curing of cement-based materials. However, traditional pre-wetted LWAs often have low water absorption capacity and poor water retention, necessitating a large volume of LWAs to achieve effective internal curing [19]. This increased demand can lead to a significant reduction in the material's overall strength. Alternatively, mesoporous superfine powders provide water to the surrounding cementitious matrix while also enhancing strength through pozzolanic activity [20]. Despite these advantages, both LWAs and superfine powders generally exhibit limited water absorbability, restricting their widespread application.

Bentonite clay is an exception, as it can absorb up to 10 times its weight in water. When used as a partial cement replacement, it acts as an internal water reservoir to mitigate autogenous shrinkage [20], [21]. However, incorporating bentonite clay as a partial replacement for cement can negatively impact the flowability of fresh concrete, posing challenges in practical applications.

1.2.2 Super Absorbent Polymer (SAP)

Superabsorbent polymers (SAPs) are specialized materials capable of absorbing and retaining large amounts of water, often more than 300 times their weight. This remarkable property is attributed to their three-dimensional, crosslinked hydrophilic polymer structure [16]. Common examples of chemically-based SAPs include sodium polyacrylate and polyacrylamide copolymers, widely used in applications such as diapers, hygiene products, agriculture, and industrial processes. Bio-based SAPs, on the other hand, are primarily composed of natural materials like starch, cellulose, or chitosan and are commonly used in agriculture, food packaging, and disposable hygiene products.

The water absorption capacity of SAPs is influenced by factors such as chemical composition, crosslink density, and particle size [22]. SAPs are synthesized from monomers, typically acrylic acid and acrylamide, in the presence of an initiator and a cross-linker [23]. The hydrophilic groups in acrylic acid form bonds with water molecules, enabling absorption. Increasing the initiator concentration during synthesis (up to a critical threshold) enhances water absorption by generating more monomer radicals. Conversely, increasing the cross-linker concentration raises the crosslink density of the polymer network, reducing solubility in water and improving water retention [23], [24].

Hydrogels retain water through two primary mechanisms: Van der Waals forces and hydrogen bonding [25], [26]. Van der Waals forces, a relatively weak attraction between the hydrogel surface and nearby water molecules, allow water to be easily separated. SAPs with smaller particle sizes rely more on Van der Waals forces due to their larger surface area [27]. Hydrogen bonding, a stronger interaction, primarily retains water in SAPs with larger particle sizes. This is facilitated by the side chains of polymers located near the hydrogel core, which enhance the bonding with water molecules [28], [29].

1.3 SAP-Cementitious Matrix Interaction

SAPs have been incorporated into cementitious materials in small quantities (0.05%–1% by weight of cement) as internal curing agents due to their ability to retain water in their swollen state and release it to mitigate shrinkage and sustain cement hydration [30], [31]. However, selecting an appropriate SAP for internal curing requires more than evaluating its pure water absorption capacity. Several methods have been proposed in the literature to measure SAP absorption and desorption behavior in a cementitious environment [30]–[37]. Among these, the tea-bag method and filtration method are widely used.

Typically, absorption tests involve the use of cement pore solutions extracted from cement slurries prepared with various W/C ratios, such as 0.36, 1, 2, 2.5, 4, 5, and even 10 [34]–[40]. Cement pore solutions are extracted through techniques like compressed nitrogen extraction [41], cellulose membrane filtration [42], microfiber filtration [38], or decantation after constant stirring for variable durations [36]. Additionally, some studies have estimated SAP absorption in cement paste by analyzing heat evolution and capillary pressure changes [43]. Increased water content delayed the hydration peak and reduced capillary pressure, with both variations linked to water uptake by SAPs. This relationship was used to calculate SAP absorption [44]. However, these tests

often fail to represent the actual behavior of SAPs within mortar or concrete due to the lack of interaction with aggregates, time-dependent ion concentration changes, and the distinct interactions between SAPs and the hardened cementitious matrix after setting.

The interaction of SAPs with the hardened cementitious matrix is notably different from their interaction with cement pore water or slurry. To address this, some studies [44]–[47] evaluated swollen hydrogel performance in hardened cementitious systems. For instance, a saturated hydrogel dyed with pigmented water was placed in a dish surrounded by cement paste, and its water release and the resulting internal humidity changes during cement hardening were monitored. Initially, a rapid water release occurred due to ion concentration gradients, followed by a slower release driven by humidity gradients [24]. The region around the SAP showed increased hardness and reduced porosity due to enhanced hydration product formation [45].

Another approach involved placing a swollen hydrogel layer between polished hardened concrete sections and measuring volume changes in the hydrogel using optical profilometry over intervals up to 28 hours. This revealed that capillary adhesion at the interface increased desorption due to Laplace pressure development [46]. Similarly, saturated SAPs dyed with ink were inserted into hardened cement paste, and the spread radius of the color was used to estimate internal curing effects [47]. Despite these efforts, current literature has not thoroughly investigated the in-situ behavior of hydrogels during the fresh, initial setting, and final setting phases of concrete, leaving a critical gap in understanding their real-time interaction with the cementitious matrix.

1.4 Air Entrainment Agents

Concrete structures in cold climates face significant challenges due to freezing temperatures. When water trapped within the concrete's pores freezes, it expands, creating internal pressure that can damage the cement matrix. This often results in surface scaling, cracks, or delamination [48]. To mitigate these effects, deicing agents such as sodium chloride and calcium chloride are frequently used to lower water's freezing point. However, these agents pose additional risks. Chloride ions react with cement hydration products like monosulfate (AFm), forming expansive Friedel's salt [49]–[51], which exacerbates internal stress. Furthermore, deicing solutions can leach calcium ions from key components like calcium hydroxide and C-S-H gel, leading to gradual strength loss [51], [52]. The combined impact of freezing, chemical reactions, and calcium depletion accelerates concrete deterioration over time.

One effective strategy to counter freeze-thaw damage is optimizing the air void structure within the concrete. Properly distributed small air voids provide space for freezing water to expand, reducing stress on the matrix. These voids are intentionally introduced using air-entraining admixtures or air-entraining cement. In contrast, larger, irregularly distributed entrapped air voids, formed during mixing and compaction, can weaken the concrete's strength and durability [53]. Effective vibration and consolidation techniques are necessary to minimize such voids and maintain structural integrity [54], [55].

The composition of an air-entrained agent typically includes a water-soluble polar hydrophilic head and a water-insoluble non-polar hydrophobic tail. The hydrophilic end can have various charges or be non-ionic (neutral) [56]. When the air-entrained agent interacts with the air-

water interface, it undergoes adsorption. The surfactant arranges itself by extending the hydrophobic end inward towards the air bubble, while the hydrophilic head forms a stable outer layer with lower surface tension, surrounded by water molecules (Figure 1.2). This mechanism of air entrainment is crucial for the formation of a well-distributed network of air voids within the concrete matrix.

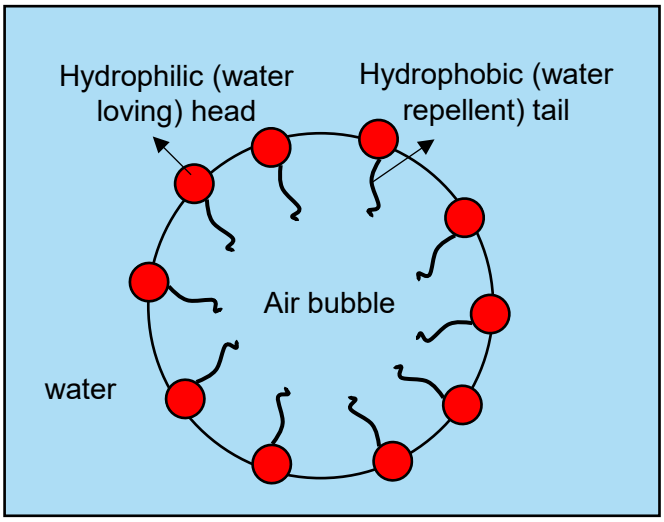

Figure 1.2: Working principle of surfactant-based air-entrained agents.

Air entrainment agents can be classified into two broad categories: bio-based and chemically synthesized materials [57]. Bio-based agents include natural wood resins, petroleum acids, and vegetable and animal fats [58]. These substances can react with calcium hydroxide, which is produced during cement hydration, resulting in the formation of hydrophobic calcium salts. This reaction plays a crucial role in generating stable air bubbles within the concrete mixture [57]. However, the widespread availability of bio-based materials in large quantities can pose challenges in meeting the industry's demands. On the other hand, chemically synthesized air entrainment agents are primarily derived from aliphatic, aromatic, and sulfonated hydrocarbons [59]. These synthetic agents are specifically designed to create and stabilize air voids in concrete by reducing the surface tension of water films on air bubbles [60]. The effectiveness of these agents can vary based on the composition. For instance, an air-entrained agent with a positively charged hydrophilic head (cationic surfactant) exhibits a strong attraction toward negatively charged cement particles, while anionic surfactants interact with the positive portion of cement particles [61]. Anionic surfactants are commonly available and cost-effective, resulting in a finer void system. However, non-ionic surfactants have the weakest attraction to cement particles. To strike a balance between achieving a finer air void structure and maintaining compression strength, a combination of non-ionic and anionic surfactants can be used. This combination limits the adsorption of cement particles, thereby providing a cost-effective solution with a more refined air void structure [62].

Air-entraining agents are commonly incorporated into concrete to introduce an air content of about 5–7%, enhancing durability against freeze-thaw damage [63]. However, this approach has some drawbacks. The additional air voids reduce the overall density of the solid matrix, leading

to a notable strength reduction—approximately 5% for every 1% increase in air content [64]–[67]. Unlike SAPs, air-entraining agents do not contribute to cement hydration and may even interfere with it [68]. Their molecular structure, which includes polar groups, can interact with the water phase in the mix, causing adsorption onto cement particles and potentially disrupting hydration [69], [70]. The increased void content also promotes quicker water evaporation, raising the risk of shrinkage [71]. Achieving effective freeze-thaw protection requires numerous small, evenly distributed air voids [72]–[74], which demand careful control over factors such as mixing time, vibration, and concrete placement [54], [75], [76]. Furthermore, the performance of air-entraining agents can be affected by interactions with other admixtures, such as superplasticizers and supplementary cementitious materials like fly ash [77]–[80]. Proper balance and compatibility are critical to ensure the desired properties of the concrete.

1.4.1 SAP as an Air Entrainment Agent

The incorporation of SAP in mortar or concrete creates a concentration gradient between the water stored within the SAP and the surrounding cement pore solution, leading to osmotic pressure development. This osmotic effect drives water out of the SAP, resulting in its deswelling and creating additional voids within the cementitious matrix over time [81], [82]. These voids, both initially present and those formed through the SAP's deswelling process, are critical to enhancing the matrix's freeze-thaw (F-T) performance.

Researchers has explored the potential of SAP in extending its application to frost resistance [10], [83], [84]. However, the void structure formed via SAP-based internal curing is often less optimal compared to the well-distributed, finely sized voids created by commercial air-entraining agents [85], [86]. Despite this, the performance of SAP in enhancing F-T resistance is influenced by several key factors, including particle size, dosage, synthesis method, and mixing conditions [84], [87]–[90]. For example, smaller SAP particles and lower dosages contribute to finer voids, which are more effective in improving F-T resistance [89], [90]. Additionally, the synthesis method significantly impacts the void structure; suspension polymerization often produces more spherical and evenly distributed voids, while bulk polymerization leads to irregularly shaped voids [88]. SAPs in dry form are particularly effective in creating smaller void spacings, which further enhances F-T resistance [84].

While internal curing agents improve durability and mitigate scaling to some extent, their performance still surpasses that of cement mixtures without any air entrainment. To overcome the trade-off between durability and the mechanical strength reduction caused by air entrainment, combining SAPs with air-entraining agents has shown better results. This hybrid approach achieves improved freezing resistance and durability, striking a balance between mechanical and durability requirements [86], [91].

1.5 Motivation for Using Bio-Based Hydrogel

Recent challenges such as COVID-19, geopolitical instability, and climate change have disrupted supply chains for raw materials used in chemical admixtures. The gap between demand and production has led to higher costs for these additives, making construction more expensive [92], [93]. To promote sustainability and reduce environmental impact in internal curing and air

entrainment, there is a growing need for bio-based admixtures derived from locally available, renewable resources instead of synthetic chemicals.

Starch, particularly cornstarch, is a promising alternative due to its ability to absorb water when heated or chemically modified through a process called gelatinization. This occurs as hydrogen bonds form between starch molecules and water, causing the granules to swell and thicken the surrounding liquid [94]. Cornstarch, which accounts for 80% of global starch production, is widely available and abundant, with United State alone producing approximately produces 390 million metric tons annually [95]. Its granular structure, mainly composed of amylose and amylopectin, undergoes swelling when exposed to heat, releasing these components and forming a gel structure that contains suspended glucose particles and bonded water [96], [97].

1.6 Research Gap

A significant research gap exists in developing internal curing systems sustainably sourced materials with simple synthesis methods, particularly for low W/C mortars. Despite the growing interest in bio-based hydrogels, there is limited exploration of their application in cementitious matrices. Specifically, the potential of cornstarch-based hydrogels as dual-functioning internal curing and air-entrainment agents remains largely unexplored, leaving a gap in understanding their impact on freeze-thaw resistance and overall performance in cement-based systems. Additionally, there is a lack of research investigating the interactions of hydrogels in in-situ conditions during the fresh, initial setting, and final setting phases of concrete, leaving a critical gap in understanding hydrogel behavior over time.

1.7 Research Objectives

This project addresses the identified research gap by fulfilling the following objectives:

1. To synthesize cornstarch-based hydrogels using the heat gelatinization process in both swelled and ground forms.
2. To quantify the internal curing potential of synthetic and bio-based hydrogels within mortar under gravitational and capillary forces during the initial curing stages over a 56-day period.
3. To improve the air void system and properties of low W/C ratio mortar using cornstarch-based hydrogels with varying cornstarch contents, comparing their performance to commercially available air-entraining agents and SAPs.
4. To investigate the influence of commercially available SAPs, varying in size and composition, and cornstarch-based hydrogels in both swelled and ground forms on the freeze-thaw resistance of low W/C ratio mortar under severe freeze-thaw cycling in a brine solution.

1.8 Organization of the Report

The rest of the report is organized as follows: Chapter 2 outlines the methodology for synthesizing cornstarch-based hydrogels in both swollen and ground forms through the heat gelatinization process. It also introduces a novel approach to quantify the internal curing potential of hydrogels. Additionally, the chapter presents the findings from studying the interactions between the cementitious matrix and the incorporated hydrogels (both commercial and cornstarch-

based) and includes insights gained from microstructural investigations. Chapter 3 presents the Micro-CT scanning methodology and results employed to analyze various parameters of the void structure in air-entrained and internally cured specimens. Chapter 4 examines the performance of SAPs and cornstarch-based hydrogels under severe freeze-thaw cycles in a brine solution, with a discussion of results in terms of variation of mechanical properties and microstructural behavior. Finally, Chapter 5 summarizes the key findings of the study and provides recommendations for future research.

1.9 Research Products

The following journal articles and conference presentations are produced from this study:

1.9.1 Journal Papers

1. A. Jalal and **R. Kiran,** (2023) "Quantifying the water donation potential of commercial and corn starch hydrogels in a cementitious matrix," Journal of Materials Research and Technology, vol. 24, pp. 4336–4352, 2023, DoI: https://doi.org/10.1016/j.jmrt.2023.04.031
2. J. Asif and **R. Kiran**, (2024) "Sustainable Biobased Hydrogel as an Alternative Air-Entrainment Agent in Cement-Based Materials," Journal of Materials in Civil Engineering, vol. 36, no. 11, p. 4024342, DoI: https://doi.org/10.1061/JMCEE7.MTENG-17763
3. J. Asif and **R. Kiran**, (2025) "Freeze-thaw resistance of concrete with biobased hydrogels and super absorbent polymers," In preparation.

1.9.2 Conference presentations

1. A. Jalal and **R. Kiran.** (2022) "A Sustainable Air-entraining and Internal Curing Agent," in 2022 Mid-Continent Transportation Research Symposium, Ames, IA.
2. A. Jalal and **R. Kiran**, (2023) "Enhancing Pavement Durability through the Application of Superabsorbent Polymers and Cornstarch-Based Hydrogels as Internal Curing Agents," in IRF Global R2T Conference & Exhibition, Phoenix, AZ.
3. A. Jalal and **R. Kiran**, (2023) "Commercial and Sustainable Hydrogels for Internal Curing and Shrinkage Control in Concrete," in Engineering Mechanics Institute Conference, Atlanta, GA.

Chapter 2. Quantifying the Water Donation Potential of Commercial and Corn Starch Hydrogels in a Cementitious Matrix

External curing alone may not be sufficient in the case of concrete with a W/C ratio of less than 0.36. Dry Super Absorbent Polymers (SAPs) weighing 0.05% to 1% wt. of cement are popularly used for internal curing purposes. The swollen SAP crystals act as water reservoirs at later curing stages, donating water to the surrounding cementitious matrix for hydration. Currently, there is no method available in literature to quantify the water donation potential of SAPs in a cementitious matrix. Moreover, the water transfer mechanism between the swollen SAP and the surrounding cementitious matrix is not understood in the first eight weeks of the curing period. In this chapter, a capsule filled with swollen SAP is embedded in a cement mortar cube. The internal wetting area around the swollen SAP capsule is monitored for 56 days by periodically slicing the mortar cube. The internal wetting area around the swollen SAP capsule is taken as a proxy metric for the internal curing potential of the SAP. Five commercially available SAPs, along with a newly synthesized corn starch hydrogel, are investigated in this study.

2.1 Materials and Methods

2.1.1 Materials

2.1.1.1 Commercial Superabsorbent Polymers (SAPs)

The internal curing potential of five different types of commercially available SAPs are investigated in this study designated as A (LiquiBlock™ HS Fines), B (LiquiBlock™ 40F), C (LiquiBlock™ 2G-110), D (LiquiBlock™ WHS 2) and E (LiquiBlock™ WHS 1). These SAPs can be differentiated based on their chemical composition, particle size, and water absorption ability. The properties of the SAPs used in the current study and their commercial names as provided by the supplier (Emerging Technologies) are presented in Table 2.1. All the five commercial SAPs are sodium salts of crosslinked polyacrylic acid, except SAP type B is potassium salt of crosslinked polyacrylic acid/polyacrylamide copolymer. SAP types C, D, and E have relatively high-water absorption when compared to A and B owing to their larger particle sizes. As discussed in section 1.2.2, smaller SAP particles have a larger surface area, which allows them to retain water through relatively weaker Van der Waals forces. In contrast, larger SAP particles predominantly retain water through stronger hydrogen bonding interactions [25], [26], [98].

2.1.1.2 Cement, superplasticizer, and hydrogel capsule

Type-1 Portland cement as per ASTM C150 [99] was procured from TCC Materials®. Superplasticizer (MasterGlenium® 7500 made by BASF corporation) was employed to achieve the desired workability set at 90% in the flow table test. Superplasticizer fulfils the requirements of type A and type F admixture provided in ASTM C 494/C 494M [100]. Clear gelatin capsules were used in this study to introduce hydrogel into mortar cubes to investigate the internal curing potential of hydrogels. The body part (height 22.2 mm and external diameter 9.55 mm) of a size "000" gelatin capsule (1.142 ml volume) was used to store swollen hydrogel. The gelatin capsule

takes approximately 10 minutes to dissolve in water [101]. The hydrogel was injected into the capsule body using a 60 ml syringe without a needle, while a dropper was used to add water to the capsule whenever applicable.

Table 2.1: Properties of commercially available SAPs as provided by the supplier

SAP ID	A	B	C	D	E
Commercial name	LiquiBlock™ HS Fines	LiquiBlock™ 40F	LiquiBlock™ 2G-110	LiquiBlock™ WHS 2	LiquiBlock™ WHS 1
Particle size distribution (in microns)	1-140	1-200	<600	2% @ 850, 3% @ 150	0-850
Absorption (g/g) of deionized water	>180	>200	>490	~450	>400
Chemical composition	Sodium salt of crosslinked polyacrylic acid	Potassium salt of crosslinked polyacrylic acid/polyacrylamide copolymer	Sodium salt of crosslinked polyacrylic acid	Sodium salt of crosslinked polyacrylic acid	Sodium salt of crosslinked polyacrylic acid

2.1.1.3 Synthesis of cornstarch hydrogel

ARGO® brand corn starch was used to synthesize cornstarch hydrogel through heat gelatinization. Approximately 1% wt. corn starch is mixed in water and heated at a temperature of 180° F for 15 minutes. Cornstarch has a granular microstructure with the dominant region of glucose, mainly composed of amylose and amylopectin. With the input of heat energy, the starch particles in water solution swell until they release amylose and amylopectin and this process is referred to as the heat gelatinization [96]. The continuous heat forms a gel structure containing suspended glucose particles with bonded water molecules [97].

2.1.2 Preparation of specimen with hydrogel capsules

The sample preparation and curing were conducted according to ASTM C192/C192M-16a [102]. All samples were prepared with the same mix proportion to maintain consistency. Low water to cement ratio of 0.3 was used, which will require an internal curing source to complete the hydration process [7]. The weight of the fine aggregate was 1.75 times the weight of cement. Superplasticizer (0.6% wt. of cement) is added to the cement to maintain workability (90% flow table value), and the weight fraction of the superplasticizer is evaluated by a trial and error method. A cube of 50.8 mm side was used to cast specimens embedded with hydrogel or water capsules to investigate the internal curing offered by the hydrogels. 1% wt. hydrogels were prepared by mixing dry all the dry SAPs with 100 times their weight of water.

A novel test protocol was developed to investigate the water donation ability of SAPs. This understanding is vital as water availability to the cementitious matrix with low W/C ratios is necessary to complete the hydration process. Figure 2.1 illustrates the procedure employed to introduce hydrogel capsules while casting the cement mortar cubes. First, the freshly prepared mortar was poured into a cubic mold until $1/4^{th}$ of the total depth Figure 2.1 (a)) and compacted

using a rubber tamper to ensure proper compaction. Next, the body of the transparent gelatin capsule was inserted into its cap for strengthening the capsule and placed near each corner of the cube using gentle thumb force. Finally, a syringe without a needle was used to insert 1% wt. hydrogels and cornstarch-based hydrogel into capsules. A cube embedded with capsules filled with water is considered a benchmark sample in this study. Finally, the remaining 3/4th portion of cubic molds was filled with mortar (Figure 2.1 (c)) and compacted. Two sets of samples were prepared, one to observe water donation under gravitational force and the other under capillary force (see Figure 2.2). The set of samples for the investigation of water donation by the hydrogel under gravity force were placed upside down so that the open end of the inside capsules faced down (Figure 2.2 (a)), while the second set was placed in the face-up direction (Figure 2.2 (b)). All samples were covered with a wet, thick cloth for 24 hours to avoid any water loss before demolding and water immersed in the water tank until they were tested.

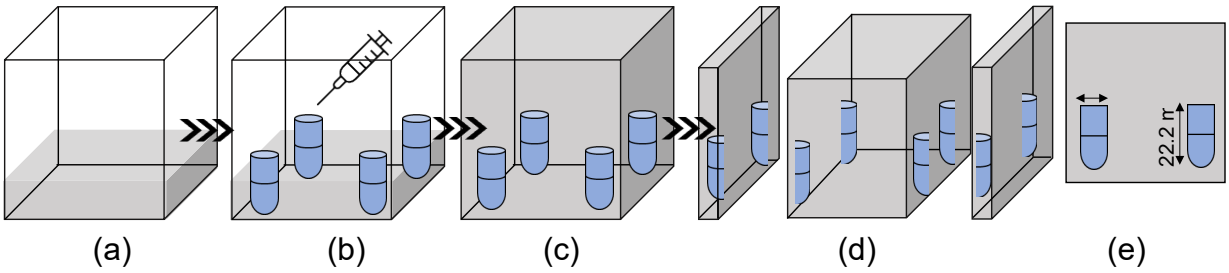

Figure 2.1: Procedure for casting mortar cubes with hydrogel capsules: (a) pour mortar up to 1/4th depth, (b) insert hydrogel capsules near each corner, (c) complete the casting,(d) slice through the center of hydrogel capsules after required curing time, and (e) cross-sectional view of a sliced portion

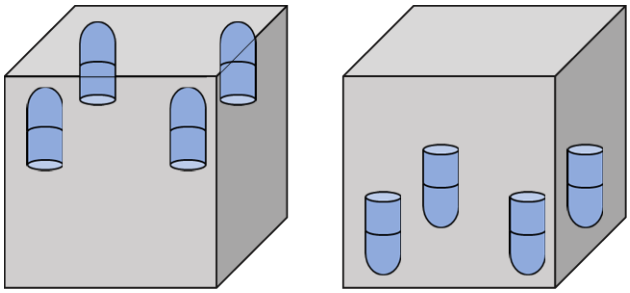

Figure 2.2: Position of specimens during curing time period (a) open ends face downwards under gravitational force and (b) open ends face upwards for under capillary force case

2.2 Testing program

2.2.1 Tea-bag method

The intended function of an SAP is to absorb enough water so that it can supply to the surrounding cementitious matrix. The water-absorbing ability of the hydrogels when exposed to fresh water and the cement pore solution was investigated using tea-bag method. The cement pore solution was prepared by mixing water with five times the weight of cement. The solution was

magnetically stirred for 24 hours and filtered for the tea-bag test [20]. In the tea-bag method, dry SAP weighing around 0.1 g was inserted into a premoistened cotton tea bag before completely immersing it in an airtight water container to avoid evaporation and carbonation, as shown in Figure 2.3. Carbonation occurs when carbon dioxide from the environment interacts with the target solution. Especially in the case of cement pore solution, carbonation of calcium hydroxide produces calcium carbonate that increases calcium ion concentration around SAP, which reduces water absorption of the hydrogel [22], [47]. The tea-bag with the SAPs immersed in the solution was taken out, wiped with a dry cloth, and weighed at 5, 10, 30, 60, 180, and 1440 minutes. The average solution absorption in grams per gram weight of the dry SAP is evaluated from three samples using Eq. 2.1.

$$AC = \frac{W_3 - W_2 - W_1}{W_1} \qquad \text{Eq. 2.1}$$

where, AC is the solution absorption capacity of SAP, W_1 is the mass of dry SAP, W_2 is the mass of wiped wet tea bag, and W_3 is the mass of wiped wet tea bag containing swollen hydrogel.

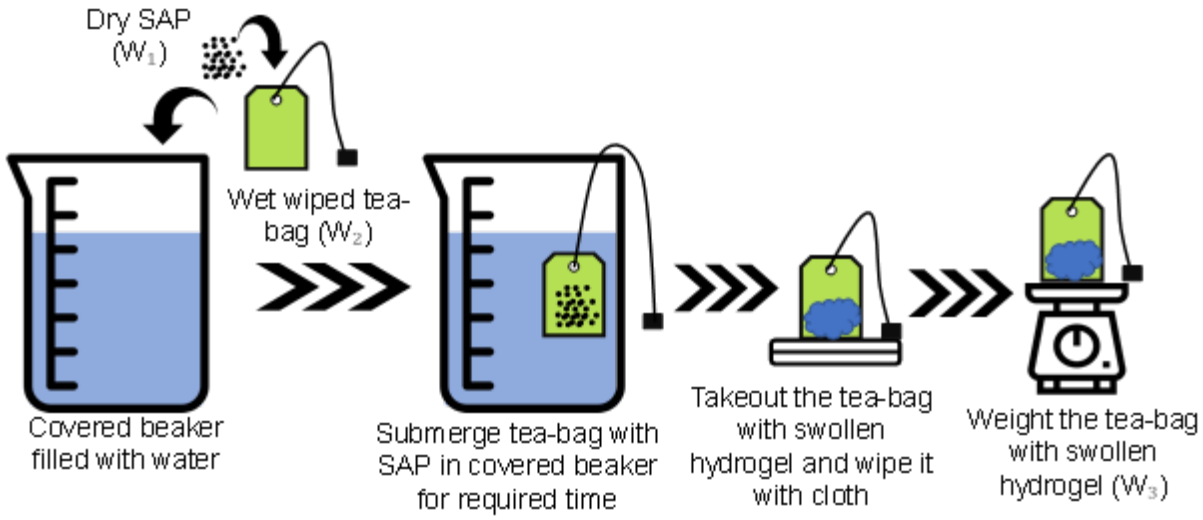

Figure 2.3: Procedure for tea-bag test used to quantify the absorption capacity of dry SAPs in the pore solution.

2.2.2 Wetting Area as a proxy measure for water donation ability of SAPs

The functionality of hydrogels is to supplement water to the surrounding cement matrix in the initial stages of hydration to aid the hydration process [23]. In practice, SAPs are added during the concrete mixing process and the SAPs encounter cementitious materials in fresh and hardened states of concrete. Few studies [42], [43] introduced swollen SAP with colored water between hardened polished concrete pieces or through a hole into a concrete cylinder. The extent of internal curing was linked to the spread of colored water. However, the current study introduced swollen hydrogel in a fresh mortar and measured the variation in the wetted area around the embedded hydrogel over time to understand the performance of SAPs inside the cementitious matrix. In this study, we employ the water wetting area as a proxy measure for the water donation ability of SAPs

in the cementitious matrix. In other words, the higher the wetted area, the higher the ability of the SAP to donate the water and vice versa.

The water donation is quantified by determining the wet area around the swollen hydrogel capsule inside mortar cubes after 1, 3, 7, 14, 28, and 56 days. After each specified period of curing, mortar cubes were cut vertically at 5 mm from any two opposite side ends using a dry diamond saw cutter blade (see Figure 2.1 (d)). Dry cutting was adopted to avoid the intrusion of moisture from surrounding sources. The cutting was initiated from the opposite side to the position of the hydrogel capsule to reduce the dispersion of desorbed water due to the sliding movement of the blade (Figure 2.1: (d)). This entire process of cutting cubic samples results in four cross-sections exposing wet areas due to the water desorption by hydrogels, as shown in Figure 2.1 (d) and Figure 2.1 (e). Immediately after cutting, the wetted cross-sectional images were captured with a 24.2 MP resolution Canon® EOS 800D camera. The images were processed using ImageJ software to determine the wet area around the hydrogel capsule. A thresholding approach is used to quantify the wet area in ImageJ. A sample input image used for the ImageJ analysis is provided in Figure 2.4 (a) the output of the ImageJ thresholding method is provided in Figure 2.4 (b). The red region is identified as wet area by ImageJ. Some edges and dry regions are also identified as wet regions in this method. However, this region is less than 3% of the wet region which is within the acceptable error limits. It should be noted that the capsule region is always wet for all the samples and hence not subtracted from the total wet region. Images of at least 2 sections per mortar cube were used for quantifying the wet region.

Figure 2.4: (a) Picture of a sectioned mortar cube after 1-day of curing with 1%-HB capsule under gravity force, and (b) wet area color coded as red by the ImageJ software.

2.2.3 XRD, SEM, and EDX analysis

Chemical and microstructure analyses were conducted to determine the changes in the cement mortar due to the interaction with the hydrogels. The X-ray diffraction (XRD) was conducted in the vicinity of the hydrogel capsules after 28 days of external curing and these results are compared with the XRD results of the control specimen (cement mortar cubes with water capsule). The capsule region was extracted using a dry diamond blade and the obtained material is finely powdered and sieved through a mesh size of 200 microns. This powder is then used to

perform XRD at a scanning angle (2θ) ranging from 5° to 80° with a speed of 4° per minute. In addition, scanning electron microscopy (SEM) and energy-dispersive X-ray spectroscopy (EDX) analysis were carried out at four different distances from the capsule region to assess variation in microstructure and chemical composition, respectively, when moving away from the internal curing source (hydrogel capsule) after 28 days of external curing. Four points were selected at distances of 15, 25, 35, and 45 mm from the side containing the hydrogel capsules, presented as red rectangles in Figure 2.5. After casting, the pressure from the surrounding mortar pushes the hydrogel inside, reducing the capsule cavity area. As a result, it was observed the capsule cavity height reduced up to the 10 mm mark from the bottom. The SEM and EDX analyses were performed in the area between the capsule and the cube's surface with an increment of 10 mm, excluding 5 mm from each end to avoid the direct influence of the external curing and hydrogel. The mortar cube with water capsules (CW) is considered a control specimen for both the SEM and EDX analysis.

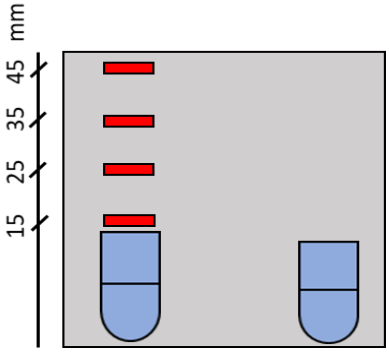

Figure 2.5: The target locations for SEM and EDX analysis to quantify the microstructure and hydration product density, respectively.

2.3 Results and Discussion

2.3.1 Water absorption of hydrogels

The distill water absorption capacity of hydrogels is provided by the supplier (see Table 2.1). However, tap water is used for concreting purposes which contains calcium and sodium minerals that alter the water absorbability of hydrogels. The tea-bag method described in section 2.2.1 was adopted to determine water absorption of SAPs after 5, 10, 30, 60, 180, and 1440 minutes of immersion in tap water. Figure 2.6 shows the tap water absorption of commercial SAPs as a function of time. It was observed that water absorption in the first 5 minutes was rapid, and maximum water absorption by the hydrogels occurred around 30 minutes after exposure to the tap water (see Table 2.2). After approximately 30 minutes, some desorption occurred, and the quantity of absorbed water decreased gradually. Among the SAPs investigated, type A and B showed relatively low water absorption (~150 g/g at 30 minutes), while SAPs type C, D, and E exhibited more than 200 g/g absorption. These differences can be attributed to the larger particle sizes of high-water absorbing SAPs as the chemical composition is more or less the same among all hydrogels except for the type B. Smaller particle-sized SAPs (A and B) have more surface area and hold water molecules with weaker Van der Walls forces. In contrast, SAPs with bigger

particles (SAP type C, D, and E) have more space inside the individual particles to hold water through stronger hydrogen bonds with water molecules [26]. These trends are similar to what was provided by the supplier for the distilled water absorption ability of the SAPs (presented in Table 2.1). However, the lower water absorption of tap water is due to the presence of calcium and sodium minerals in the tap water [97], [103].

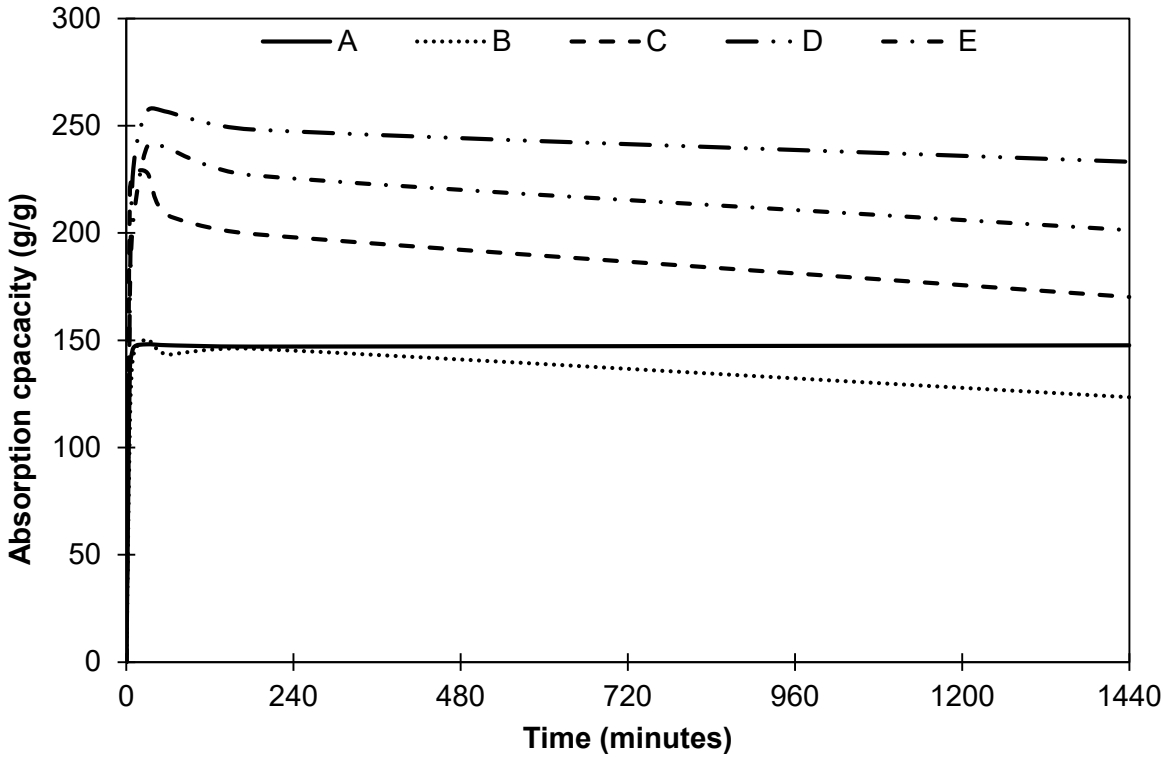

Figure 2.6: Tap water absorption of commercial SAPs as a function of time

Table 2.2: Absorption capacity of SAPs immersed in tap water and cement pore solution after 30 minutes of interaction

	A	B	C	D	E
Tap water absorption after 30 minutes (g/g)	148.1	150.4	228	256.8	240.4
Cement pore solution absorption after 30 minutes (g/g)	38.5	68.0	42.7	69.2	76.4

The SAPs will be exposed to the water mixed with cementitious materials and other deleterious materials during the concreting process. With this, it is important to quantify the water absorption ability of these SAPs in an environment that closely mimics the fresh concrete. Therefore, the tea-bag water absorption test was also performed in the cement pore solution which was described in section 2.2.1. Figure 2.7 illustrates the water absorption of SAPs in cement pore solution as a function of time. Similar to the SAPs exposed to the tap water (see Figure 2.6Figure 2.6:), there is a rapid initial water absorption by the SAPs in the cement pore solution, and the

maximum absorption was observed approximately after 5 minutes of immersion. Furthermore, the water absorption ability of all SAPs except the B type decreased steeply after this exposure time. In the case of type B, the water absorption increased even after the initial peak, and this increase has been steady.

The development of osmotic pressure due to ion concentration difference between the surrounding solution and inside SAP causes water transfer into the SAP. In addition, SAP possesses negatively charged carboxylate groups that interact with water through a hydrogen bond and thus hold it. However, the combination of water with cement initiates the hydration reaction that output products which have cations like Ca^{2+}, $Al^{3+,}$ and Na^{+} [104], [105], which attract the negatively charged carboxylate groups in SAPs that lead to the screening effect. The screening effect dampens the development of osmotic pressure and, consequently, the swelling of SAP [106]. In addition, stable ions like Ca^{2+} combine with the negatively charged carboxylate group of SAPs to produce complexes that reduce the anionic charge of the hydrogel and, accordingly, the osmotic pressure because of the smaller ion concentration difference [107]. Both screening effect and formation of complexes considerably decrease the water absorption capacity of SAPs in cement pore solution [30]. SAPs quickly store water at the beginning before the development of the screening effect and formation of complexes. However, the low carboxylate group concentration may be the reason for maintaining the water absorption behavior in hydrogel type B that reduces the attraction between pore solution cations, and hydrogel's negatively charged carboxylate group decreases the screening effect and complex formation [107]. The tea-bag method does not apply to the cornstarch-based hydrogel because of its high mobility and inability to contain porous cotton tea-bags. For this reason, the internal curing potential is directly tested.

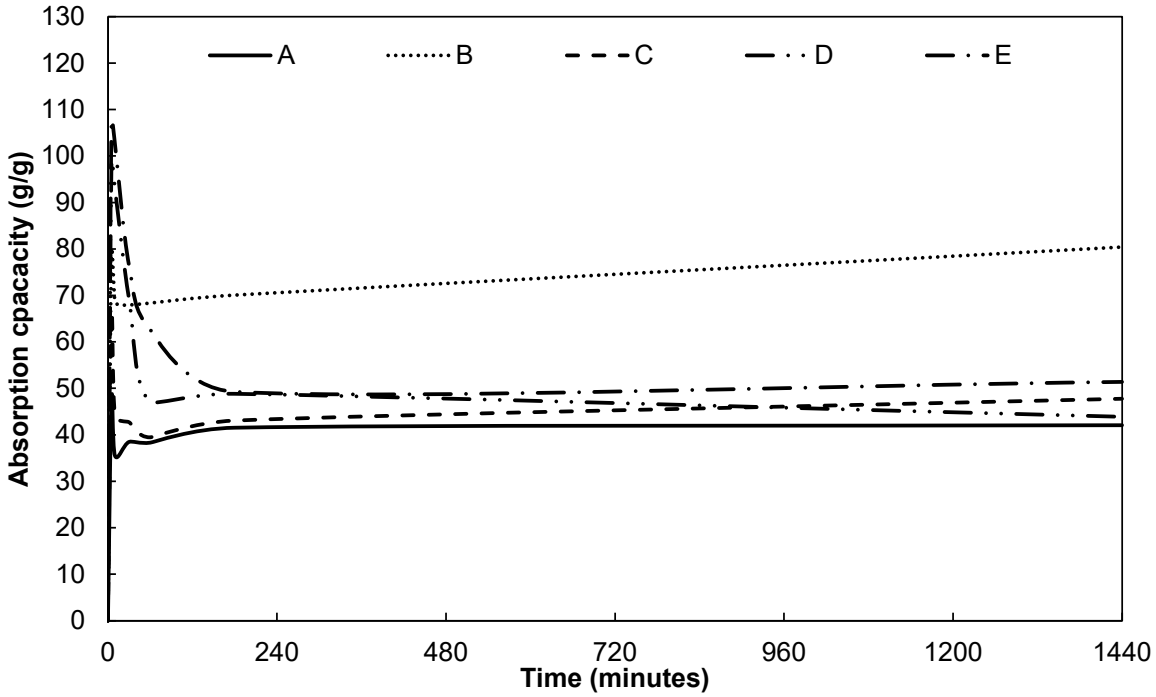

Figure 2.7: Water absorption of commercial SAPs in the cement pore solution as a function of time

2.3.2 Internal curing

The water donation ability of saturated hydrogel has to be investigated in the fresh and hardened state of the cementitious matrix, which is not similar to quantifying the water desorption in solution or hardened cementitious matrix [108]–[110]. Many factors govern the deswelling or desorption of hydrogels. The ion concentration difference between stored water in hydrogel and pore cement solution (ions such as Ca^{+2}, Na^{+1}, S^{-2}, $K^{+1,}$ and OH^{-1}) leads to osmotic pressure at the curved surface of the cavity that sucks water from the hydrogel to the surrounding region and accumulates hydrogel on the surface of the cavity in the form of a membrane [13], [111]. Furthermore, the mortar matrix forms a network of pores that results in a capillary pull of water from the hydrogel [112]. In addition, the mechanical, hydrostatic pressure from the nearby mortar squeezes the water from the hydrogel into the matrix. Finally, self-weight facilitates water movement from the hydrogel in the direction of gravity. Several studies in the past [113] suggested that hydrogel desorption depends on the kinetics of hydration of cement. However, no studies have investigated hydrogels' desorption (introduced during the mortar's casting) throughout the hydration process. This study investigated the hydrogel desorption in cement mortar cubes over 56 days using the water spread method discussed in Section 2.2.2.

As mentioned previously, the internal curing potential of a hydrogel is indirectly characterized by evaluating the water wetting area in a 50.8-inch cement mortar cube with an embedded hydrogel gelatin capsule (1.142 ml volume). It is important to note that for standardization purposes, all hydrogels were instantaneously swelled to 100 gram/gram and are not fully saturated except for the corn starch hydrogel. In the case of cornstarch hydrogel, 1% cornstarch solution was used to prepare the hydrogel using the heat gelatinization method described in section 2.2.1. The wetting area was tracked for all the hydrogels until 56 days (1 day, 3 days, 7 days, 14 days, 28 days, and 56 days). The water donation ability under gravitational pull and capillary force are summarized in Figure 2.8 and Figure 2.9, respectively.

The difference in the ion concentration propels the initial desorption. However, later the ion concentration becomes relatively uniform in the system, including cement matrix and hydrogel. Subsequently, the humidity gradient plays a role in moisture transmission to or from the hydrogel instead of osmotic pressure. Figure 2.8 illustrates the variation in the wet area due to encapsulated hydrogels when samples were placed upset down – gravity force case (see Figure 2.2 (a)). In most cases, it was observed after the day-1, wet areas were high because of water desorption due to ion concentration differences. However, after three days, osmotic pressure was gradually eliminated, and the wet area dropped. The SAP type A follows this trend perfectly, as it initially supplied the water to 40% of the cross-sectional area, then suddenly dropped approximately 40% and then doubled at 7 days of curing because of the positive humidity gradient developed between hydrogel and cement mortar matrix. The variation in desorption continues because hydration of cement and evaporation causes the reduction in the wet area after 14 days, elevates again at 28 days, and remains relatively constant until 56 days due to the almost completion of the hydration process at 28 days.

The change in a wet area with time differs among the types of hydrogels because of differences in their absorption capacity, desorption rate, chemical compositions, and crystal sizes. However, the cyclic pattern of variation remains the same rather than a continuous increase or decrease in a wet area in almost all the SAPs. After the final setting of mortar, the void network remains intact, eliminating the influence of external mechanical and hydrostatic pressure on the hydrogel. At the same time, hydration of cement and evaporation results in a positive humidity gradient until the hydration process nears completion. SAP type C has maximum absorption capacity and shows a high variation in the wet area. Initially hydrated more than half of the area, then suddenly dropped at 3 days and abrupt enhancement at 7 days and in a similar way fell after 14 days. However, that variation becomes stable after 28 days until 56 days. Despite the low water absorption capacity, cornstarch-based hydrogel showed better performance. After one day, the CS hydrogel supplied water to almost the same area as that of type HC hydrogel, but after 3 days, it lost almost 35% of the area that remained stable until 14 days. However, CS hydrogel resulted in a significant wet area after 28 days. Cornstarch-based hydrogel's stable performance is due to the high fluidity that improves the penetration into pores in all directions due to gravity force and capillary pull, which was not possible in other hydrogels as they are more viscous when compared to the CS hydrogel. The hydrogel capsule mimics a single particle of swollen SAP and its way of internal curing around its vicinity. Overall, it was observed that hydrogels provide water for internal curing throughout the hydration process. In addition, cornstarch-based hydrogel operated better in terms of initial high-water supply and acted as a stable curing source throughout the hydration process.

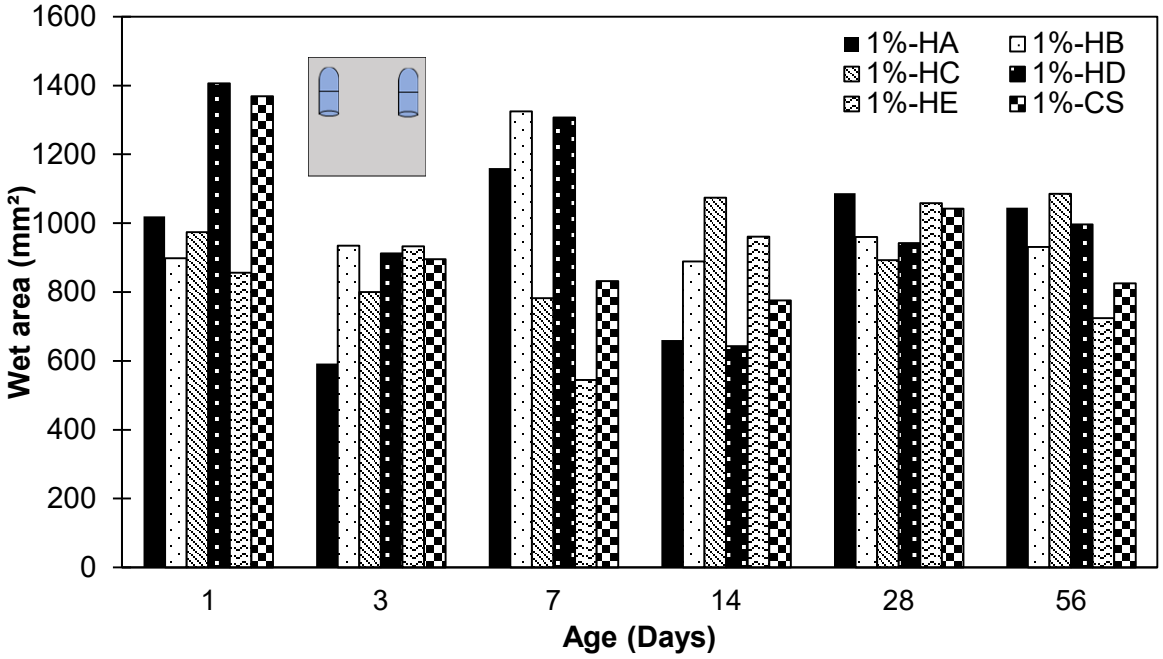

Figure 2.8: Wet area variation with time around the encapsulated hydrogel under the gravity force.

Past studies [34], [113] proposed the capillary force to be the driving force behind the spread of water throughout the matrix from the hydrogel for internal curing. Figure 2.9 presents

the wet area around the capsule full of hydrogel when placed upright (open ends of capsules face up as shown in Figure 2.2 (b)) to observe internal curing under capillary action. Overall, the wet area dropped when compared to the gravity case, but still, hydrogels provided water to a significant area. Initially, commercially available hydrogels irrigate lesser areas due to their high viscosity. As the water content is the same in all types of hydrogels, an SAP with a higher absorption capacity forms a denser gel. Hydrogels produced from types of C and D initially irrigated lower area, while the water from the hydrogels produced from types A and B exhibited more wet areas by capillary action owing to their less viscosity due to low water absorbing capacity.

In most cases, the cyclic variation in the wetting area observed in the gravity case remained the same, verifying the dependence of desorption rate on humidity and ion concentration gradients. Hydrogel type A again showed the falling and rising trend more clearly because of comparatively low water absorption capacity but still firm enough to hold position and water, unlike cornstarch-based hydrogel. The high-water absorbent hydrogels produced from types C, D, and E had low wet area initially and this area gradually increased until 7 days and then almost remained constant with a small increment at the end of 56 days of external curing. The 1% cornstarch-based hydrogel performed better even against the gravity pull. Initially, corn starch hydrogel almost irrigated 1100 mm^2 of the surrounding area and decreased by a small margin after 14 and 28 days, maybe due to a shift in humidity gradient direction but the wetting area is regained at 56 days. There is no significant difference between cornstarch-based hydrogel under gravity and capillary forces due to its high fluidity which makes it easy to penetrate into pores to provide curing water.

Overall, it was observed that the swollen hydrogels desorb water under both capillary force and gravitational pull irrigating the neighboring regions. However, the water desorption is found to be dominant when the direction of flow of water aligns with the gravitational force. Furthermore, the stored water from the low water absorbent hydrogels can be easily accessible to the surrounding area, especially in the initial stage, but the cyclic variation in water desorption is more prominent when compared to the high-water absorbent hydrogels which have a more stable trend of desorption. The superior performance of the corn-starch hydrogel can be attributed to it low viscosity due to low water absorption capacity.

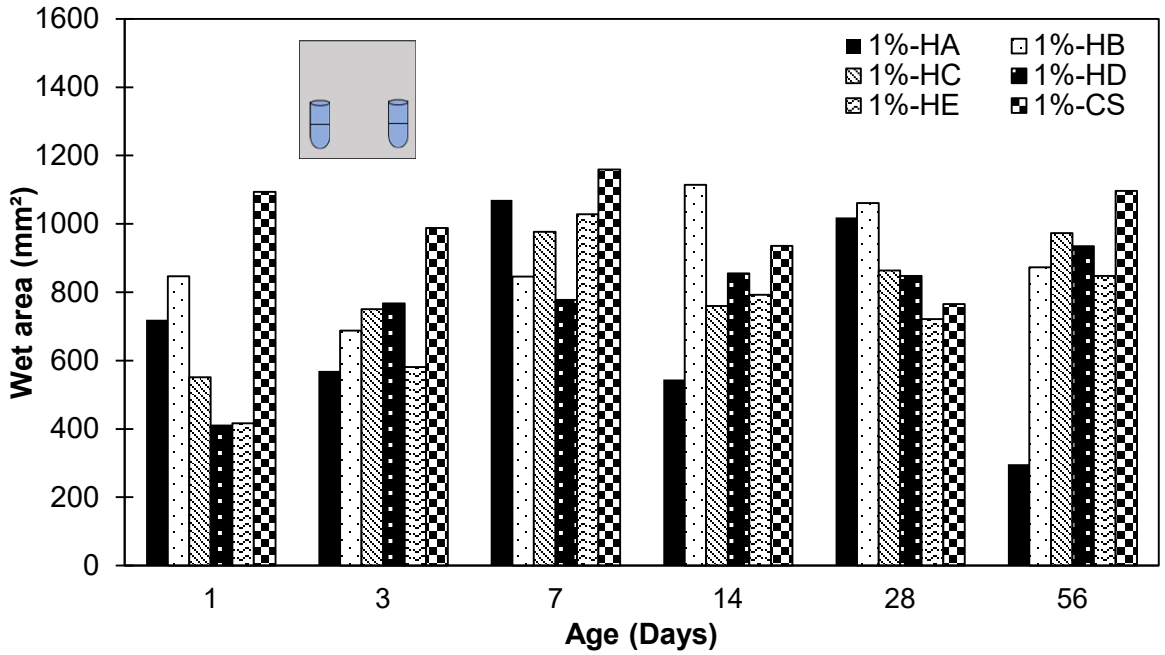

Figure 2.9: Wet area variation with time from the encapsulated hydrogel under capillary force.

2.3.3 SEM and EDX Analysis

Higher wet areas in the case of samples with hydrogel capsules are an indirect measure of internal curing. However, a higher density of hydration products can be directly associated with hydrogel water contribution to the hydration process of cement. To this end, SEM and EDX analyses were performed to characterize the morphology of the interface between the hydrogel capsule and cement mortar and the presence of hydration products, respectively. The SEM and EDX analyses were performed employing the procedures described in section 2.2.3, after 28 days of curing to observe the contribution of hydrogels towards the completion of the hydration process. The hydration of cement primarily results in CSH gel at the initial stage that densifies as hydration provides strength to the mortar. SEM and EDX analyses were performed 24 hours after sectioning to allow all released water from the hydrogel to evaporate. A cavity was formed where the hydrogel capsule was placed during the casting process. The outer surface of the cavity which acted as a hydrogel-mortar interface is where the hydrogel and mortar directly interact when the gelatin capsule is dissolved (Figure 2.10 (a)). The region around the hydrogel-mortar interface has a distinctive rough, grainy texture area, whose thickness varies depending on the type of SAPs embedded in the hydrogel capsules (see Figure 2.10 (a)). The EDX analysis of the granular texture region around the hydrogel capsule region (Figure 2.10 (b)) shows high peaks of Si and Ca, demonstrating the presence of dense clusters of CSH gel. However, that dense cluster of CSH gel fades when moving away from the hydrogel capsule region, confirming the positive impact of hydrogel on cement hydration in the vicinity of the mortar-hydrogel interface region.

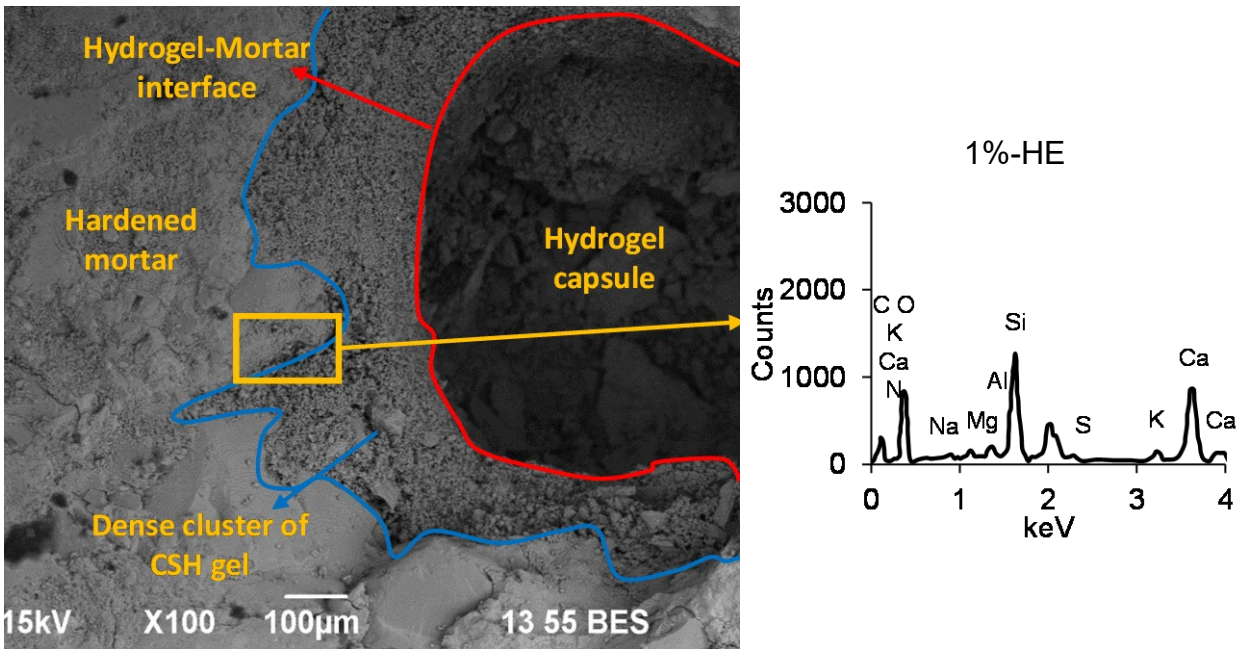

Figure 2.10: (a) Typical hydrogel capsule region surrounded by dense granular morphology region; and (b) EDX analysis of surrounded granular cluster showing high peaks of Si and Ca.

In current research work, the performance of hydrogel was gauged by the extent of the wet area around the hydrogel capsule; therefore, SEM and EDX analyses were carried out at different distances from the source hydrogel capsule to determine the efficiency of hydrogel in improving the density of hydration products. Figure 2.11 presents the change in the morphology of the mortar surface when moving away from the hydrogel capsule obtained through SEM images at a resolution of 10 µm. The variation in surface morphology is due to changes in the extent of the hydration process. The spots in the SEM images are labeled as CH, and CSH, representing calcium hydroxide and CSH gel, respectively, determined by using peaks from EDX analysis. CSH gel was observed in granular type morphology while CH has a slightly smooth structure. The sample with embedded water capsules labeled as "CW" is considered a control specimen that exhibited lesser clusters of CSH gel primarily found in the vicinity of the water capsule. However, the region near the surface with only access to external water for curing showed lower density of CSH gel, indicating that external curing alone may not be sufficient to completely hydrate all the available cementitious materials. In contrast, the cubes with hydrogel capsules had comparatively more area of concentrated CSH gel region that gradually decreased when moved away from the hydrogel capsule.

Furthermore, individual hydrogel performance varies due to differences in their properties like water absorption capacity, viscosity, and particle size. Hydrogel type HA had high density of CSH gel near the hydrogel capsule which gradually decreased after 35 mm distance (from the bottom of the sample) until the edge of the sample. In the case of hydrogel type HB, the hydration products get denser at 25 mm from the bottom of the sample. The water content in all types of hydrogel was the same which causes the flowability of higher water absorbent capacity polymers (1%-HC, 1%-HD, and 1%-HE) relatively low. Low flowability hurdles the movement of these

hydrogels inside mortar cube, therefore, most of the dense regions of CSH gel were observed near the capsule region. The HE-type hydrogel having the highest absorption capacity managed to spread a very dense accumulation of CSH gel up to a distance of 35 mm in a non-uniform pattern. The bio-based cornstarch hydrogel performed well with uniform distribution of dense clusters of CSH gel in all the regions, even at the highest point of 45 mm. The water content in 1% cornstarch solution exceeds the water absorption capacity of cornstarch-based hydrogel, therefore, decreasing it viscosity. Despite the lower water holding capacity, cornstarch-based hydrogel provides sufficient moisture throughout the process of hydration due to low viscosity. The cornstarch is composed of amylopectin and amylase, which are glucose molecules. Heating the cornstarch solution swells the particles, and continue heating bursts and disperses glucose molecules in the solution. When the solution settles and reaches normal temperature in the mortar, the amylase particles recombine to retain water and provide curing moisture throughout the hydration period [97]. In addition, some micro-voids were also observed in the vicinity of the corn-starch hydrogel capsule with the accumulation of hydrate products such as calcium hydroxide (Figure 2.11). These micro-voids may be have resulted from the mobility of the hydrogel releasing the stored water leaving behind voids containing calcium hydroxide that is reported in previous studies [114], [115].

A significant amount of cement clinker remains un-hydrated when W/C ratio is 0.3. Therefore, an internal curing source is needed to complete hydration and gain full strength [115]. Figure 2.12 illustrates the effect of hydrogel on elemental peaks observed in EDX analysis. The addition of hydrogel capsules decreased the sodium, magnesium, and aluminum contents while increasing the amount of calcium, silicon, carbon, and oxygen, displaying a considerable improvement in hydration products and thereby the degree of hydration. Overall, it was observed that adding swollen SAPs significantly improves the hydration products.

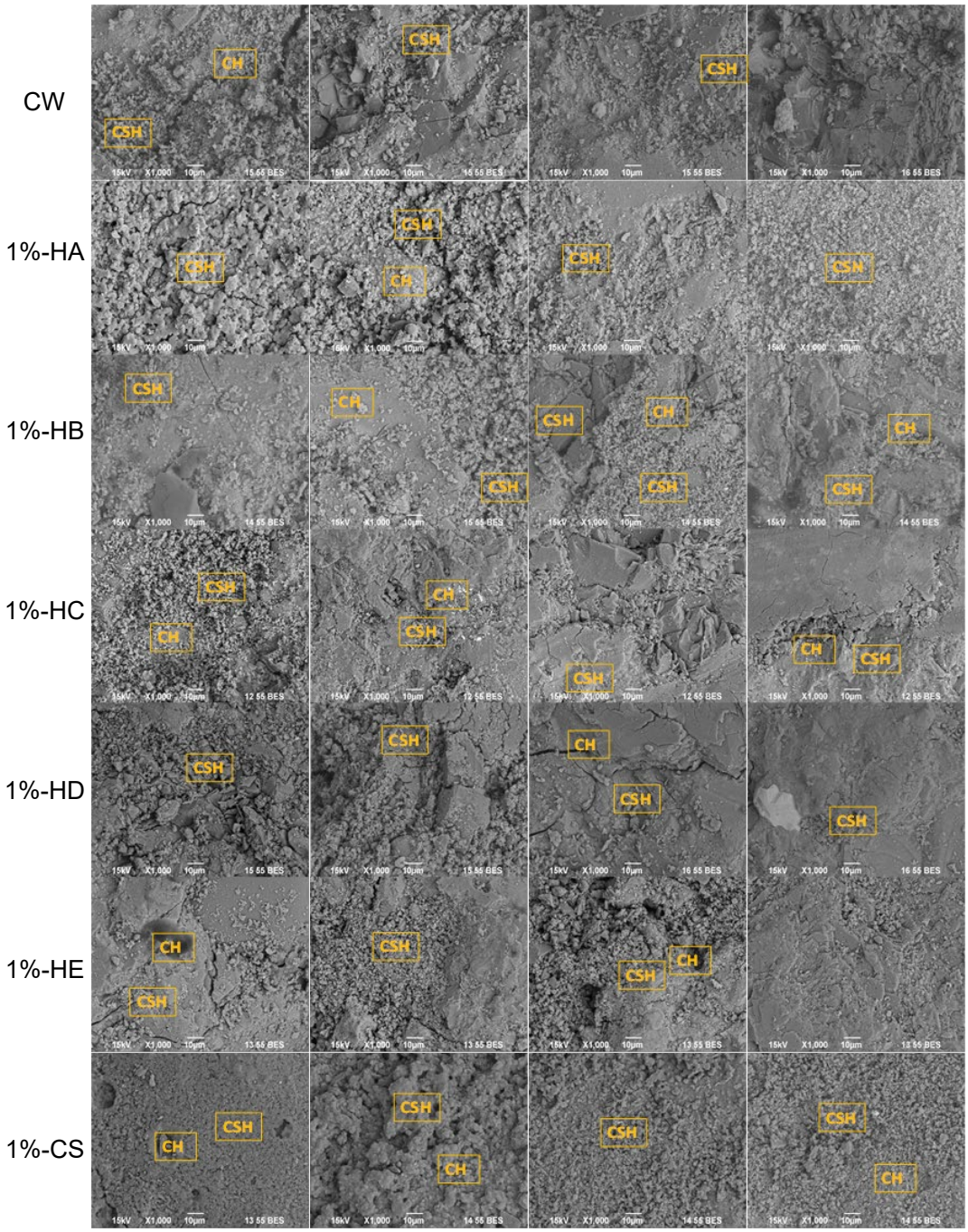

Figure 2.11: Variation in mortar surface morphology with increasing distances from the hydrogel capsule and the water capsule using SEM images at 10 µm resolution

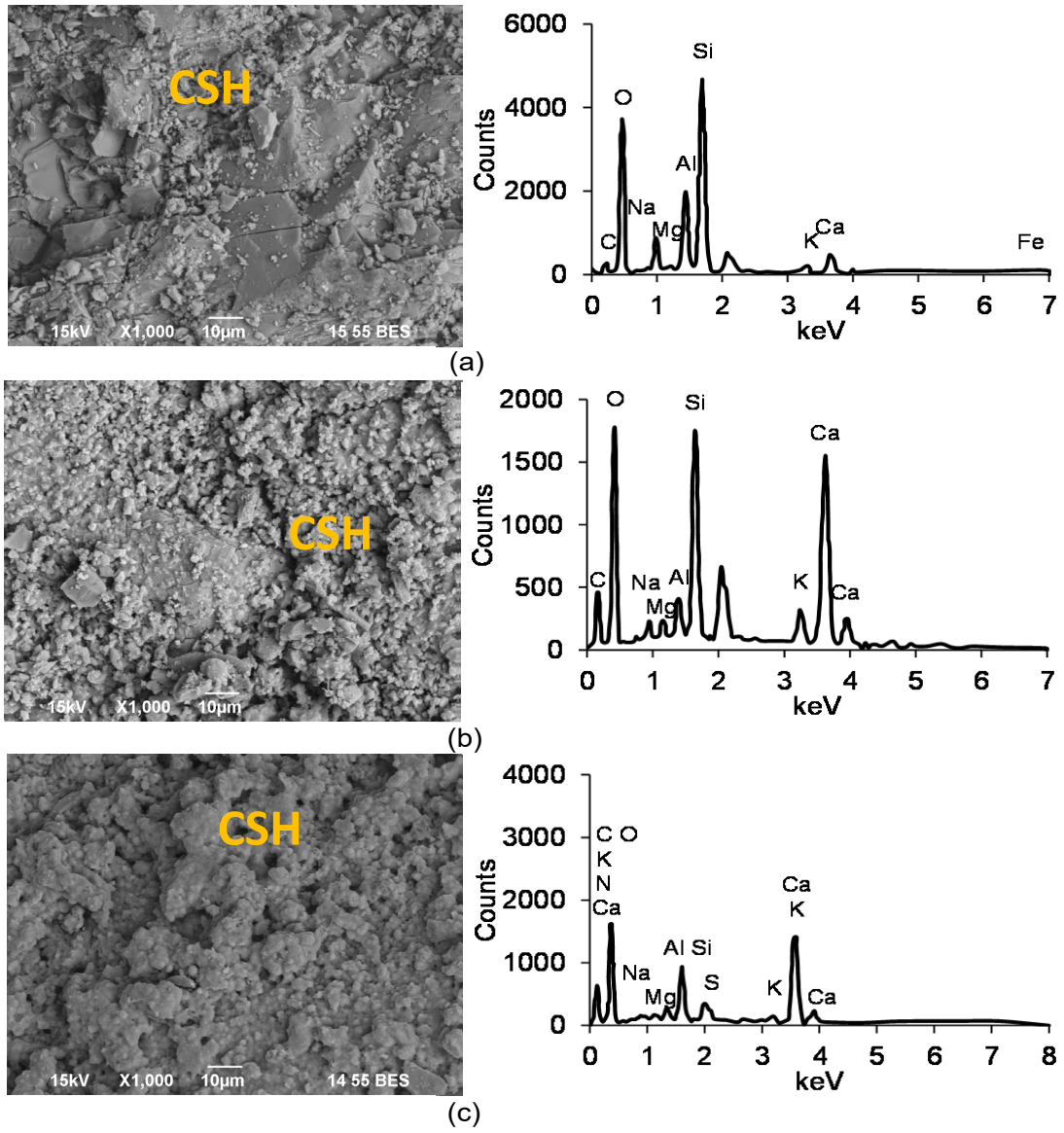

Figure 2.12: Comparison of EDX peaks for (a) control specimen (CW), (b) 1%-HA, and (c) 1%-CS at a 15 mm distance from the capsule

2.3.4 XRD Analysis

The variation in water supply for hydration may alter the crystalline phases and their quantity over time due to changes in the degree of hydration. XRD pattern was obtained to compare peak intensity to study cement hydration products and the formation of any new chemical phases when different types of swollen SAPs were embedded. The capsule region (referred to as the hydrogel-mortar interface) was extracted and powdered for evaluating XRD spectra 28 days after casting. Figure 2.13 was obtained when XRD analysis was performed on the powder extracted from the vicinity of the hydrogel capsule region 28 days after casting and compared with the water capsule region of the control sample. The peak of quartz is cut short to highlight other significant peaks. Quartz represents sand in the mortar that has no contribution to the hydration process. There is no new peak observed in the XRD pattern (Figure 2.13) due to the addition of SAP indicating

no formation of any new hydration product [116]. The hydration process initiates when the main component of cement clinkers, such as tricalcium silicate and dicalcium silicate, interact with water [117]. Figure 2.13 shows the drop in tricalcium silicate and dicalcium silicate peaks of samples with hydrogel capsules, indicating that a higher fraction of cementitious material has undergone the hydration process. The drop-in hydration reactant is more prominent in the case of hydrogel type D, E, and CS, while hydrogel type C presented minimum fall. The Hydrogel type C also showed a minimum wet area in the water spread test 28 days after casting (Figure 2.8), proving that the water spread test is an effective measure of internal curing. Furthermore, samples with hydrogel capsules showed a slight drop in the final hydration product calcium hydroxide peaks indicating its lower presence. While calcium hydroxide constitutes 20-25% of hydrated cement paste, its main responsibility is to maintain the high pH of the concrete [118]. On the other hand, calcium hydroxide can easily leach out into the water and react with sulfates [119] and carbon dioxide [120] deteriorating the cementitious matrix. With this, the slight decrease in the calcium hydroxide in the internally cured samples can be seen as an advantage and the reason for this should be investigated further, which falls outside the scope of the current study.

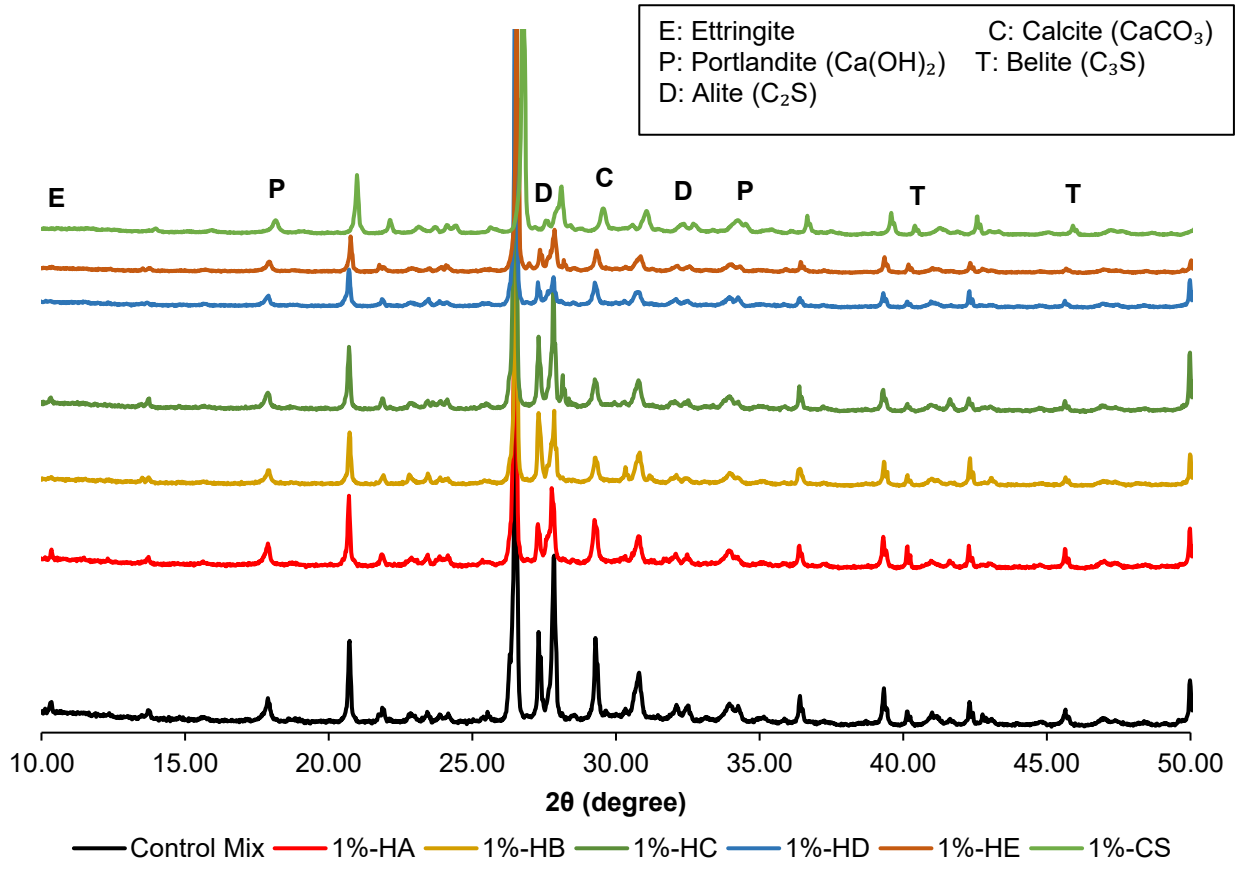

Figure 2.13: XRD analysis after 28 days of curing near capsule region.

2.4 Conclusions

This chapter investigated the internal curing potential of SAPs and corn-starch hydrogels, and the following are the important conclusions of this study:

1. All five SAPs absorbed more than 150 g/g of tap water. D and E showed the highest absorption (~250 g/g), followed by C (228 g/g), A, and B (~150 g/g). This high absorption in D and E is due to their larger particle sizes, which allow them to retain more water through stronger hydrogen bonds.
2. Water absorption of HA, HB, HC, HD, and HE dropped significantly in cement pore solution by 74%, 55%, 81%, 73%, and 68%, respectively. This reduction is caused by the screening effect, which shields the SAPs' functional groups, and the formation of ion complexes that hinder water absorption.
3. All encapsulated hydrogels, including cornstarch, created larger wet areas in the matrix. HA achieved the highest wetted area with 43% under gravity and 41% under capillary forces, while cornstarch reached 42% and 31%, respectively. Water capsules, however, showed no wetting. Gravitational forces, combined with capillary action, were key in transferring water from hydrogels to the matrix.
4. Hydrogels released water cyclically, more prominently in low-absorption hydrogels like A. Initially, high osmotic pressure from ion concentration differences drove water release. Later, as ion concentrations equalized, humidity gradients controlled the fluctuating water mobility.
5. Hydrogels (A and CS types) enhanced CSH gel distribution, as SEM/EDX revealed dense, uniform hydration near capsules. C and D hydrogels improved hydration up to 25 mm away. In contrast, control specimens with water capsules exhibited sparse, uneven CSH clusters near the capsule. Continuous water supply from hydrogels contributed to denser hydration.
6. Internal curing boosted the hydration degree without forming new products. XRD at 28 days showed lower peaks for unhydrated reactants (C3S, C2S) compared to the control, confirming improved hydration facilitated by hydrogels.

Chapter 3. Sustainable Bio-based Hydrogel as an Alternative Air Entrainment Agent in Cement-Based Materials

This chapter focuses on synthesizing a bio-based hydrogel from local, renewable raw materials to enhance the freeze-thaw resistance of hardened cementitious matrices. The study aims to improve the air void system and parameters of low W/C ratio mortar using cornstarch-based hydrogel with varying cornstarch content, compared to a commercially available air-entraining agent and SAPs. A bio-based hydrogel was produced through a thermal gelatinization process using cornstarch contents ranging from 1% to 3% of the mortar mixing water. The effectiveness of the cornstarch hydrogel was assessed by comparing its void structure with two commercial SAPs, used at 0.2% of cement weight, and an air-entraining agent, used at 0.49 percent of total mortar weight. The void structures were analyzed by evaluating porosity, void size distribution, spacing factor, and void shape using micro-CT scanning with a sensitivity of 10 μm.

3.1 Materials and Methods

3.1.1 Materials

In this study, Type-1 Portland Cement (TCC Materials®) is used as the binding material, meeting the requirements of ASTM C150 [99]. Fine aggregate was obtained from Quikrete® sand. To maintain workability between 85% to 90% flow table value, the proportion of the superplasticizer was adjusted. The superplasticizer used was MasterGlenium® 7500, a high-range water reducer manufactured by BASF Corporation, which satisfies the type A and type F admixture requirements (ASTM C 494/C 494M [100]). Additionally, for air entrainment, the liquid air entrainment admixture Akona®, meeting the ASTM C260 [121] requirements, was used as the reference commercial air entraining agent. This air entraining agent improved the air void system to enhance resistance against freezing-thawing cycles.

SAPs are commonly used for internal curing and to mitigate autogenous shrinkage [122]–[124]. These SAPs have the ability to absorb water many times their weight and release it into the cementitious matrix, providing an alternative curing mechanism [124], [125]. In this study, a bio-based hydrogel was synthesized using naturally abundant cornstarch, which was employed for air entrainment purposes. Additionally, two different types of commercially available SAPs with distinct particle sizes and chemical compositions were selected for comparison. These SAPs, referred to as type B and D, were procured from Emerging Technologies, and their properties are summarized in Table 2.1, along with their water absorption capacities. Both SAPs have different chemical composition and sizes. SAP-type B is a potassium salt of crosslinked polyacrylic acid with a comparatively smaller particle size and water absorption capacity. In contrast, SAP type D is a sodium salt of crosslinked polyacrylic acid with a larger water absorption capacity due to its larger particle size. SAP type D have larger water absorption due to higher size while SAP type B have higher water absorption in cement pore solution due to lower anionic ion concentration as explained in discussion in Section 2.3.1.

3.1.2 Synthesis of Cornstarch Hydrogel

Cornstarch is a semi-crystalline material with both crystalline and amorphous regions [126]. The crystalline portions contain amylopectin polymers, while the amorphous regions of the starch granules contain both amylose and amylopectin [126]. Specifically, corn starch is composed of 20-30% amylose and 70-80% amylopectin [127]. When combined with water and heated, the starch granules undergo swelling due to the absorption of water by the amorphous regions containing amylose and amylopectin. The degree of swelling increases with a higher volume fraction of amylopectin. As heating continues, the crystalline structures within the corn starch become unstable, leading to a rapid reduction in the size and number of crystalline regions. Ultimately, the amylose leaches out, causing the disintegration of the starch granules. This process results in the irreversible dissolution of corn starch in water [97]. The leached amylose acts as a hydrocolloid, capable of forming hydrogels when water is present. Hydrogels are networks of crosslinked hydrophilic polymers that can absorb significant amounts of water. When the cornstarch gel is cooled, it thickens and solidifies into a firm gel. The firmness of the resulting gel depends on the length of the amylose molecules and the volume fraction of amylopectin in the original corn starch.

In this research, cornstarch was mixed with water at different weight percentages (1%, 2%, and 3%) and heated at 180° F for 8 minutes to synthesize the cornstarch hydrogel. During the heating process, some water evaporates, but it is replenished to maintain the required water content in the mixture. The viscosity of the hydrogel was measured in centipoise (cP) using a rotational Brookfield viscometer® model DV-II+Pro with an LV-1 spindle operating at a speed of 100 rpm. The viscosity values for the cornstarch hydrogel are presented in Table 3.1, and it was observed that higher cornstarch content leads to increased viscosity of the hydrogel.

Table 3.1: Impact of cornstarch weight percentage on the viscosity of hydrogel

Cornstarch (% of water wt.)	1%	2%	3%
Viscosity (cP)	4.09	5.96	10.40

3.2 Mix Proportions

To investigate the mechanical behavior, pore structure, and chemical characterization, mortar cubes were prepared in accordance with ASTM C192/C192M-16a [102] standard. The proportions and types of admixtures added to the mixtures, while maintaining a ratio of 1:1.75:0.3 for cement, sand, and water respectively, are provided in Table 3.2. In order to evaluate the impact of the cornstarch-based hydrogel on mortar properties, particularly the entrained air content, different percentages of cornstarch (1%, 2%, and 3% of total water) were added. The cornstarch-based hydrogel, in the form of a viscous fluid (preparation outlined in section 3.1.2), was incorporated into the dry cement-sand mix during casting, replacing the water. In previous literature [90], [128], the optimal amount of commercially available SAP was reported as 0.2% of the cement weight. Therefore, the same quantity was used in this research. However, since

absorbent polymers reduce the fluidity of the mixture, a superplasticizer was added to achieve the desired workability, targeting a flow table value of 85% to 90%. To compare the performance of specimens containing the cornstarch-based hydrogel and commercially available SAPs, a control mix (CM) was prepared and mixed with a commercially available air-entraining agent. The supplier recommended adding 0.49% of the total mortar weight of the air-entrained agent to achieve 8% (±2%) air entrainment and this recommendation was implemented in this study.

Table 3.2: Mix Proportions for cement mortar

Sample	Superplasticizer (% of cement wt.)	Cornstarch (% of water wt.)	Commercial SAP (% of cement wt.)	Air entraining agent (% of mortar wt.)
CM	0.60	0	0	0
1%CS	0.95	1	0	0
2%CS	1.30	2	0	0
3%CS	2.20	3	0	0
0.4%AE	0.60	0	0	0.49
0.2%SB	1.85	0	SAP B (0.2)	0
0.2%SD	1.37	0	SAP D (0.2)	0

3.3 Testing Program

3.3.1 Workability

When working with concrete with a low water-to-cement ratio (W/C) of 0.3, ensuring proper workability is crucial for proper compaction [129]. The hydrogel in the cementitious matrix absorbs additional water and reduces the effective W/C ratio and hence may negatively impact workability. To overcome this challenge, an appropriate amount of superplasticizer is added to address the workability issues. To measure workability, the flow table test, following ASTM C1437 [130], was employed. The amount of superplasticizer was adjusted in each mixture to achieve a similar flow table value, aiming for approximately 85% to 90% consistency. Multiple trials, typically around three, were conducted for each mixture type with varying amounts of superplasticizer to attain the desired workability. Immediately after mixing, the freshly prepared mortar underwent the flow table test. The test involved dropping the table 20 times, and the average of the four mortar diameters was calculated. The Eq. 3.1 was then used to determine the percentage flow table value of the mixture.

$$Workability\ (\%) = \frac{average\ mortar\ diameter - mold\ base\ diameter}{mold\ base\ diameter} \times 100 \quad Eq.\ 3.1$$

3.3.2 Compressive strength

To evaluate the compressive strength, 50 mm mortar cubes were prepared in accordance with ASTM C109 [131] specifications. The compressive strength tests were conducted at various time intervals: 3, 7, 14, 28, and 56 days, while externally cured until tested. The compressive strength measurements were performed for the control mix (CM) as well as the mixes containing a commercial air-entraining agent (0.4%AE) and SAPs at concentrations of 0.2% SB and 0.2% SD. The results were obtained by averaging three test samples for each mix.

3.3.3 Void analysis

The primary objective of using an air-entraining agent is to enhance the pore structure of the concrete matrix [132]. One of the peculiar characteristics of water is its anomalous expansion, where it expands rather than contracts as the temperature drops from 4°C to 0°C, resulting in decreased density. This density reduction continues as water freezes, as the molecules arrange themselves into open crystal structures in solid form. The existence of a fine void network within the microstructure of concrete allows for the accommodation of hydrostatic stresses that can arise from this expansion phenomenon. Conversely, the presence of larger voids that are widely spaced apart can compromise the overall quality and strength of the cementitious base material [133].
Micro-CT scanning is employed to conduct void analysis in the hardened cementitious matrix. Micro-CT scanning provides a three-dimensional view, allowing for the examination of the final void structure after approximately 28 days of external curing. This time frame corresponds to the near completion of cement hydration and the attainment of intended strength. By utilizing micro-CT scanning at this stage, it is possible to accurately evaluate the void structure in the cementitious matrix, especially when SAPs are used for air entrainment. This technique provides valuable insights into the overall void distribution and characteristics in the concrete, aiding in the assessment of the impact of SAPs on the hardened material.

The variation in voxel size, sensitivity, and resolution of the 3D micro-CT scanner depends on the size of the sample being analyzed [134]. Generally, as the sample size decreases, the resolution and ability to identify smaller void features (sensitivity) improve. In this study, two different sample sizes were used to examine both general porosity and detailed characteristics of air-entrained voids (presented in Figure 3.1). For void structure analysis, the GE Phoenix v|tome|x s X-ray computed tomography system (micro-CT) with a 180 kV nano focus X-ray tube was employed. Initially, a 3D micro-CT scan was performed on the entire 50 mm length cube, using a voltage of 160 kV and a current of 315 µA. This scan resulted in a magnification of only 2.65x, a voxel size of 75.4 µm, and a sensitivity capable of detecting voids around 180 µm in diameter. Since including the surface of the mortar sample in the volumetric results might not provide an accurate void structure owing to surface defects, the scanned data was further digitally cropped using myVGL software. The cube was digitally reduced to a length of 40 mm cube for precise analysis and examination using the viewer application for projects created in VGStudio Max.
According to ASTM C125 [135], air-entrained voids are defined within a size range of 10 µm to 1000 µm. To ensure that all air-entrained voids are included in the analysis, it is necessary to reduce the sample size. In order to achieve a sensitivity of 10 µm, a sample with a maximum dimension of 10 mm is required. To obtain the desired sample size, a smaller cube was extracted from the core of a 50 mm length cube. The extracted cube had a maximum dimension (diagonal length) roughly equivalent to 10 mm, resulting in a side length of 7.07 mm as shown in Figure 3.1. A diamond cutter was employed to carefully perform the extraction. For the subsequent 3D micro-CT scanning on the reduced sized cube, a voltage of 100 kV and a current of 550 µA were utilized. This scanning configuration provided a magnification of 22x, a voxel size of 9.1 µm, and a sensitivity of 10 µm. It's important to note that the cutting action of the diamond blade may split

some voids, which the micro-CT scanner may interpret as surface defects. Consequently, a digitally cropped cube with a length of 4.5 mm was considered for the analysis of major voids to eliminate the surface roughness and striations left behind by the diamond saw. For void analysis, the specimens were cured in a water tank for 28 days, and two specimens were selected from each mixture for testing and examination. This ensured a representative assessment of the void characteristics in the cementitious matrix for each mix.

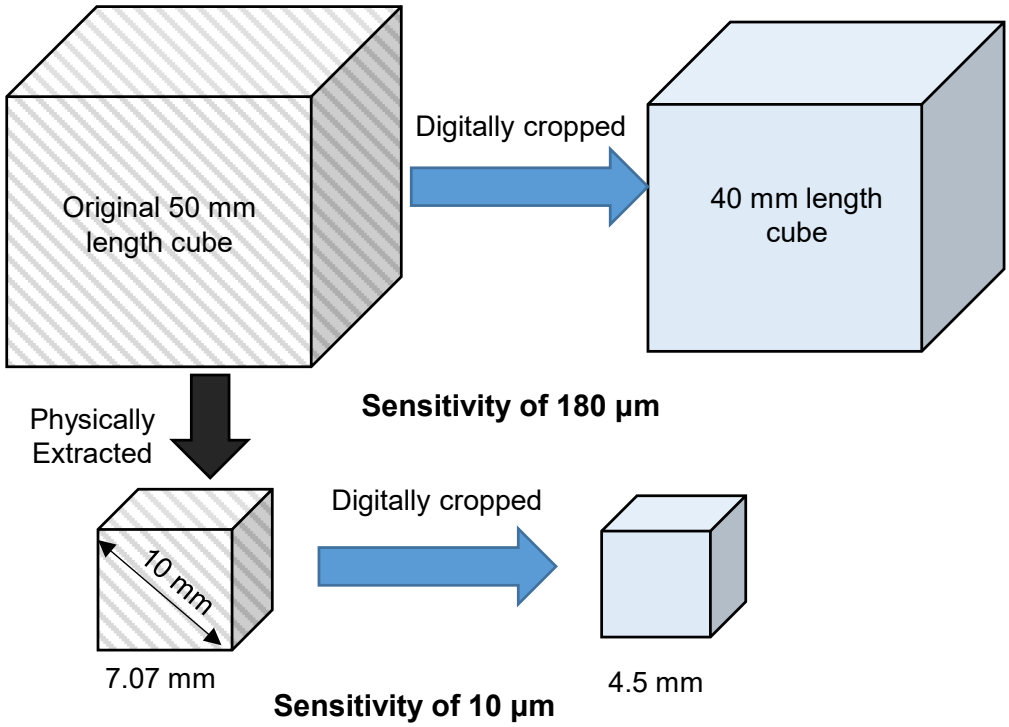

Figure 3.1: Digital cropping strategy to eliminate surface abnormalities and physical extraction method to achieve a sensitivity of 10 µm to quantify small air-entrained voids as per ASTM C125.

3.3.4 X-ray Diffraction (XRD) analysis

XRD analysis is a technique used to investigate the crystal structure of cementitious materials. In the context of this study, XRD analysis was conducted to examine the effects of SAPs, cornstarch hydrogel, and a commercial air-entrainment agent on the formation of deleterious crystalline phases in the cementitious matrix, if any. To perform the analysis, a sample was extracted from the core of the mortar cube, which had been externally cured for 28 days. Prior to XRD analysis, the extracted sample was finely ground until it passed through a 200-micron size mesh, ensuring a homogenous and representative sample. The XRD measurements were then performed using two theta (2θ) scanning angles ranging from 5° to 80°, with a scanning speed of 4° per minute.

3.4 Results and Discussion

3.4.1 Achieving consistent workability across mixes

When employing a low W/C ratio, concerns may arise regarding workability, especially when incorporating air entrainment agents and hydrogels. These additives have a significant impact on the rheological properties of the mixture [136]. Surfactant-based air entrainment agents play a crucial role in reducing surface tension, leading to the formation of small air bubbles. These bubbles assist in the movement of coarser particles within the mixture, ultimately improving workability [137]. On the other hand, the presence of hydrogels results in additional water absorption, which reduces the flowability of the mixture [40]. This decrease in flowability can pose challenges when trying to achieve the desired flow table value of 85% to 90%. To overcome these challenges and ensure suitable workability, superplasticizers are added instead of altering the W/C ratio. These additives modify the viscosity of the mortar, effectively enhancing its flow characteristics [138].

Table 3.3 presents the variations in superplasticizer demand for different mixtures, including those containing cornstarch hydrogel, commercial SAPs, and air entrainment. The inclusion of a minimal amount of air entrainment agent (0.49% of total weight) slightly improved workability while maintaining the same quantity of superplasticizer (0.6% of cement content). Workability remained within the targeted flow table value range of 85% to 90%. However, the addition of cornstarch-based hydrogel had a significant impact on superplasticizer demand, showing a nearly linear relationship. As the cornstarch content increased (1%, 2%, and 3%), the required amount of superplasticizer increased by approximately 1.58, 2.3, and 3.7 times, respectively, to achieve adequate workability for proper compaction. Similarly, the incorporation of commercial SAPs (0.2%HB and 0.2%HD) substantially reduced flowability, necessitating approximately 3 and 2.3 times more superplasticizers, respectively, compared to the control mixture, to attain the required workability. The hydrogel's water absorption capacity resulted in a reduction of the effective W/C ratio, leading to a higher demand for superplasticizers to achieve the desired mixture mobility.

Table 3.3: Superplasticizer content to achieve 85% to 90% flow table value.

Mixture	Superplasticizer (% of cement content)
CM	0.6
1%CS	0.95
2%CS	1.4
3%CS	2.2
0.4%AE	0.6
0.2%SB	1.85
0.2%SD	1.37

3.4.2 Void Analysis

3.4.2.1 Porosity

Figure 3.2 compares the porosity of digitally cropped samples of different sizes: 40 mm and 4.5 mm cube lengths. The analysis also includes the porosity of the sample with a 7.06 mm cube side from which the 4.5 mm cube is digitally extracted to demonstrate the influence of boundary conditions. The results reveal that the 4.5 mm length cropped specimens exhibited significantly higher porosity compared to the 40 mm length cube. This emphasizes the importance of micro-CT scanner resolution. For the larger cube size (40 mm length), the scanner had a sensitivity of approximately 180 μm, which resulted in the exclusion of void volumes smaller than that, leading to an overall decrease in measured porosity. Conversely, the micro-CT scanner demonstrated high sensitivity (10 μm) when the smaller cube size (4.5 mm length) was used. This increased sensitivity allowed for the detection of smaller void volumes, resulting in an overall increase in porosity. The results obtained from the 4.5 mm length digitally cropped cube met the air-entrained void diameter criteria outlined in ASTM C457 [139], which specifies a minimum void diameter of 10 μm. However, an exception was observed in the case of commercial SAPs (0.2%SB and 0.2%SD). This discrepancy may be attributed to large particle sizes in the case of both the SAPs and their non-uniform spatial distribution. This alone will be a hurdle for the use of commercial SAPs as air-entraining agents. The superior results in the case of cornstarch hydrogels are due to their smaller particle size and uniform spatial distribution, unlike the commercial SAPs. Another noteworthy observation is that, despite having the same resolution, the digitally cropped specimen with a length of 4.5 mm displayed higher porosity compared to the original extracted cube size of 7.07 mm. This discrepancy arose due to the action of the cutter blade during the extraction process, causing voids to split and be detected as surfaces by the micro-CT scanner. Consequently, the extracted cube exhibited a relatively lower void volume, resulting in lower porosity and accuracy when compared to the digitally cropped 4.5 mm length cube. To ensure more accurate and reliable results while still satisfying the air entrainment void size criteria outlined in ASTM C457 [139], the 4.5 mm length cropped cube was selected for further analysis and discussion. This choice avoids potential inaccuracies introduced by the cutter blade and ensures consistency in meeting the specified void size criteria. Two cubes were selected from each mix and the average porosity is reported.

The analysis of a digitally cropped cube with a length of 4.5 mm reveals interesting findings regarding the impact of cornstarch-based hydrogel and commercial air-entrained agents on porosity. Comparing samples with varying percentages of cornstarch-based hydrogel, it is observed that the addition of 1% and 2% hydrogel increases porosity by 15% and 38%, respectively, compared to the sample without an air-entraining agent. However, further increasing the cornstarch content to 3% only results in a 24% increase, indicating that there is no significant advantage in terms of air entrainment beyond 2%. This increase in porosity can be attributed to the desorption of the initially swollen hydrogel, which leaves behind voids that contribute to the higher porosity [140]. Interestingly, while increasing cornstarch content enhances internal curing by increasing water release as noted in previous studies [141], a higher fraction of cornstarch can

lead to the formation of additional hydration products that fill some of the voids left by the desorbed hydrogel. Consequently, the porosity is reduced, as seen in the case of the 3% cornstarch sample. In contrast, the addition of commercial air-entrained agents (0.4% AE) results in 22% less porosity compared to the control mix, despite using a consistent compaction time. Notably, the use of a finer particle-sized SAP type B (0.2% SB) leads to a moderate 22% increase in porosity, whereas the larger particle-sized SAP type D (0.2% SD) results in a lower 15% porosity compared to the sample without an air entraining agent. It is worth mentioning that the porosity of the SAP type D sample with a 40 mm length cube exhibits the maximum porosity, confirming that larger SAP particles can create larger voids [142]. These varying porosity values for different-sized cubes when commercial SAPs are used highlight the non-uniform spatial distribution of these particles throughout the sample.

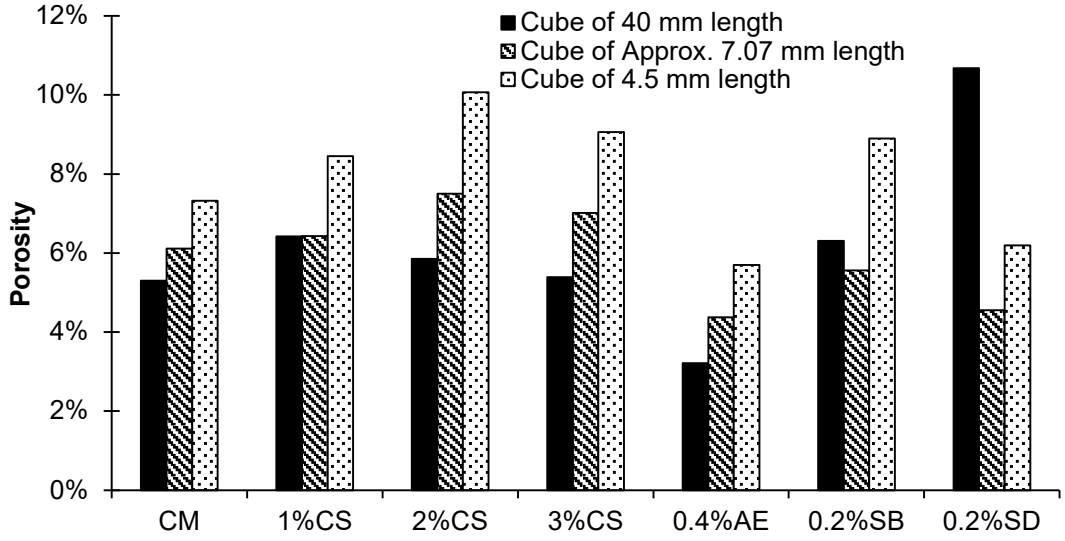

Figure 3.2: Porosity measured using different sized cubes to study the effect of micro-CT resolution and surface abrasion defects.

3.4.2.2 Void size distribution

The size and distribution of voids are crucial factors that influence the properties of cementitious matrices. Generally, voids ranging from 10 μm to 1000 μm are categorized as air-entrained voids [135]. However, to optimize both freeze-thaw performance and mechanical properties, it is desirable to have a higher number of smaller air-entrained voids. European standard EN 206-1 [143] and some previous studies [144]–[146] have highlighted the significance of voids with diameters equal to or smaller than 300 μm in enhancing the durability and resistance of concrete to freeze-thaw cycles. Consequently, these voids, are referred to as A_{300} in this study and the corresponding void fraction will be considered as micro air content.

Figure 3.3 illustrates the distribution of air-entrained void sizes, specifically categorizing them into micro-air content (A_{300}) and larger voids with diameters between 300 μm and 1000 μm. For the control sample, the micro-air content is approximately twice as high as the larger voids volume. However, the ratio of micro-air content to larger voids varies with the addition of cornstarch hydrogels and the air entrainment agent. The use of a 3% cornstarch-based hydrogel

and the commercial air-entrained agent significantly improved the micro-air-entrained voids, increasing them threefold compared to the larger voids. Notably, the 3% cornstarch-based hydrogel exhibited a 10% higher micro-air-entrained void content than the sample with the commercial air-entrained agent. On the other hand, the 1% and 2% cornstarch-based hydrogel samples displayed an increase of only 17% and 10% in micro-air entrained voids compared to the larger air-entrained voids. Furthermore, the commercial SAPs (0.2%SB and 0.2%SD) had almost equal proportions of micro-air content and large voids volume, likely due to their larger particle size compared to cornstarch. The analysis of air-entrained voids reveals that the 3% cornstarch-based hydrogel shows promise as a viable alternative to commercial air entrainment agents.

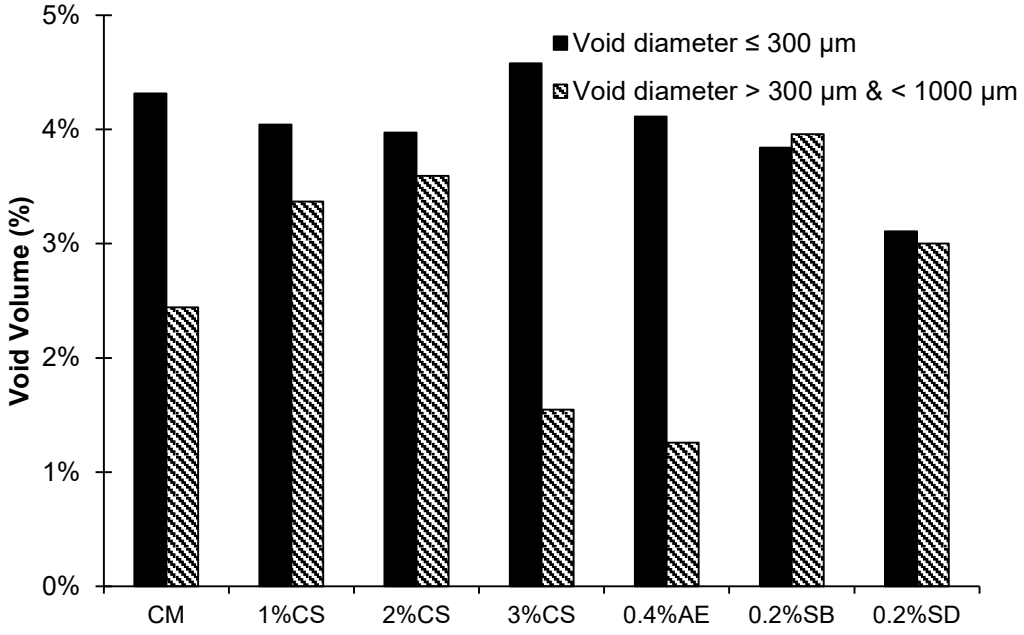

Figure 3.3: Effect of addition of CS hydrogels and commercial air entrainment agent on the volume of micro air entrained voids and larger entrained voids at a resolution of 10 µm.

Figure 3.4 presents the micro-CT scan images of the digitally cropped cube samples with a length of 4.5 mm, providing a visual representation of the voids and their distribution. These images offer valuable insights into the impact of different air entrainment agents on void characteristics. Notably, Figure 3.4 (c) and (d) demonstrate the distinctiveness of the 3% cornstarch-based hydrogel (3%CS) and the commercial air-entrained agent (0.4%AE) for obtaining desirable air content. 3%CS and 0.4%AE present a smaller number of larger distinguished entrapped voids. In contrast, the control specimen, the sample with 2% cornstarch-based hydrogel, and the samples with commercial hydrogels (0.2%SB and 0.2%SD), as depicted in Figure 3.4 (a), (b), (e), and (f), show a higher number of visible larger entrapped voids. Furthermore, the larger voids in these samples are relatively non-uniformly distributed indicating a less favorable void structure compared to the 3%CS and 0.4%AE samples.

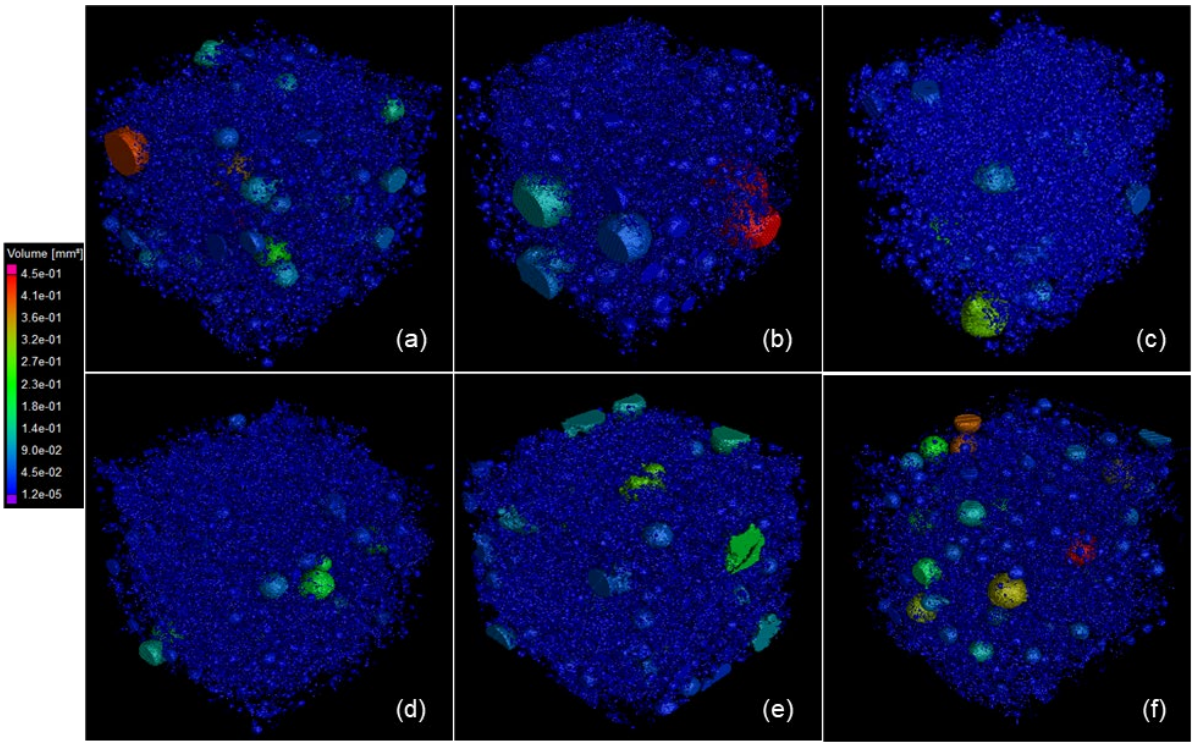

Figure 3.4: Sample micro-CT scanned images showing the entrapped voids distribution at a 10 micron resolution obtained from 4.5 mm digitally cropped cubes (a) CM (b) 2%CS (c) 3%CS (d) 0.4%AE (e) 0.2%SB (f) 0.2% SD.

Figure 3.5 provides an insightful representation of the distribution of void sizes, shedding light on whether the voids tend to be more prevalent in smaller or larger sizes. For the samples containing cornstarch-based hydrogel, the curve rises and levels off at smaller sizes for the 1% and 3% cornstarch content, indicating a relatively higher proportion of smaller voids compared to the control mix. Notably, the best results in terms of void size distribution were achieved with the commercial air-entrained agent (0.4% AE), which had a majority of voids in smaller sizes compared to other specimens. This can be attributed to the stable film created by commercial air-entraining agents around air bubbles, reducing surface tension and preventing their transformation into larger bubbles especially when there is no excessive compaction as done in this case [56]. However, it is worth noting that the 3% cornstarch-based hydrogel yielded comparable results to the commercial air-entrained agent, supporting the previous findings from Figure 3.3 and Figure 3.4. The higher content of cornstarch in 3% cornstarch hydrogel not only promotes hydration and partial filling of voids but also results in an increased number of smaller voids. In contrast, the curves for the commercial SAPs start at relatively larger void diameters, indicating a higher proportion of larger voids due to their larger particle size and greater water absorption capacity when compared to the cornstarch hydrogels. It is important to note that the commercial air entraining agent is sensitive to compaction, unlike the hydrogel infused specimens and is not guaranteed to yield good results when there is vibration and excessive compaction [60].

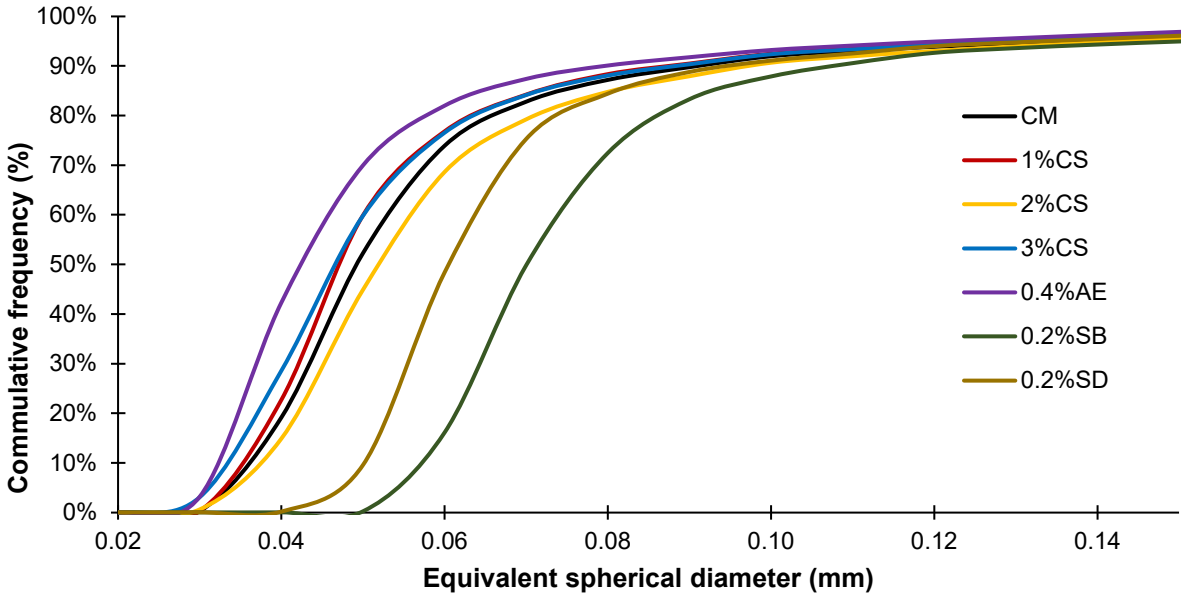

Figure 3.5: Effect of CS hydrogels and air-entrained agent on void size distribution (scans obtained at a resolution of 10 μm).

3.4.2.3 Sphericity of air-entraining voids

Sphericity plays a crucial role in discerning different types of voids, such as random irregular entrapped air voids, cracks, and air-entrained voids. Air-entrained bubbles tend to have a shape close to a sphere [107, 108]. Sphericity is calculated by comparing the surface area of the actual void to the surface area of a perfect sphere with the same volume. A sphericity value close to 1 suggests that the void has a shape resembling a sphere, indicating a higher likelihood of being an air-entrained void [109, 110]. Figure 3.6 showcases the average sphericity evaluated at a resolution of 10 μm, for two samples of each mixture type. The average sphericity values for all the mixtures range from 0.56 to 0.58. It is observed that the addition of cornstarch hydrogel, commercial SAP, and air-entrained agent has a minimal effect on sphericity, although influencing void sizes and distribution. The voids in the 2%CS mix are slightly more spherical, while a slight decrease in sphericity was observed in the 0.2%AE specimen.

Figure 3.7 provides the percentage distribution of voids for sphericity values ranging from 0.4 to 0.8 that were observed in this study. The distributions for both samples per mix are plotted in Figure 3.7 and these results overlapped as there is no discernable difference. Furthermore, there is no significant difference between the various air entraining agents. However, all samples had an approximate 24% of voids with a sphericity value close to 0.6. At the same time, it is worth noting that the 2% cornstarch-based hydrogel mixture displays a slightly increased void proportion at higher sphericity values, indicating a positive influence of cornstarch on void shape. However, the difference is marginal and may not have any practical implications.

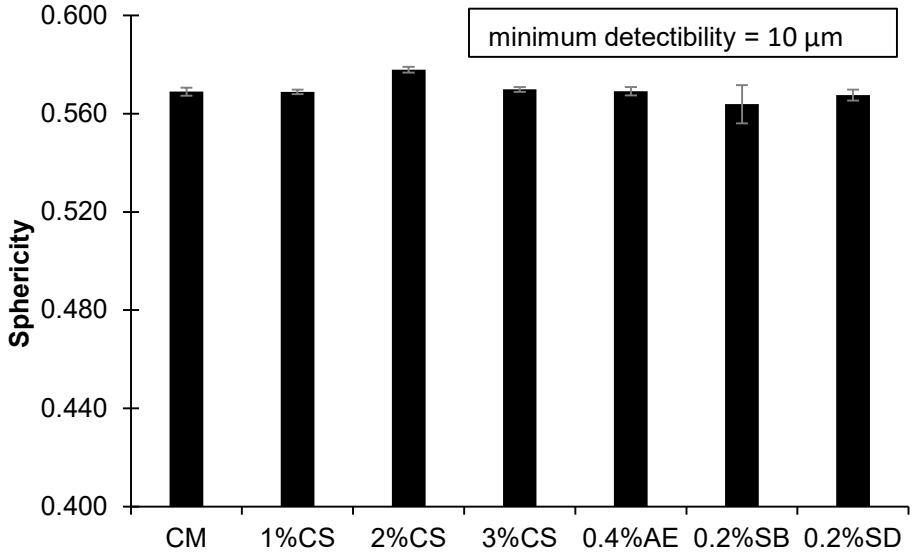

Figure 3.6: Effect of hydrogel and air entrained agent on average sphericity of voids (obtained at a resolution of 10 µm)

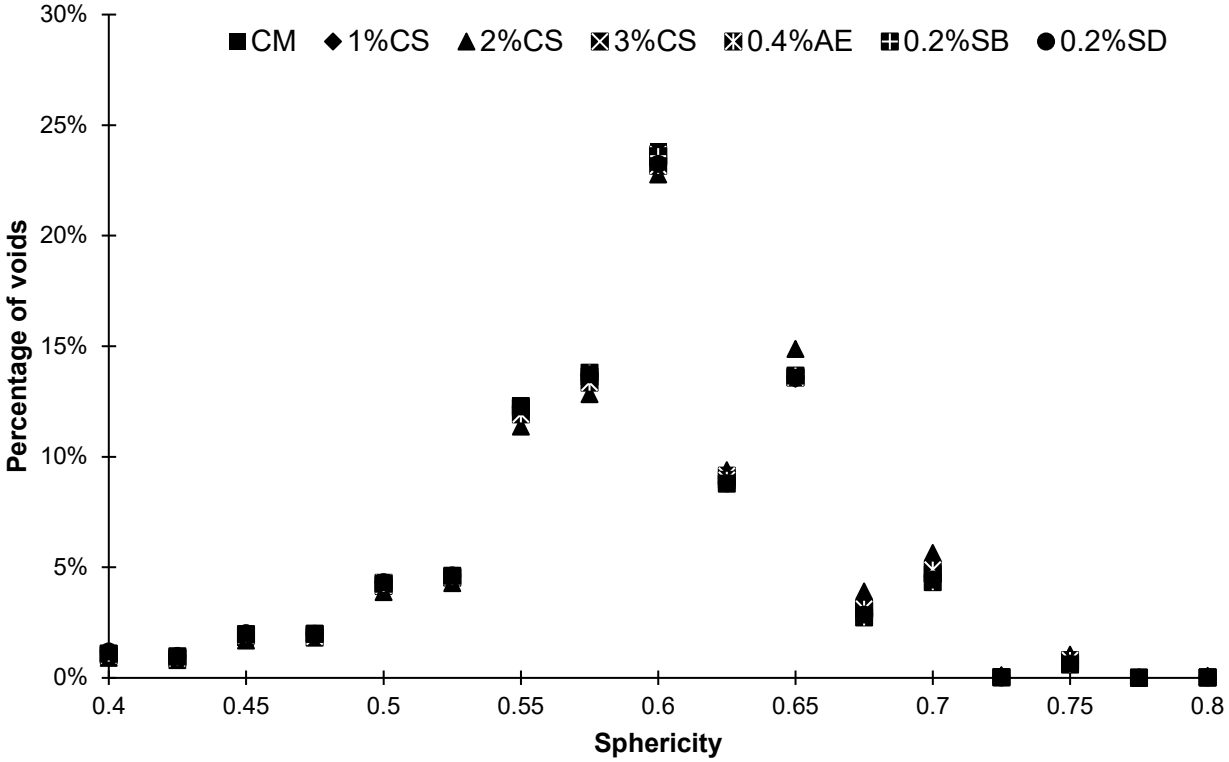

Figure 3.7: The impact of hydrogels and commercial air-entraining agent on the distribution of sphericity, ranging from 0.4 to 0.8.

3.4.2.4 Spacing factor

The spacing factor characterizes the spatial distribution of voids within a cementitious matrix. It provides a quantitative measure of the average distance between air bubbles in the material. A lower spacing factor is desirable for optimal freeze-thaw resistance, as it indicates a shorter distance for water to travel to reach voids during freezing temperatures, thereby

accommodating anomalous water expansion more effectively [73]. ASTM C457 [139] sets a requirement of a spacing factor of less than 0.2 mm for sufficient freeze-thaw resistance.
ASTM C457 [139] provides two equations for calculating the spacing factor based on the ratio of hardened cement paste volume (p) to air void volume (A). If the volume of cement paste remains constant, a reduced p/A ratio results in a greater volume of air voids within the fixed volume of cement paste. This outcome is achievable when smaller voids are densely packed, leading to a larger overall surface area. According to followed standard [139] and literature [151] this situation occurs when $p/A < 4.342$ and calculation of spacing factor is based on surface area. On the other hand, if p/A is greater than 4.342, a few larger voids can significantly influence the surface area, leading to inaccurate spacing factor results. To address this issue, all air voids are treated equally as nodes of the same size within a 3D lattice [152]. In the current study, the ratio of paste volume to air void volume for all samples exceeded 4.342, indicating that the equation 3 can be used for the calculation of the spacing factor.

$$SF = \frac{3}{a}\left[1.4\,(1 + \frac{p}{A})^{\frac{1}{3}} - 1\right] \qquad \text{Eq. 1}$$

Where, SF, a, p/A are space factor in mm, specific surface in $mm^{-1,}$ and paste-air ratio, respectively. Micro-CT scanner outputs, total pore volume (V_p) and total surface area (S) of voids. Subsequently, the specific surface (a) can be calculated as

$$a = \frac{S}{V_p} \qquad \text{Eq. 2}$$

Figure 3.8 presents the average variations in the spacing factor for all the considered mixes. The calculations follow the guidelines of ASTM C457 [139] with a 10 μm sensitivity. The graph includes the mean values of two samples covering around 200,000 number of voids for each mixture, accompanied by error bars. It is important to note that concrete with a larger but smaller number of voids within a given volume, results in a reduced total void surface area and, consequently, larger spacing between the remaining voids. This observation is consistent with the results obtained in the current study, where the spacing factor correlates with the volume of larger voids. As voids increase in size, the spacing factor also increases due to a lower number of voids per unit volume, resulting in greater distances between them. However, despite these variations, all mixtures had a spacing factor within the acceptable limit of 0.2 mm, as recommended by the ASTM C457 [139] standard.

Notably, the commercial air entrainment agent exhibits the lowest spacing factor, which is 17% lower than the control sample with no air entraining agent. Among the mixtures incorporating cornstarch hydrogel, the 3%CS sample has the smallest spacing factor, attributed to a higher proportion of smaller-sized voids (as discussed in section 3.4.2.2). It is worth mentioning that there is a noticeable variation between the two samples of commercial SAP type B, possibly due to the non-uniform distribution of larger voids, as shown in Figure 3.4 (e), resulting in a larger error bar. Previous studies [153], [154] have also highlighted the issue of uneven distribution of SAP within the concrete matrix. However, it is important to note that the differences in the spacing factor

among the different mixture types are not significant enough to adversely impact the performance of the cementitious matrix.

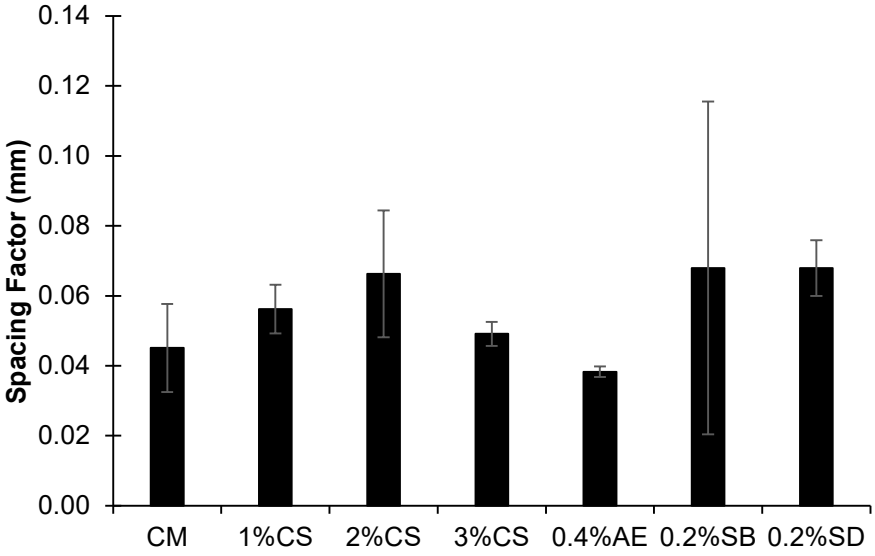

Figure 3.8: Effect of hydrogels and air-entrained agent on average spacing factor calculated as per ASTM C457 evaluated with a resolution of 10 μm.

3.4.3 Compression Strength

The use of air-entrained agents and hydrogels will increase the air content within the microstructure of the matrix, potentially impacting its compressive strength over time. Figure 3.9 presents the compressive strength for all mixtures after 3, 7, 14, 28, and 56 days of external water curing. The reported values represent the average strengths of three samples, accompanied by error bars to indicate variations among sample strengths within the same batch, particularly for mortar specimens containing the hydrogel. The variations in compressive strength observed in the cornstarch and commercial hydrogel samples are comparable to those of the reference mortar specimens. This consistency in variation can be attributed to the uniform workability achieved, which facilitated proper compaction [155]. Additionally, the commercial SAPs were dry mixed, and the entire mixing water was dedicated to preparing the cornstarch-based hydrogels, ensuring a homogeneous distribution within the matrix. For this reason, the variations in compressive strength for hydrogel-based samples remained within acceptable limits and were comparable with control and air-entrained specimens.

The inclusion of any admixture, whether it be cornstarch hydrogel, commercial SAPs, or a commercial air-entrainment agent, leads to a decrease in compressive strength. This decline is particularly noticeable in the initial stages of curing (3 and 7 days) for mixtures incorporating water-absorbent polymers. In the case of cornstarch-based hydrogel samples, an increase in the cornstarch content corresponds to a more pronounced initial drop in strength due to the creation of additional pores by the increased number of starch particles. Furthermore, the higher cornstarch content enhances the hydrophilic group chains within the absorbent polymer, resulting in an increased initial water retention capacity and increasing pore sizes [156].

Both cornstarch and commercial hydrogels release stored water at later stages of hydration. This release of water creates empty spaces, increasing porosity and reducing compressive strength [157]. Nevertheless, in the later stages of curing (28 and 56 days), the hydrogel samples begin to regain some of their strength, and the strength difference compared to the control specimen becomes less significant. This can be attributed to the internal curing process that promotes cement hydration [158] which leads to the increase in hydration products, which partially fill the voids left behind by the desorption of the hydrogel [159]. As a result, specimens containing a higher cornstarch content-based hydrogel exhibit improved performance in the later stages of curing.

The void structure analysis of cornstarch-based hydrogels confirms that the sample containing 3% cornstarch exhibits finely distributed voids, as discussed in section 3.4.2. After a curing period of 28 days, all cornstarch-based hydrogel specimens exhibit approximately similar strength (Figure 3.9). However, after 56 days, specimens with higher cornstarch content (2%CS and 3%CS) showed a slight increase in strength compared to the control mix (CM). On average, at the end of the 56-day curing period, the addition of 1%, 2%, and 3% cornstarch-based hydrogel to the control mix results in a reduction of compression strength by 25%, 15%, and 18%, respectively. For the commercial superabsorbent polymer (SAP) samples, the strengths at 28 days and 56 days are nearly identical, with an average decrease of approximately 11% and 15%, respectively. In contrast, the addition of a commercial air-entrained agent to the simple mortar mixture (CM) significantly reduces the 56-day strength by 22%. Despite the lower air content in the air-entrained agent sample (Figure 3.2), it was unable to regain strength, as it does not positively influence cement hydration [7]. On the other hand, the hydrogel's internal curing process leads to the generation of additional hydration products that partially fill the initially formed pores through hydrogel desorption. This mechanism plays a crucial role in restoring the compression strength of the material.

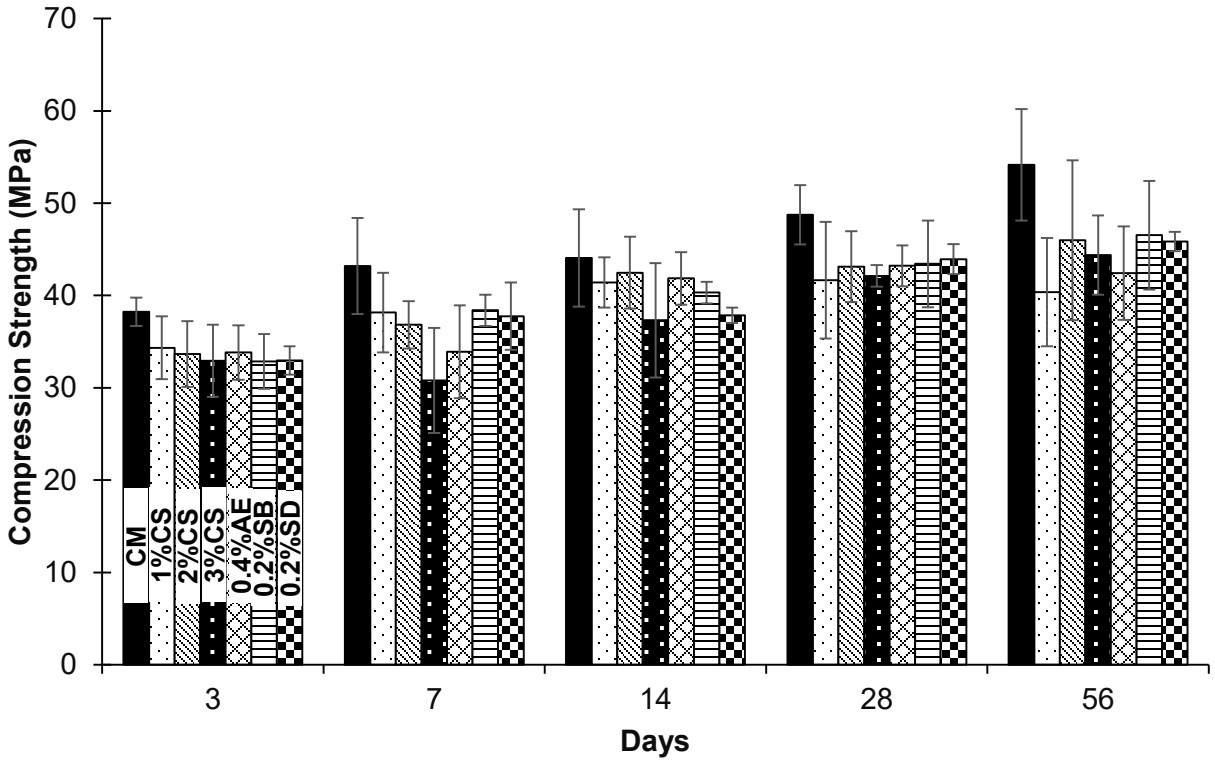

Figure 3.9: Influence of hydrogel and air-entrained agent on compression strength

3.4.4 XRD Analysis

The primary objective of this study is to improve the void structure in a cementitious matrix with a low water-to-cement ratio by introducing bio-based hydrogels. It is important to investigate the chemical changes induced by these air-entraining agents and hence X-ray diffraction (XRD) analysis was conducted. Figure 3.10 presents the XRD results obtained from a sample taken from the center of a mortar cube that underwent external curing in a water tank for 28 days.

The analysis revealed no significant chemical variations, except for an increase in the dicalcium silicate (C_2S) component caused by the commercial air-entrained agent. Previous studies [69] had already identified this phenomenon, where an excessive amount of air entrainment agent could slow down the hydration process of cement due to steric hindrance. This hindrance is a non-bonding interaction between the polar part of the air-entrained agent and the aqueous phase of the matrix, leading to the adsorption of cement particles and reduced hydration. However, in current research work the air entrainment agent is added in adequate amounts but its combined action with superplasticizer promotes considerable adsorption of cement particles that was amplified by a low W/C of 0.3 [70]. On the other hand, the introduction of a cornstarch-based hydrogel reduced the unhydrated components, aka, tricalcium silicate (C_3S) and dicalcium silicate (C_2S) in the cementitious matrix. This promoted the hydration process, converting more cement clinker into hydration products (CSH gel). These hydration products partially filled the voids left behind by the hydrogel droplets, resulting in an improved void structure and the recovery of some compressive strength, as discussed in sections 3.4.2 and 3.4.3. Regarding the commercial superabsorbent polymers (SAPs), they had an insignificant impact on the C_2S peak, although there

was a slight shift in the peak positions. This observation could be attributed to lattice contraction and a decrease in the size of the hydration crystals, which warrants further investigation [126–128].

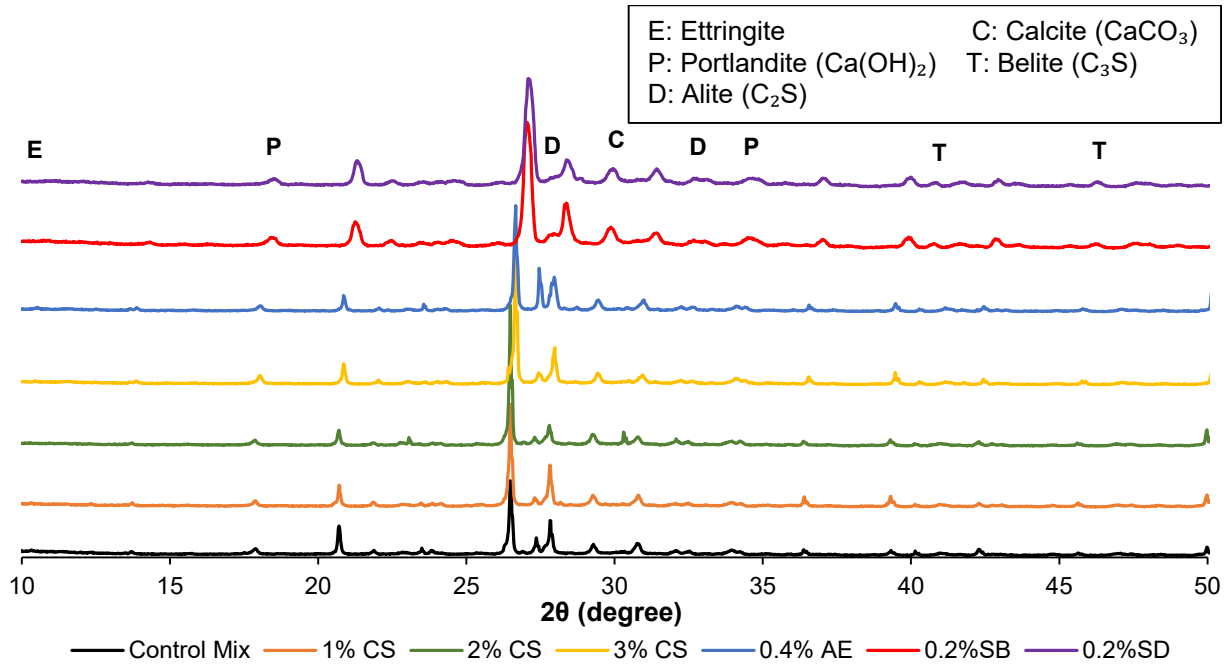

Figure 3.10: XRD analysis to quantify the effects of CS commercial hydrogels and the air entraining agent on the chemical composition

3.5 Conclusions

The chapter investigated cornstarch-based hydrogel as an alternative to commercial air-entraining agents, focusing on its effects on the void structure of cementitious matrices. Key findings include:

1. Adding 1%, 2%, and 3% cornstarch hydrogel increased porosity by 15%, 38%, and 24%, respectively, due to water desorption from hydrogel droplets during hydration. The reduced porosity at 3% is attributed to additional hydration products partially filling voids.
2. The 3% hydrogel and commercial air-entraining agent improved micro-air voids, increasing their volume threefold compared to larger voids. The 1% and 2% hydrogels, as well as commercial SAPs, resulted in similar void structures.
3. All agents achieved spacing factors within ASTM C457 limits. The 3% hydrogel and commercial agent had the lowest spacing factors, indicating better freeze-thaw resistance due to more voids and reduced spacing.
4. No significant reduction in compressive strength was observed with cornstarch hydrogels, SAPs, or the commercial agent. Strength reductions at early stages with higher cornstarch were partially recovered through internal curing, with 3% hydrogel outperforming the commercial agent.

5. XRD analysis showed no harmful chemical phases in cornstarch hydrogel samples. Higher cement hydration products were observed, attributed to the hydrogel's internal curing ability during later hydration stages.

Overall, 3% cornstarch hydrogel is a sustainable and economical alternative to commercial agents, providing higher porosity, comparable micro-air content, favorable spacing factors, and equivalent compressive strength. Compaction effects were excluded as cornstarch hydrogels are unaffected by them, unlike surface tension-modifying agents.

Chapter 4. Effect of Commercial Superabsorbent Polymers and Cornstarch Hydrogels on Freeze-Thaw Resistance of Cementitious Materials

The Salt Belt region of the United States experiences frequent freeze-thaw cycles during winter, resulting in an annual road maintenance cost of approximately $2.3 billion [163]. When temperatures drop, the pore solution within the cementitious matrix begins to freeze. Since ice occupies a greater volume than liquid water, its expansion generates internal stresses within the concrete, which can cause cracking and reduce durability over time. To address these internal stresses, air entrainment agents are commonly incorporated into concrete mixtures. These agents introduce small, uniformly distributed air voids that provide space for ice to expand, thereby reducing internal stresses and preventing any cracking. The inclusion of these voids significantly enhances the freeze-thaw resistance of concrete, making it more durable in cold climates [164]–[167].

Air entrainment agents can be classified into two broad categories although other minor categories exist: bio-based and chemically synthesized materials [57]. Bio-based air entrainment agents are derived from natural sources such as wood resins, petroleum acids, and vegetable or animal fats [58]. These agents react with calcium hydroxide, a byproduct of cement hydration, to form hydrophobic calcium salts. These salts help stabilize air bubbles generated during mixing process by reducing surface tension in the concrete mixture [57]. However, large-scale production of bio-based air entrainment agents to meet industrial demand remains a challenge. In contrast, chemically synthesized air entrainment agents are typically composed of aliphatic, aromatic, and sulfonated hydrocarbons [59]. These synthetic agents are specifically developed to efficiently create and stabilize air voids by lowering the surface tension of water films on air bubbles. However, the addition of extra voids reduces the compression strength [64]–[67]. In addition, air entrainment agent adsorption onto cement particles reduces cement hydration [69], [70].

Superabsorbent polymers (SAPs) are commonly used to provide internal curing in cementitious materials by absorbing water during mixing and gradually releasing it over time [124]. When cement hydration begins due to the interaction between cement and water, an ion concentration gradient develops between the water within the swollen SAP and the surrounding matrix pore solution. This gradient drives the release of water from the SAP into the cementitious system [81], [82]. As the polymer releases water, its volume decreases, creating empty spaces known as voids. In Chapter 3, it was found that hydrogels generate an air void structure in mortar that is comparable to that produced by commercial air entrainment agents. However, their effectiveness in enhancing F-T resistance still requires further investigation. Existing literature indicates that the void structure formed by hydrogel water release is generally less ideal than that created by commercial air-entrainment agents [85], [86]. Research suggests that several factors, including particle size, dosage, synthesis process, and mixing conditions, significantly impact the freeze-thaw resistance of absorbent polymers [84], [87]–[90]. For example, smaller particle sizes and lower SAP dosages lead to finer voids, which improve freeze-thaw durability [89], [90].

Additionally, suspension polymerization tends to produce more spherical voids, whereas bulk polymerization results in irregularly shaped voids [88]. Furthermore, SAPs in dry form create void structures with smaller spacing, contributing to improved freeze-thaw resistance [84]. Understanding and optimizing these factors is crucial for enhancing the performance of SAPs in cementitious materials, particularly in environments subject to freeze-thaw cycles.

Despite their potential, SAPs have shown mixed results in freeze-thaw resistance in the literature, highlighting the need for further investigation into how factors like composition, particle size, and water absorption capacity influence their performance. Similarly, bio-based hydrogels present a promising but underexplored solution for enhancing concrete properties. This study evaluates the freeze-thaw behavior of mortar specimen incorporating commercial SAPs and a cornstarch-based hydrogel in the presence of a deicing solution. Two commercial SAPs with varying compositions and particle sizes, along with the bio-hydrogel in swelled form, were introduced into cementitious matrix. Their performance was compared against specimens containing a commercial air-entrainment agent and a control mix with no admixtures.

4.1 Materials and Methods

4.1.1 Materials

Mortar samples were prepared using Type I Portland cement (TCC Materials®), conforming to ASTM C150 standards [99], combined with fine aggregates from Quikrete® and tap water. Current study employed a low W/C ratio of 0.3 mixture which lack workability due to limited amount of mixing water. Therefore, a high-range water reducer (superplasticizer), MasterGlenium® 7500 (BASF), was added. This superplasticizer meets ASTM C494/C494M standards for Type A and Type F admixtures [100]. For enhanced freeze-thaw resistance, the reference mix included Akona® liquid air-entraining admixture (TCC Materials®), compliant with ASTM C260 [121].

4.1.2 Superabsorbent Polymers (SAPs)

The current chapter evaluates the impact of two commercial SAPs, designated B, and D (details in Table 2.1) on the freeze-thaw resistance of the mortar. These SAPs, which vary in size and composition, were sourced from Emerging Technologies. SAP D is composed of a sodium salt of crosslinked polyacrylic acid, while SAP B consists of a potassium salt of crosslinked polyacrylic acid/polyacrylamide copolymer. Additionally, SAP D has a larger particle size than SAP B but exhibits lower absorption of cement pore solution.

4.2 Cornstarch hydrogel forms and synthesis

This report investigates the application of a cornstarch-based hydrogel to improve the properties of cementitious mixtures. Chapter 2 explores its potential for internal curing in mortar, while Chapter 3 examines its impact on the void structure of mortar. The current chapter focuses on evaluating its effect on the freeze-thaw resistance of mortar. Similar to the approach in Chapters 2 and Chapter 3, the cornstarch-based hydrogel was synthesized using the heat gelatinization process, where a cornstarch-water solution was heated to 82.2°C for 15 minutes [97] as show in Figure 4.1. Cornstarch was used at 0.2% by weight of cement, matching the proportion used for commercial SAPs contain mortar mixture.

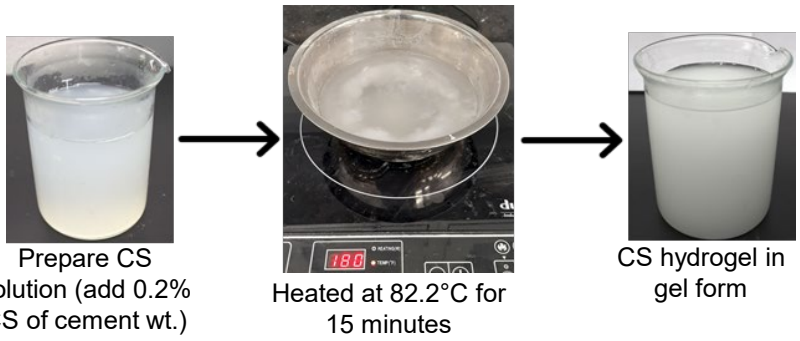

Figure 4.1 Preparation of cornstarch hydrogel in form of gel

4.3 Mix Proportions

Five mortar mixtures were cast to investigate the effect of cornstarch-based hydrogels and commercial SAPs on freeze-thaw resistance of mortar. The inclusion of absorbent polymers in the mixtures led to the absorption of some mixing water during mortar preparation, which consequently lowered the effective W/C ratio. To compensate for this reduction and maintain effective W/C during mixing and consistent workability, additional water was introduced. This adjustment ensured that mixtures containing absorbent polymers achieved the target workability of 90±2% on the flow table, matching the workability of the control mixture without absorbent polymers [40], [168], [169]. The workability of the mortar was evaluated using the flow table test, conducted in accordance with ASTM C1437 [130].

Table 4.1 summarized all the mixes detail used in a current study. The control mixture was prepared with a W/C ratio of 0.3 and a sand-to-cement ratio of 1.75. A superplasticizer, constituting 0.6% of the cement weight, was included in mixtures to achieve the target workability of 90±2% on the flow table. Air-entraining agents were used at 0.49% of the total mortar weight to achieve an air content of 8% (±2%), as per the manufacturer's recommendations [57].

Both commercial and bio-based hydrogels were added at 0.2% of the cement weight, based on prior studies [170]–[173]. The commercial SAPs were first dry-mixed with cement and sand. In contrast, cornstarch gel (CSG) was incorporated into the water-superplasticizer mixture first.

Table 4.1 Mix Proportions for mixes used in research work

Sample ID	Type of admixture	Condition	Additional W/C*	Total W/C
CM	---	---	---	0.3
0.2%-CSG-0.045	CS-based hydrogel	Swollen	0.045	0.345
0.2%-SB-0.05	SAP B	Dry	0.05	0.35
0.2%-SD-0.011	SAP D	Dry	0.011	0.311
0.4%-AE	Air entrainment agent	Liquid	----	0.3

4.4 Testing Program

4.4.1 Typical Freezing-thawing Cycle

A 24-hour FT cycle was selected for this study, with each specimen subjected to a maximum of 200 FT cycles. Each cycle consisted of a freezing phase and a thawing phase. The cement mortar cubes were water-cured for 28 days before being immersed in a salt brine solution for F-T testing. In the Northern United States, concrete pavements are frequently exposed to snow, and salt brine is commonly used as a deicing agent during winter months. However, salt brine has been shown to contribute to surface scaling issues [174] and hence chosen as the immersion liquid in the FT cycles in this study. During the freezing phase, specimens were cooled from room temperature to a target temperature of -22°C over 5 hours, then held at this temperature for 10 hours. The -22°C freezing temperature was selected because a 23% salt brine solution, used as the immersion liquid, freezes below -21.1°C [175]. Following this, the thawing phase involved gradually warming the specimens back to 20°C (room temperature) over 5 hours, after which specimen were maintained at this temperature for an additional 4 hours. The full 24-hour FT cycle is illustrated in Figure 4.2.

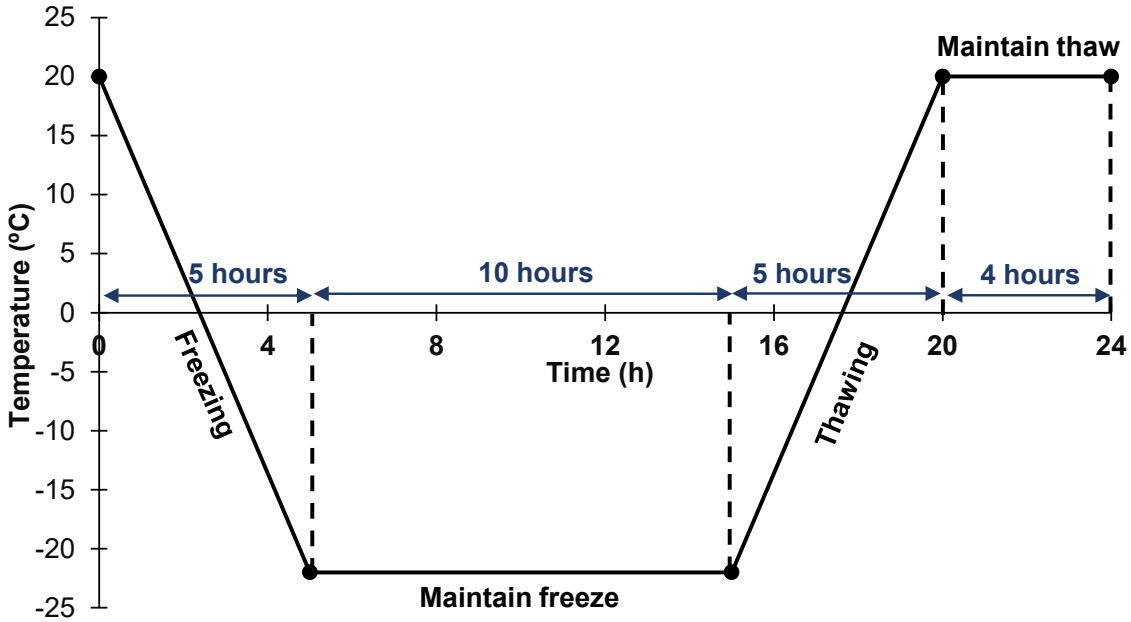

Figure 4.2 Schematic diagram of the freeze-thaw cycle

4.4.2 Compression Strength

Compression tests, following ASTM C109 [102], were conducted to evaluate the impact of F-T cycles on specimen strength. For each mix, 15 cube specimens (50 mm sides) were cast to analyze strength variations over different F-T cycles. The specimens were water-cured for 28 days before being placed in a freeze-thaw cabinet. Initial compression strength was recorded as a baseline prior to F-T exposure. Further tests were performed after 30, 60, 110, and 200 F-T cycles to track strength changes.

4.4.3 Mass Change, Scaling and Chloride Penetration

Low temperatures cause the pore solution in concrete to freeze, leading to an increase in volume that generates significant internal stresses within the matrix. This stress buildup can cause surface material to peel off (scaling), eventually resulting in mass loss [176]. Additionally, chloride ions from the surrounding brine solution can penetrate the matrix and react with cement hydration products, resulting in the formation of Friedel's salt. Due to its expansive nature, Friedel's salt promotes concrete scaling [174].

Cube specimens (50 mm sides) were water-cured for 14 days before being subjected to F-T cycles [177], [178]. The average mass and scaling of three specimens from each mix were recorded after 30, 60, 110, and 200 F-T cycles. Mass measurements were taken immediately after removing the samples from the solution, ensuring that the surfaces were wiped using dry cloth before weighing. Scaling was visually assessed and classified according to Table 4.2 [179].

Deep penetration of chloride ions can also contribute to the corrosion of embedded steel reinforcement. To evaluate chloride penetration, the affected area was determined after 200 F-T cycles. Specimens were halved, and their cross-sections were sprayed with a 0.1 M silver nitrate solution. Chloride ions reacted to form a white precipitate, which turned gray upon light exposure, indicating chloride presence [180]. The penetration area was then measured using ImageJ software by analyzing photographs of the cross-sections.

Table 4.2 Description of the visual scale of scaling deterioration in mortar specimens

Scale	Description
0	No scaling
1	Slight scaling
2	Slight to moderate Scaling
3	Moderate Scaling
4	Moderate to severe scaling
5	Severe scaling

4.5 Results and Discussion

4.5.1 Scaling

Scaling was assessed through visual inspection of the specimens after 30, 60, 110, and 200 F-T cycles. Three specimens were visually examined for each mixture. No signs of scaling were observed until 110 F-T cycles in any of the mortar mixtures, and hence the visual appearance at 110 and 200 F-T cycles are reported. Figure 4.3 illustrates the visual appearance of cubes after 110 and 200 F-T cycles when compared to their original state which is before exposure to F-T cycles.

The lack of scaling prior to the 110 F-T cycles can be attributed to low W/C ratio which leads to denser and impermeable microstructure [181]. In this study, the increased roundness of the edges and corners and relative increase in the surface roughness of the cubes is considered as

basis for assessing the extent of scaling damage. After exposure to 110 F-T cycles, most mortar cubes showed signs of scaling noticed as wear of edges and corners resulting in their rounding. At later stages (at 200 F-T cycles), in certain cases, scaling was observed as increased surface roughness caused by particle shedding in addition to corner and edge rounding.

The control mix cubes exhibited visually discernable scaling around their edges after exposure to 110 F-T cycles (see Figure 4.3 first row, second column). This scaling has resulted in more rounded corners when compared to the unexposed control mortar cubes. Among the specimens containing hydrogel, slight scaling was observed with the addition of SAP D, which has a lower additional water demand (see Figure 4.3 fourth row, second column). The relatively low scaling in this case manifested as slight rounding and blunting of edges. Conversely, the cubes containing hydrogels with higher water demand (CSG and SAP type B, as seen in the second column of row 2 and row 3, respectively, of Figure 4.3) and those with a commercial air-entraining agent (column 2 of row 5 in Figure 4.3) maintained their edge sharpness and corner integrity, showing minor signs of scaling through slight increase in the surface roughness and corner rounding.

By the end of 200 F-T cycles, surface deterioration became more apparent in some specimens. The control mix cubes (row 1, column 3 of Figure 4.3) showed significantly rounded edges with rougher surfaces indicating higher scaling at the end of 200 F-T cycles. The mix with the low water demand hydrogel, SAP type D (row 4, column 3 in Figure 4.3), exhibited small flakes near the edges but maintained their relative edge sharpness, when compared to what they experienced at the end of 110 F-T cycles. In contrast, specimens with higher water demand hydrogels, like SAP type B (column 3 of row 3 in Figure 4.3) and CSG (column 3 of row 2 in Figure 4.3), were more prone to scaling through increased surface roughness. The air-entrained mortar specimens exhibited the least scaling, with only minor surface roughness in the vicinity of the corners and edges even after the exposure to 200 F-T cycles.

Scaling ratings are assessed based on descriptions provided in Table 4.2, following the guidelines of ASTM C672/C672M-12 [182]. It is classified on a scale from 0 (no scaling) to 5 (severe scaling), with minor scaling up to level 1, slight to moderate scaling up to level 2, and moderate scaling designated as level 3. However, none of the specimens displayed scaling at moderate-to-severe (level 4) or severe (level 5) levels. A total of three specimens were selected from each mixture, and the average scaling after 110 and 200 F-T cycles is presented in Figure 4.4, along with error bars. The addition of hydrogel moderately improved scaling resistance, whereas the incorporation of an air-entraining agent had a more pronounced effect. After 110 F-T cycles, hydrogels with higher water demand exhibited a moderate reduction in scaling. In contrast, hydrogels with lower water demand showed only a slight reduction in scaling. On the other hand, the incorporation of an air-entraining agent significantly improved scaling resistance, as one out of three specimens exhibited only slight scaling at the end of 110 F-T cycles.

After 200 F-T cycles, all control specimens exhibited moderate scaling, marked as level 3. The addition of various hydrogels moderately enhanced scaling resistance, with most specimens showing a reduction to severe-to-moderate scaling (level 2), while a few still exhibited moderate

scaling (level 3). Although this improvement was evident, the overall scaling remained lower than the control mix. At the end of 200 F-T cycles, the incorporation of any type of hydrogel resulted in the same average scaling, regardless of differences in particle size and absorption properties. The most significant improvement was observed in specimens containing the air-entraining agent, which consistently reduced scaling across all three specimens to only slight scaling (level 1) at the end of 200 F-T cycles.

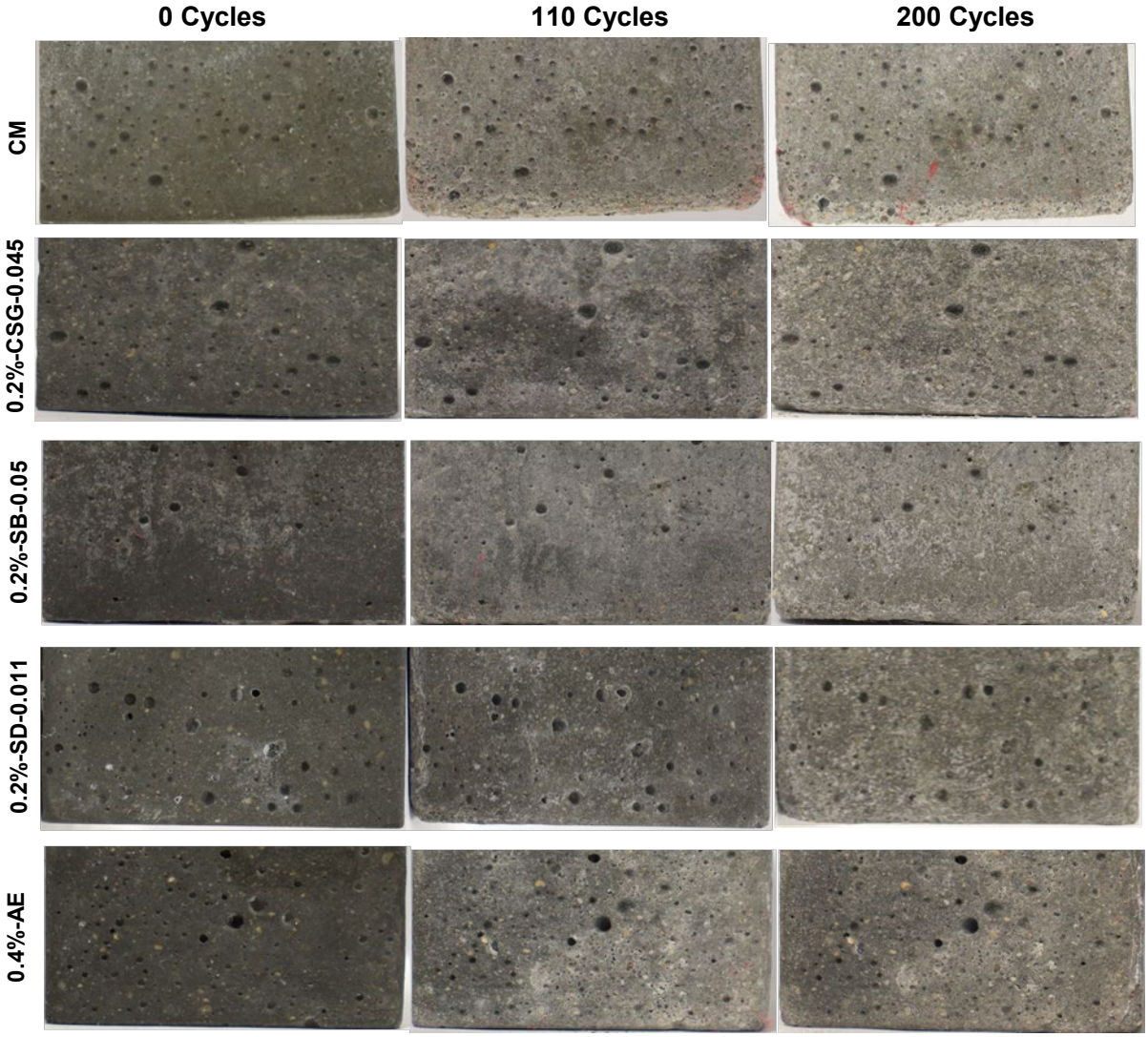

Figure 4.3 The visual appearance comparison of specimens before and after exposure to 110 and 200 F-T cycles

Three forms of damage lead to scaling of mortar cubes: 1) the freezing pore solution expands in volume and exerts hydrostatic tension stresses in the pore network leading to microcracks that promote scaling, 2) chloride ions in the salt brine accelerate calcium leaching, particularly from calcium hydroxide ($Ca(OH)_2$) and calcium silicate hydrate (C-S-H) gel, which weakens the cementitious matrix due to increased porosity leading to scaling [51], [52], [183], and 3) at temperatures below freezing point that are prevalent in the colder cycle of the F-T cycles,

oxychloride compounds can form in the presence of calcium hydroxide and chloride salts which are highly expansive and cause internal stresses, leading to surface scaling and cracking. Among these three mechanisms, the increase in the volume of pore solution is the most damaging and occurs immediately up on freezing. This is mitigated by introducing a void network that provides additional space for the frozen pore solution to expand without causing internal stresses.

From the previous chapter, it was demonstrated that the commercial air entraining agent produces a superior network of voids, and this has been proven to be effective in reducing the scaling damage in this chapter. Furthermore, the enhanced scaling resistance observed in mixes containing higher water demand hydrogels, compared to those with lower water demand, may be attributed to their efficient internal curing [184], [185]. Additionally, higher swelling hydrogels create relatively larger voids, which may require more F-T cycles to accumulate enough salt precipitation to cause slight to moderate scaling. As a result, higher water demand hydrogels initially exhibited slight scaling. However, by the end of 200 F-T cycles, all hydrogel types resulted in the same level of scaling. [90], [186].

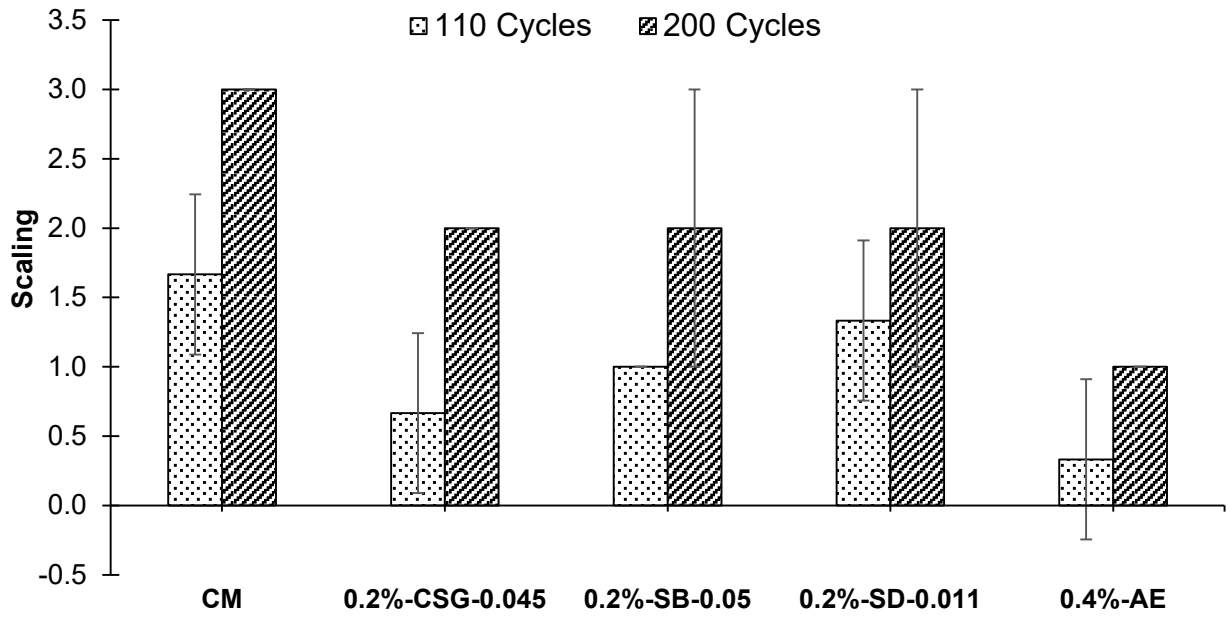

Figure 4.4 Average scaling level when exposed to 110 and 200 F-T cycles in brine solution.

4.5.2 Mass Change

In this study, the mass change of mortar cubes was measured after 30, 60, 90, 110, and 200 F-T cycles, and is plotted in Figure 4.5. Positive bars indicate mass gain relative to the mass before exposure to F-T cycles, while negative bars indicate mass loss.

In most cases, specimens demonstrated mass gain rather than loss, with only a few exceptions. The control mix exhibited relatively lower mass gain, with a slight spike at 110 F-T cycles, which later returned close to the original mass after 200 F-T cycles. However, a net positive mass was still observed, as mass gain was partially offset by mass loss due to scaling. Among hydrogel-incorporated specimens, those with higher water demand hydrogels (CSG and SAP type B) exhibited relatively higher mass gain at the end of 200 F-T cycles. However, the incorporation

of relatively lower water absorbent and larger particle size hydrogel (SAP type D), maintained the mass with minor fluctuations. On the other hand, the inclusion of a commercial air entrainment agent moderately increased the mass.

The variation in mass measurements can be attributed to multiple factors. Mass loss primarily results from scaling, which causes the peeling of matrix particles or, in some cases, flaking [187], [188]. However, as discussed in Section 4.5.1, only a moderate level of scaling was observed overall, making its contribution to mass loss insignificant. In contrast, mass gain can be linked to the ongoing cement hydration process. The specimens were exposed to F-T cycles after 14 days of external curing [189]. Since cement hydration usually continues for about 28 days, it may have slightly contributed to the mass gain [190]. However, previous studies [191] indicate that this effect is minimal and can generally be ignored. The more likely cause of mass gain is the accumulation of salt precipitates within voids or microcracks [177], [192]. In addition to the mass of the salt itself, its hygroscopic nature allows it to absorb water, leading to further mass increase [193], [194]. Given that all specimens in this study were submerged in a highly concentrated (23.3%) sodium chloride solution, salt accumulation was a significant factor contributing to mass gain in most specimens.

For the control mix, the mass reduction at 200 F-T cycles compared to 110 F-T cycles could be attributed to the significant scaling observed (discussed in Section 4.5.1). Specimens incorporating higher water-demand hydrogels (CSG and SAP type B) exhibited a notable mass increase, likely due to an increase in void volume which will be discussed in a later section. Literature [90], [186] suggests that high-swelling hydrogels create larger voids upon water release, which can accommodate more salt precipitates, thereby increasing mass. This could explain why specimens with lower water-demand hydrogel (SAP type D) showed comparatively less mass gain. SAP type D has a larger particle size, meaning it contains fewer particles than SAP type B when the same mass is used. This results in a smaller number of voids introduced by the hydrogel, limiting the space available for salt accumulation. This could explain why the addition of SAP type D led to relatively lower mass gain but remained consistent throughout the F-T cycles. In contrast the addition of air-entraining agents increased the porosity of the mortar [70] when compared to the control specimens, providing additional void space for salt accumulation from the surrounding solution. However, since air entrainment agents are designed to create smaller, well-distributed voids, the resulting mass increase was moderate [177], [195], [196]. Overall, the results indicate that the addition of hydrogel to cementitious materials does not lead to substantial mass changes when exposed to F-T cycles and deicing solutions. Instead, it contributes to mass gain, similar to air-entraining agents, governed by the void formation and salt accumulation.

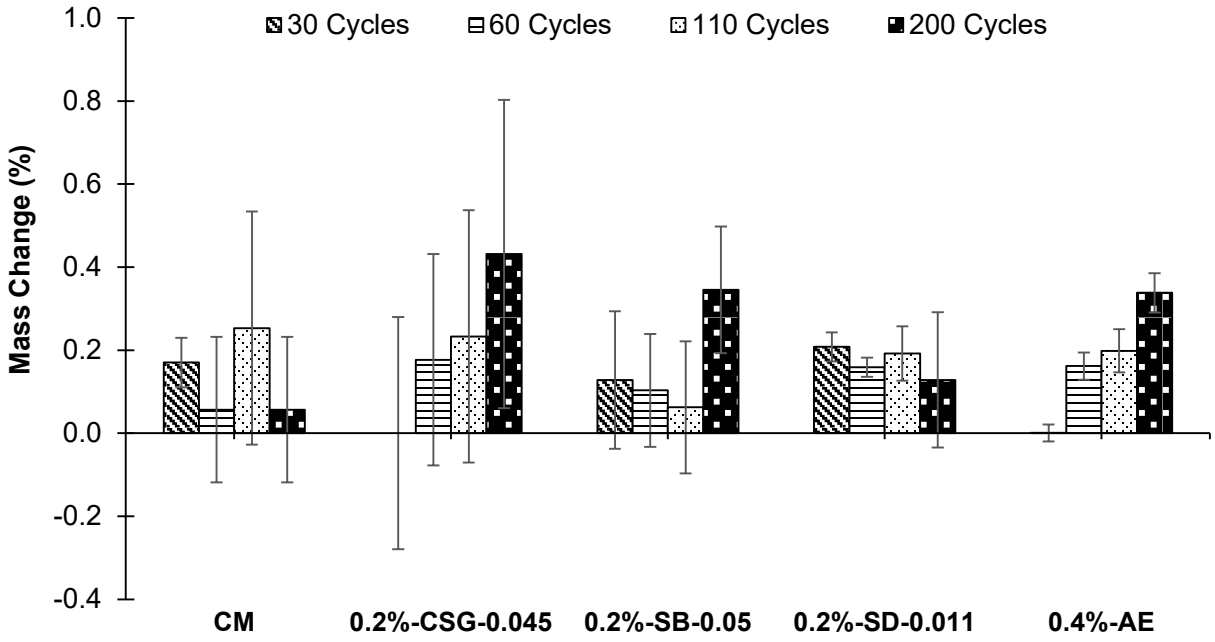

Figure 4.5 Percentage change in mass relative to the initial mass before exposure to F-T cycles.

4.5.3 Compression Strength

To assess the impact of hydrogels and air entrainment agent on cementitious materials exposed to F-T cycles and deicing solutions, compressive strength tests were conducted after 30, 60, 90, 110, and 200 F-T cycles. Figure 4.6 illustrates the impact of hydrogel and air-entraining agent addition on the compressive strength of mortar subjected to F-T cycles in a brine solution. Additionally, Figure 4.7 presents the changes in compressive strength compared to the initial strength before F-T cycles exposure. In the chart, positive bars indicate strength gain, while negative bars represent strength reduction. Error bars denote the range of values obtained.

Overall, the addition of hydrogel and air entrainment agent resulted in a reduction in mortar compressive strength, as shown in Figure 4.6. The initial strength drop before exposure to F-T cycles was more pronounced with hydrogel incorporation, particularly for the hydrogel with the highest water demand, SAP type B, which caused a 25% decrease in strength. However, as the F-T cycles progressed, this difference became smaller. By the end of 200 F-T cycles, the higher water demand hydrogels, CSG and SAP type B, reduced the strength by only 1% and 3%, respectively, compared to the control mix strength after 200 F-T cycles. In contrast, the lower water demand hydrogel, SAP type D, demonstrated superior performance, significantly increasing strength by 9.5%. The inclusion of an air-entraining agent resulted in a slight reduction in strength compared to the control mix, but both showed nearly identical strength after 200 F-T cycles.

Figure 4.7 provides a more comprehensive view of the impact of F-T cycles and the deicing solution on the initial compressive strength of each mix. The results showed that, in most cases, strength increased up to 110 F-T cycles. However, as the F-T cycles continued, particularly beyond 200 cycles, the negative effects of freeze-thaw action and the deicing solution became more evident. The control mix and the mix containing a commercial air-entraining agent experienced a strength reduction of approximately 12% after 200 F-T cycles. In contrast, specimens

incorporating dry commercial SAPs, SAP types B and D, exhibited a significant strength increase of approximately 15% after 200 F-T cycles compared to their initial strength. Meanwhile, the addition of cornstarch-based hydrogel in its swelled form effectively maintained compressive strength, showing an initial strength gain up to 110 F-T cycles before returning to its original strength level.

Several factors influence the strength of mortar. Environmental conditions, such as exposure to freeze-thaw (F-T) cycles and deicing solutions, play a significant role in determining the durability of cementitious materials. Additionally, the incorporation of hydrogels and air-entraining agents alters the mortar's microstructure, further impacting its overall strength. The cementitious matrix typically experiences a reduction in compressive strength when exposed to F-T cycles and deicing solutions [197]. The expansion of freezing pore solution and the crystallization of salt precipitates in pores generate internal stresses within the matrix, leading to surface degradation (scaling) and ultimately causing strength reduction [198], [199]. Additionally, chloride ions from the surrounding deicing solution contribute to the leaching of calcium ions from cement hydrates (C-S-H gel), which are essential for strength development, further weakening the matrix [51], [52], [183].

The addition of hydrogels and air-entraining agents also impacts the compressive strength of mortar. By increasing air content, these additives alter porosity, which in turn affects overall strength [200]. The addition of hydrogels, particularly those with high water demand, results in a noticeable reduction in compressive strength due to an increased W/C ratio. As the hydrogel releases water, it increases porosity and thus reducing strength [201], [202]. This explains why SAP type B, which absorbs a larger volume of water, caused a significant drop in compressive strength. The use of air-entraining agents also led to strength reduction, though to a lesser extent, as the introduced voids were smaller and well-distributed, mitigating their negative impact on overall mechanical performance [56].

As exposure to F-T cycles and deicing solutions continued, their deteriorative effects became increasingly evident. However, an initial increase in strength was observed in all mixtures, consistent with previous studies [196], [203], [204]. This increase in strength can be attribute to the brine solutions can initially accelerate cement hydration by increasing ion concentration in addition to ongoing cement hydration. Sodium chloride promotes the early hydration of C_3S (tricalcium silicate) and C_2S (dicalcium silicate), leading to the formation of C-S-H gel, which is crucial for strength development. Over time, as F-T cycles progressed beyond 200 cycles, the negative effects of freeze-thaw damage and deicing solutions intensified, leading to strength loss. In the control mix, this strength drop was due to lack of mechanism to mitigate internal stresses generated from pore solution expansion and salt crystallization. The use of an air-entraining agent increased the air content in the mortar, enhancing scaling resistance but slightly compromising structural integrity due to the presence of additional voids.

The negative effect of F-T cycles and deicing solution was more pronounced after 200 F-T cycles. However, all mixtures experience initial increase in strength when exposed to F-T cycles and deicing solution observed aligns with previous studies [196], [203], [204]. This increase in

strength can be attribute to the brine solutions can initially accelerate cement hydration by increasing ion concentration in addition to ongoing cement hydration. Sodium chloride promotes the early hydration of C_3S (tricalcium silicate) and C_2S (dicalcium silicate), leading to the formation of C-S-H gel, which is crucial for strength development. However, as the F-T cycles progressed, particularly beyond 200 cycles, the negative effects of freeze-thaw action and deicing solution became more pronounced. In the control mix, the strength reduction occurred due to the absence of a mechanism to counteract internal stresses caused by pore solution expansion and salt crystallization. The use of an air-entraining agent increased the air content in the mortar, enhancing scaling resistance (as discussed in Section 4.5.1) but slightly compromising structural integrity due to the presence of additional voids [60].

The incorporation of hydrogels, however, demonstrated either maintained or improved compressive strength while providing moderate scaling resistance as F-T cycles advanced. This aligns with existing literature [91], [205], [206] suggesting that scaling occurs due to the presence of larger voids in the matrix compared to air-entraining agents. However, the gradual release of water from hydrogels over time acts as an internal curing mechanism, enhancing cement hydration and ultimately improving strength [124]. The use of powdered dry commercial SAPs proved to be more effective than pre-saturated bio-based hydrogels. This observation supports the finding that pre-wet hydrogels lead to higher porosity [207] and a less homogeneous distribution of hydrogel within the matrix [82]. Nevertheless, the addition of corn-starch hydrogel maintained the original strength, indicating its viability as an alternative. The use of SAP type D exhibited superior performance, surpassing both the control and air-entrained mortar strength after 200 F-T cycles, even with additional water content. This exceptional performance can be attributed to its lower water demand. Studies [208] suggest that SAPs with lower water absorption create less porosity compared to those with higher water absorption. Additionally, SAP type D, having a larger particle size, resulted in a smaller number of particles dispersed within the matrix. Fewer SAP particles produced fewer pores, enhancing overall matrix integrity while still providing sufficient space to accommodate freezing-induced expansion.

Overall, the addition of hydrogels reduces the compressive strength of mortar but mitigates strength loss due to F-T cycles and deicing solutions. Particularly, the incorporation of larger particle-sized SAPs with lower water demand significantly enhances the freeze-thaw resistance of cementitious materials.

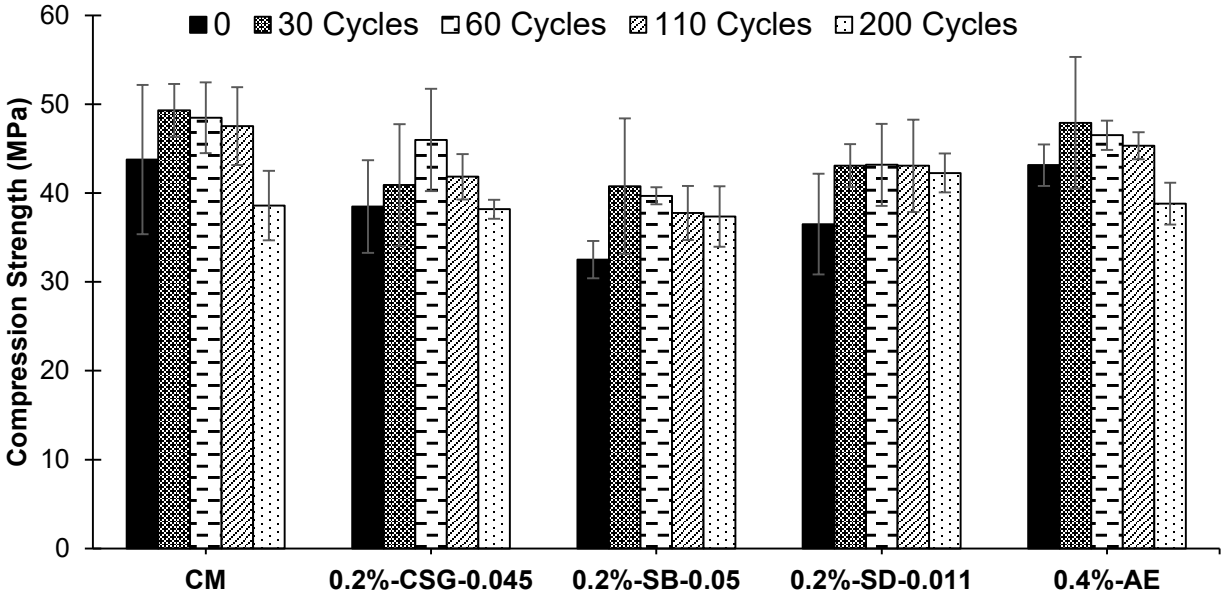

Figure 4.6 Effect of F-T cycles on compression strength when exposed to brine solution

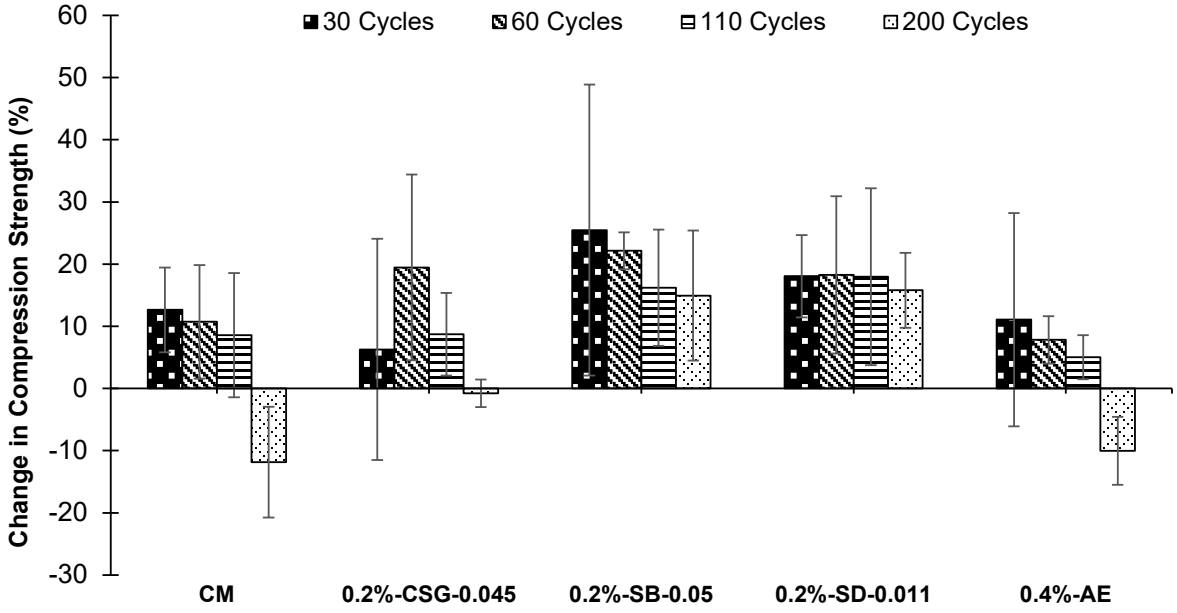

Figure 4.7 Change in compression strength (%) compared to strength after 28 days of external curing (0 cycle) for each mix

4.5.4 Chloride Penetration

In this study, mortar cubes submerged in a brine solution and subjected to 200 F-T cycles were selected to evaluate chloride penetration. The cubes were cut in half, and the interior surface, which had not been directly exposed to the environment, was sprayed with a 0.1M silver nitrate solution. The reaction between silver nitrate and chloride ions caused the affected areas to turn grey, indicating chloride penetration. Figure 4.8 displays a cross-section of the mortar cubes after spraying with silver nitrate, with the grey zones near the surface indicating chloride ingress.

All specimens showed significant chloride penetration due to prolonged exposure to a high-concentration NaCl solution (23%) combined with 200 F-T cycles. The addition of hydrogel led to a slight increase in chloride penetration, whereas the use of a commercial air-entraining agent moderately reduced it. However, the differences in the chloride-affected area (grey region) among the specimens were not substantial enough to establish a clear trend.

To quantify the extent of chloride penetration, ImageJ software was used to determine the grey-colored area, and the results are plotted in Figure 4.9. The data is presented as a change in chloride penetration relative to the control mix (CM), where positive bars indicate increased penetration and negative bars indicate a reduction. The incorporation of all hydrogel types slightly increased chloride ingress. A quantity of additional water demand correlated with increased chloride penetration, with SAP type D exhibiting the least increase, showing only a 1.8% rise in the chloride-affected area compared to the control mix. In contrast, the inclusion of air-entraining agents effectively reduced chloride penetration.

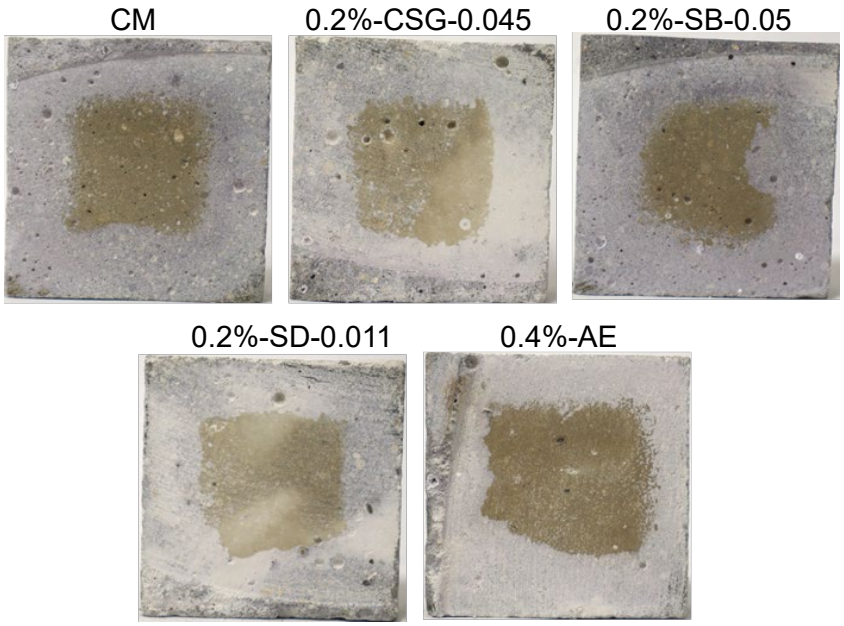

Figure 4.8 Photos of sliced cube sections sprayed with 0.1M silver nitrate solution after 200 F-T cycles (grey areas indicate chloride ion penetration).

High porosity leads to higher permeability, facilitating chloride ion penetration [209]. Furthermore, scaling reduces surface protection, promoting chloride ingress into the inner matrix [176]. The specimens incorporating hydrogel exhibited increased chloride ion penetration compared to the control mix, likely due to increased porosity. Past studies [90], [186] indicate that hydrogels with greater swelling capacity increases porosity upon water release, increasing permeability and ultimately leading to higher chloride penetration. A similar trend was observed in the current study, where SAP type B exhibited the highest chloride penetration, followed by CSG, while SAP type D showed the least increase in the chloride-affected area. This pattern aligns with the sequence of their pore solution absorption capacity or extra water demand. In contrast, the reduced chloride ingress observed with the addition of an air-entraining agent is likely

attributed to its improved scaling resistance, which effectively limited chloride infiltration from the surface [210].

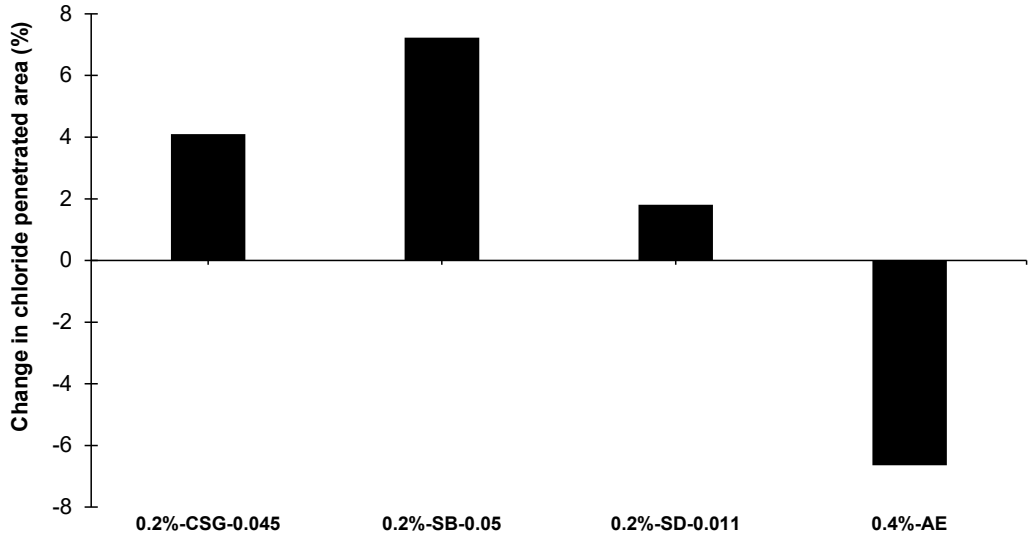

Figure 4.9 Change in chloride ion penetration at the center of the cube relative to the control mix after exposure to 200 F-T cycles in brine solution.

4.6 Conclusions

This study examined the freeze-thaw resistance of specimens with commercial air-entrainment agents, SAPs, and bio-based hydrogel. Key findings are:

1. Scaling began after 110 cycles. Specimens with commercial air-entrainment agents exhibited the least scaling. The inclusion of hydrogel to mortar moderately enhanced the scaling resistance.
2. Most specimens gained mass due to salt precipitate accumulation in pores, despite no major mass loss. Likewise, the addition of hydrogels also maintained the mass indicating relatively good freeze-thaw resistance due to mortar structural integrity.
3. The addition of hydrogel reduced the overall strength of the mortar; however, when exposed to freeze-thaw (F-T) cycles in a brine solution, it either maintained or increased strength due to enhanced internal curing. In contrast, the control mix and air-entrained mortar experienced a strength reduction, particularly after 200 cycles, due to pore stress caused by freezing of the pore solution, salt accumulation, and calcium ion leaching.
4. The addition of hydrogel increased the chloride penetration area in proportion to its extra water demand, likely due to increased porosity. In contrast, the incorporation of an air-entraining agent reduced chloride ingress, possibly due to its enhanced scaling resistance.

Overall, mixtures containing commercial air-entrainment agents effectively reduced scaling and chloride penetration but experienced a loss in strength. Mortars incorporating hydrogel moderately improved scaling resistance without mass loss. However, hydrogel effectively mitigated the reduction in mechanical strength caused by F-T cycles and exposure to the deicing

solution. Notably, SAP with larger particle size and lower water absorption demonstrated superior performance, showing an increase in strength, moderate scaling, and minimal chloride penetration.

Chapter 5. Conclusions and Recommendations

This study comprehensively investigated the potential of SAPs and cornstarch-based hydrogels for internal curing and as sustainable alternatives to commercial air-entraining agents for cement-based mixtures. It analyzed their impact on hydration, porosity, void structure, freeze-thaw resistance, and chloride penetration in cementitious matrices. The findings highlight the effectiveness of these materials in enhancing cement matrix durability while maintaining or improving mechanical properties.

5.1 Conclusions

The following are the main conclusions drawn from this study.

1. SAPs and cornstarch hydrogels exhibited high water absorption in tap water but significantly reduced absorption in cement pore solutions due to reduction in the osmatic pressure and shielding effects.
2. The newly proposed method effectively quantifies the internal curing capacity of hydrogel in cementitious specimens. It measures internal curing by assessing water distribution around the introduced hydrogel-containing capsules. Hydrogels facilitated uniform hydration near the capsules, improving CSH gel distribution and overall hydration levels without forming deleterious chemical phases.
3. The incorporation of cornstarch hydrogel increased mortar porosity, with the hydrogel derived from a 3% cornstarch solution yielding optimal results. It created smaller air voids while maintaining ASTM C457 spacing limits necessary for freeze-thaw resistance.
4. Void distribution was more consistent in specimen with cornstarch hydrogel and commercial air-entraining agents, while SAPs showed larger, irregular voids.
5. Commercial air-entraining agents enhanced scaling resistance of mortar, while cornstarch hydrogels and SAPs (especially SAP B) effectively resisted freeze-thaw damage with minimal strength loss.
6. SAP type B and SAP type D contributed to increased strength via continuous hydration, while chloride penetration resistance was best with cornstarch hydrogel and air-entraining agents.
7. Cornstarch hydrogel proved to be a sustainable and economical alternative to commercial agents, providing comparable durability and mechanical strength.

5.2 Recommendations for future study

Based on the findings of this study, the following recommendations are proposed to guide future research and practical applications:

1. *Optimization of Cornstarch Hydrogel Properties*: Investigate modifications to cornstarch hydrogel synthesis process to enhance its water absorption, water kinetics, and long-term stability in cement matrices.
2. *Compatibility with Blended Cements*: Study the performance of cornstarch hydrogel in matrices containing supplementary cementitious materials (e.g., fly ash, slag, or silica fume) to assess compatibility and hydration improvement in blended cements.

3. *Explore Additional Applications of Cornstarch Hydrogel*: Investigate the potential of cornstarch hydrogel for external curing**,** shrinkage mitigation**,** and improvement of other durability properties**,** such as resistance to sulfate attack, carbonation, and alkali-silica reaction, to broaden its usability in diverse construction scenarios.
4. *Field Trials and Scale-Up*: Implement large-scale field trials to assess the performance of cornstarch hydrogel in real-world construction projects and optimize its application methods for practical use.
5. *Cost-Effectiveness Analysis*: Evaluate the cost-benefit ratio of using cornstarch hydrogel compared to conventional admixtures, considering material production, transportation, and implementation in large-scale construction.
6. *Development of New Bio-Based Hydrogels*: Encourage research into other bio-based hydrogels that could complement or enhance the performance of cornstarch hydrogel, offering greater flexibility and tailored properties for diverse construction needs.

These recommendations aim to refine the understanding and application of cornstarch hydrogel while advancing sustainable and high-performance construction materials.

References

[1] P. Nagrale, “High Strength Concrete Market Size, Share & Industry,” 2024. [Online]. Available: https://www.marketresearchfuture.com/reports/high-strength-concrete-market-23114

[2] A. P. Fantilli, O. Mancinelli, and B. Chiaia, “The carbon footprint of normal and high-strength concrete used in low-rise and high-rise buildings,” *Case Stud. Constr. Mater.*, vol. 11, p. e00296, 2019.

[3] S. Tae, C. Baek, and S. Shin, “Life cycle CO2 evaluation on reinforced concrete structures with high-strength concrete,” *Environ. Impact Assess. Rev.*, vol. 31, no. 3, pp. 253–260, 2011.

[4] L. Wu, N. Farzadnia, C. Shi, Z. Zhang, and H. Wang, “Autogenous shrinkage of high performance concrete: A review,” *Constr. Build. Mater.*, vol. 149, pp. 62–75, 2017.

[5] K. Ozawa, K. Maekawa, and H. Okamura, “High performance concrete with high filling capacity,” *Admixtures for concrete, improvement of properties*. Chapman & Hall London, pp. 51–62, 1990.

[6] P. Lura, M. Wyrzykowski, C. Tang, and E. Lehmann, “Internal curing with lightweight aggregate produced from biomass-derived waste,” *Cem. Concr. Res.*, vol. 59, pp. 24–33, 2014.

[7] T. C. Powers and T. L. Brownyard, “Studies of the physical properties of hardened Portland cement paste,” in *Journal Proceedings*, 1946, vol. 43, no. 9, pp. 101–132.

[8] D. P. Bentz and K. A. Snyder, “Protected paste volume in concrete: Extension to internal curing using saturated lightweight fine aggregate,” *Cem. Concr. Res.*, vol. 29, no. 11, pp. 1863–1867, 1999.

[9] D. L. Stephen, “America’s Infrastructure Priorities Need Repair,” 2019.

[10] J. Asif and K. Ravi, “Sustainable Biobased Hydrogel as an Alternative Air-Entrainment Agent in Cement-Based Materials,” *J. Mater. Civ. Eng.*, vol. 36, no. 11, p. 4024342, Nov. 2024, doi: 10.1061/JMCEE7.MTENG-17763.

[11] H. U. Sajid, D. L. Naik, and R. Kiran, “Improving the ice-melting capacity of traditional deicers,” *Constr. Build. Mater.*, vol. 271, p. 121527, 2021.

[12] D. Shen, M. Wang, Y. Chen, T. Wang, and J. Zhang, “Prediction model for relative humidity of early-age internally cured concrete with pre-wetted lightweight aggregates,” *Constr. Build. Mater.*, vol. 144, pp. 717–727, 2017.

[13] C. Rößler, D.-D. Bui, and H.-M. Ludwig, “Mesoporous structure and pozzolanic reactivity of rice husk ash in cementitious system,” *Constr. Build. Mater.*, vol. 43, pp. 208–216, 2013.

[14] D. G. Nair, A. Fraaij, A. A. K. Klaassen, and A. P. M. Kentgens, “A structural investigation relating to the pozzolanic activity of rice husk ashes,” *Cem. Concr. Res.*, vol. 38, no. 6, pp. 861–869, 2008.

[15] A. Bentur, S. Igarashi, and K. Kovler, “Prevention of autogenous shrinkage in high-strength concrete by internal curing using wet lightweight aggregates,” *Cem. Concr. Res.*, vol. 31, no. 11, pp. 1587–1591, 2001.

[16] S. Ghourchian, M. Wyrzykowski, P. Lura, M. Shekarchi, and B. Ahmadi, “An investigation on the use of zeolite aggregates for internal curing of concrete,” *Constr. Build. Mater.*, vol. 40, pp. 135–144, 2013.

[17] R. Solís-Carcaño, L. V Terán-Marín, and E. I. Moreno, “Use of normal-density high-absorption limestone aggregate as internal curing agent in concrete,” *Can. J. Civ. Eng.*,

vol. 42, no. 11, pp. 827–833, 2015.
[18] B. Akcay and M. A. Tasdemir, “Effects of distribution of lightweight aggregates on internal curing of concrete,” *Cem. Concr. Compos.*, vol. 32, no. 8, pp. 611–616, 2010.
[19] R. Henkensiefken, J. Castro, D. Bentz, T. Nantung, and J. Weiss, “Water absorption in internally cured mortar made with water-filled lightweight aggregate,” *Cem. Concr. Res.*, vol. 39, no. 10, pp. 883–892, 2009.
[20] Q. Feng, H. Yamamichi, M. Shoya, and S. Sugita, “Study on the pozzolanic properties of rice husk ash by hydrochloric acid pretreatment,” *Cem. Concr. Res.*, vol. 34, no. 3, pp. 521–526, 2004.
[21] P. Shen *et al.*, “Water desorption characteristics of saturated lightweight fine aggregate in ultra-high performance concrete,” *Cem. Concr. Compos.*, vol. 106, p. 103456, 2020.
[22] A. M. Abdallah, “The effect of hydrogel particle size on water retention properties and availability under water stress,” *Int. soil water Conserv. Res.*, vol. 7, no. 3, pp. 275–285, 2019.
[23] E. M. Ahmed, “Hydrogel: Preparation, characterization, and applications: A review,” *J. Adv. Res.*, vol. 6, no. 2, pp. 105–121, 2015, doi: https://doi.org/10.1016/j.jare.2013.07.006.
[24] F. Wang, J. Yang, H. Cheng, J. Wu, and X. Liang, “Study on Mechanism of Desorption Behavior of Saturated Superabsorbent Polymers in Concrete.,” *ACI Mater. J.*, vol. 112, no. 3, 2015.
[25] W.-M. Cheng, X.-M. Hu, Y.-Y. Zhao, M.-Y. Wu, Z.-X. Hu, and X.-T. Yu, “Preparation and swelling properties of poly (acrylic acid-co-acrylamide) composite hydrogels,” *e-Polymers*, vol. 17, no. 1, pp. 95–106, 2017.
[26] M. Zhang, S. Zhang, Z. Chen, M. Wang, J. Cao, and R. Wang, “Preparation and characterization of superabsorbent polymers based on sawdust,” *Polymers (Basel).*, vol. 11, no. 11, p. 1891, 2019.
[27] R. Du, J. Wu, L. Chen, H. Huang, X. Zhang, and J. Zhang, “Hierarchical Hydrogen Bonds Directed Multi-Functional Carbon Nanotube-Based Supramolecular Hydrogels,” *small*, vol. 10, no. 7, pp. 1387–1393, 2014.
[28] J. Liu, C. Shi, X. Ma, K. H. Khayat, J. Zhang, and D. Wang, “An overview on the effect of internal curing on shrinkage of high performance cement-based materials,” *Constr. Build. Mater.*, vol. 146, pp. 702–712, 2017.
[29] K.-K. Yun, K.-K. Kim, W. Choi, and J. H. Yeon, “Hygral behavior of superabsorbent polymers with various particle sizes and cross-linking densities,” *Polymers (Basel).*, vol. 9, no. 11, p. 600, 2017.
[30] S. Friedrich, “Superabsorbent polymers (SAP),” in *Application of super absorbent polymers (sap) in concrete construction*, Springer, 2012, pp. 13–19.
[31] M. Wyrzykowski, P. Lura, F. Pesavento, and D. Gawin, “Modeling of water migration during internal curing with superabsorbent polymers,” *J. Mater. Civ. Eng*, vol. 24, no. 8, pp. 1006–1016, 2012.
[32] P. Lura, F. Durand, and O. M. Jensen, “Autogenous strain of cement pastes with superabsorbent polymers,” in *International RILEM conference on volume changes of hardening concrete: testing and mitigation*, 2006, vol. 100, pp. 57–65.
[33] O. M. Jensen, “Use of superabsorbent polymers in concrete,” *Concr. Int.*, vol. 35, no. 1, pp. 48–52, 2013.
[34] K. Farzanian, B. Vafaei, and A. Ghahremaninezhad, “The Behavior of Superabsorbent Polymers (SAPs) in Cement Mixtures with Glass Powders as Supplementary Cementitious

Materials," *Materials (Basel).*, vol. 12, no. 21, p. 3597, 2019.
[35] K. Suganya and V. Poornima, "Study on Absorbency of Superabsorbent polymer in water and cement pore fluid and its incorporation in cement mortar," *Int. J. Civ. Eng. Technol.*, vol. 8, pp. 1131–1140, 2017.
[36] D. Snoeck, C. Schröfl, and V. Mechtcherine, "Recommendation of RILEM TC 260-RSC: testing sorption by superabsorbent polymers (SAP) prior to implementation in cement-based materials," *Mater. Struct.*, vol. 51, no. 5, pp. 1–7, 2018.
[37] S. Zhao, O. M. Jensen, and M. T. Hasholt, "Measuring absorption of superabsorbent polymers in cementitious environments," *Mater. Struct.*, vol. 53, no. 1, p. 11, 2020.
[38] Y. Wehbe and A. Ghahremaninezhad, "Combined effect of shrinkage reducing admixtures (SRA) and superabsorbent polymers (SAP) on the autogenous shrinkage, hydration and properties of cementitious materials," *Constr. Build. Mater.*, vol. 138, pp. 151–162, 2017, doi: https://doi.org/10.1016/j.conbuildmat.2016.12.206.
[39] K. Farzanian and A. Ghahremaninezhad, "Desorption of superabsorbent hydrogels with varied chemical compositions in cementitious materials," *Mater. Struct.*, vol. 51, no. 1, p. 3, 2018, doi: 10.1617/s11527-017-1128-1.
[40] D. Snoeck, D. Schaubroeck, P. Dubruel, and N. De Belie, "Effect of high amounts of superabsorbent polymers and additional water on the workability, microstructure and strength of mortars with a water-to-cement ratio of 0.50," *Constr. Build. Mater.*, vol. 72, pp. 148–157, 2014, doi: 10.1016/j.conbuildmat.2014.09.012.
[41] L. Montanari, P. Suraneni, and W. J. Weiss, "Accounting for water stored in superabsorbent polymers in increasing the degree of hydration and reducing the shrinkage of internally cured cementitious mixtures," *Adv. Civ. Eng. Mater.*, vol. 6, no. 1, pp. 583–599, 2017.
[42] L. Montanari, P. Suraneni, M. T. Chang, C. Villani, and J. Weiss, "Absorption and desorption of superabsorbent polymers for use in internally cured concrete," *Adv. Civ. Eng. Mater.*, vol. 7, no. 4, pp. 547–566, 2018.
[43] J. Liu, X. Ma, C. Shi, and S. Drissi, "Internal curing of blended cement pastes with ultra-low water-to-cement ratio: Absorption/desorption kinetics of superabsorbent polymer," *J. Am. Ceram. Soc.*, vol. 104, no. 7, pp. 3603–3618, 2021.
[44] M. Li, Y. Wang, W. Wang, Q. Tian, and J. Liu, "Quantitative characterisation of absorption capacity and dosage of SAP in cement paste," *Adv. Cem. Res.*, vol. 28, no. 8, pp. 518–528, 2016.
[45] F. Wang, J. Yang, S. Hu, X. Li, and H. Cheng, "Influence of superabsorbent polymers on the surrounding cement paste," *Cem. Concr. Res.*, vol. 81, pp. 112–121, 2016.
[46] K. Farzanian and A. Ghahremaninezhad, "The effect of the capillary forces on the desorption of hydrogels in contact with a porous cementitious material," *Mater. Struct.*, vol. 50, no. 5, pp. 1–15, 2017.
[47] M. Kalinowski, P. Woyciechowski, and J. Sokołowska, "Effect of mechanically-induced fragmentation of polyacrylic superabsorbent polymer (SAP) hydrogel on the properties of cement composites," *Constr. Build. Mater.*, vol. 263, p. 120135, 2020, doi: 10.1016/j.conbuildmat.2020.120135.
[48] M. Vignes and K. M. Dijkema, "A model for the freezing of water in a dispersed medium," *J. Colloid Interface Sci.*, vol. 49, no. 2, pp. 165–172, 1974.
[49] U. A. Birnin-Yauri and F. P. Glasser, "Friedel's salt, Ca2Al (OH) 6 (Cl, OH)· 2H2O: its solid solutions and their role in chloride binding," *Cem. Concr. Res.*, vol. 28, no. 12, pp.

1713–1723, 1998.
[50] A. K. Suryavanshi, J. D. Scantlebury, and S. B. Lyon, “Mechanism of Friedel’s salt formation in cements rich in tri-calcium aluminate,” *Cem. Concr. Res.*, vol. 26, no. 5, pp. 717–727, 1996.
[51] J. J. Valenza, S. Vitousek, and G. W. Scherer, “Expansion of hardened cement paste in saline solutions,” *Creep Shrinkage Durab. Concr. Concr. Struct. Concreep*, vol. 7, pp. 12–14, 2005.
[52] N. Xie, X. Shi, and Y. Zhang, “Impacts of potassium acetate and sodium-chloride deicers on concrete,” *J. Mater. Civ. Eng.*, vol. 29, no. 3, p. 4016229, 2017.
[53] N. Papenfus, “Applying concrete technology to abrasion resistance,” in *Proceedings of the 7th international conference on concrete block paving, Sun City, South Africa*, 2003.
[54] Z. Wu, N. A. Libre, and K. H. Khayat, “Factors affecting air-entrainment and performance of roller compacted concrete,” *Constr. Build. Mater.*, vol. 259, p. 120413, 2020.
[55] P. F. G. Banfill, M. A. O. M. Teixeira, and R. J. M. Craik, “Rheology and vibration of fresh concrete: Predicting the radius of action of poker vibrators from wave propagation,” *Cem. Concr. Res.*, vol. 41, no. 9, pp. 932–941, 2011, doi: https://doi.org/10.1016/j.cemconres.2011.04.011.
[56] L. Du and K. J. Folliard, “Mechanisms of air entrainment in concrete,” *Cem. Concr. Res.*, vol. 35, no. 8, pp. 1463–1471, 2005.
[57] S. Chatterji, “Freezing of air-entrained cement-based materials and specific actions of air-entraining agents,” *Cem. Concr. Compos.*, vol. 25, no. 7, pp. 759–765, 2003.
[58] D. F. Zinkel, *Naval stores*. Springer, 1989.
[59] Z. Zhang, M. N. Vitillo, A. Maher, M. P. Szary, and F. Ansari, “Effects of Synthetic Air Entraining Agents on Compressive Strength of Portland Cement Concrete-Mechanism of Interaction and Remediation Strategy,” Citeseer, Piscataway, 2002.
[60] H. A. Shah, Q. Yuan, and S. Zuo, “Air entrainment in fresh concrete and its effects on hardened concrete-a review,” *Constr. Build. Mater.*, vol. 274, p. 121835, 2021.
[61] Q. Liu, Z. Chen, and Y. Yang, “Study of the Air-Entraining Behavior Based on the Interactions between Cement Particles and Selected Cationic, Anionic and Nonionic Surfactants.,” *Mater. (Basel, Switzerland)*, vol. 13, no. 16, Aug. 2020, doi: 10.3390/ma13163514.
[62] A. Kashani, T. D. Ngo, T. N. Nguyen, A. Hajimohammadi, S. Sinaie, and P. Mendis, “The effects of surfactants on properties of lightweight concrete foam,” *Mag. Concr. Res.*, vol. 72, no. 4, pp. 163–172, 2020.
[63] Z. P. BAŽANT, J. CHERN, A. M. Rosenberg, and J. M. Gaidis, “Mathematical model for freeze-thaw durability of concrete,” *J. Am. Ceram. Soc.*, vol. 71, no. 9, pp. 776–783, 1988.
[64] V. S. Ramachandran, *Concrete admixtures handbook: properties, science and technology*. William Andrew, 1996.
[65] M. A. A. Salem and R. K. Pandey, “Effect of air entrainment on compressive strength, density, and ingredients of concrete,” *Int. J. Adv. Mech. Civ. Eng*, vol. 4, no. 6, pp. 77–81, 2017.
[66] J.-H. Kim, A. Tugelbayev, S. H. An, J. U. Lee, and C.-W. Chung, “Dispersion quality of aqueously dispersed MWCNT affected by step sonication process and its impact on mechanical strength of cement paste: A comparison between polycarboxylate based high range water reducers and air entraining agent,” *Constr. Build. Mater.*, vol. 435, p. 136712, 2024, doi: https://doi.org/10.1016/j.conbuildmat.2024.136712.

[67] L. Hongyun, S. Xiangdong, and Z. Chunxia, “Properties of Air-Entrained Pumice Lightweight Aggregate Concrete and a Freezing-Resistance Forecasting Model,” *J. Mater. Civ. Eng.*, vol. 28, no. 3, p. 4015144, Mar. 2016, doi: 10.1061/(ASCE)MT.1943-5533.0001419.
[68] E. K. K. Nambiar and K. Ramamurthy, “Air-void characterisation of foam concrete,” *Cem. Concr. Res.*, vol. 37, no. 2, pp. 221–230, 2007.
[69] S. Ruan and C. Unluer, “Effect of air entrainment on the performance of reactive MgO and PC mixes,” *Constr. Build. Mater.*, vol. 142, pp. 221–232, 2017.
[70] X. Ouyang, Y. Guo, and X. Qiu, “The feasibility of synthetic surfactant as an air entraining agent for the cement matrix,” *Constr. Build. Mater.*, vol. 22, no. 8, pp. 1774–1779, 2008.
[71] W. Piasta and H. Sikora, “Effect of air entrainment on shrinkage of blended cements concretes,” *Constr. Build. Mater.*, vol. 99, pp. 298–307, 2015.
[72] E. Siebel, “Air-void characteristics and freezing and thawing resistance of superplasticized air-entrained concrete with high workability,” *Spec. Publ.*, vol. 119, pp. 297–320, 1989.
[73] S. Jin, J. Zhang, and B. Huang, “Fractal analysis of effect of air void on freeze–thaw resistance of concrete,” *Constr. Build. Mater.*, vol. 47, pp. 126–130, 2013.
[74] K. H. Khayat and J. Assaad, “Air-void stability in self-consolidating concrete,” *ACI Mater. J.*, vol. 99, no. 4, pp. 408–416, 2002.
[75] C. F. Ferraris, “Concrete mixing methods and concrete mixers: state of the art,” *J. Res. Natl. Inst. Stand. Technol.*, vol. 106, no. 2, p. 391, 2001.
[76] N. Puthipad, M. Ouchi, and A. Attachaiyawuth, “Effects of fly ash, mixing procedure and type of air-entraining agent on coalescence of entrained air bubbles in mortar of self-compacting concrete at fresh state,” *Constr. Build. Mater.*, vol. 180, pp. 437–444, 2018.
[77] Y. Barabanshchikov and M. Komarinskiy, “Effect of air-entraining agent lhd on the technological properties of concrete mix containing superplasticizer s-3,” in *Applied Mechanics and Materials*, 2015, vol. 725, pp. 419–424.
[78] K. M. Alexander, “The relationship between strength and the composition and fineness of cement,” *Cem. Concr. Res.*, vol. 2, no. 6, pp. 663–680, 1972.
[79] R. C. de Oliveira Romano, D. dos Reis Torres, and R. G. Pileggi, “Impact of aggregate grading and air-entrainment on the properties of fresh and hardened mortars,” *Constr. Build. Mater.*, vol. 82, pp. 219–226, 2015.
[80] Z. Peng, L. Dan, Q. Yun, Z. Sulei, S. Congtao, and Z. Tiejun, “Effect of Air Entrainment on the Mechanical Properties, Chloride Migration, and Microstructure of Ordinary Concrete and Fly Ash Concrete,” *J. Mater. Civ. Eng.*, vol. 30, no. 10, p. 4018265, Oct. 2018, doi: 10.1061/(ASCE)MT.1943-5533.0002456.
[81] P. Zhong, M. Wyrzykowski, N. Toropovs, L. Li, J. Liu, and P. Lura, “Internal curing with superabsorbent polymers of different chemical structures,” *Cem. Concr. Res.*, vol. 123, p. 105789, 2019.
[82] A. Danish, M. A. Mosaberpanah, and M. U. Salim, “Robust evaluation of superabsorbent polymers as an internal curing agent in cementitious composites,” *J. Mater. Sci.*, vol. 56, no. 1, pp. 136–172, 2021, doi: 10.1007/s10853-020-05131-2.
[83] X. Ma, J. Gao, L. Fan, and Y. Yang, “Using superabsorbent polymers (SAPs) to mitigate frost damage of cement mortar at early age,” *Constr. Build. Mater.*, vol. 394, p. 132248, 2023, doi: https://doi.org/10.1016/j.conbuildmat.2023.132248.
[84] I. S. Kim, S. Y. Choi, Y. S. Choi, and E. I. Yang, “An experimental study on absorptivity

measurement of superabsorbent polymers (SAP) and effect of SAP on freeze-thaw resistance in mortar specimen," *Constr. Build. Mater.*, vol. 267, p. 120974, 2021.
[85] V. Mechtcherine *et al.*, "Effect of superabsorbent polymers (SAP) on the freeze–thaw resistance of concrete: results of a RILEM interlaboratory study," *Mater. Struct.*, vol. 50, pp. 1–19, 2017.
[86] Y. Xu, Q. Yuan, T. Huang, S. Zuo, R. Chen, and G. De Schutter, "Effect of air-entraining agents combined with superabsorbent polymers on pore structure and frost resistance of mortar prepared under low air pressure," *Cold Reg. Sci. Technol.*, vol. 205, p. 103712, 2023, doi: https://doi.org/10.1016/j.coldregions.2022.103712.
[87] J. R. Tenório Filho, E. Mannekens, D. Snoeck, and N. De Belie, "Salt-Scaling Resistance of SAP-Modified Concrete Under Freeze–Thaw Cycles BT - Proceedings of the 3rd RILEM Spring Convention and Conference (RSCC 2020)," 2021, pp. 131–139.
[88] V. Mechtcherine, C. Schröfl, M. Reichardt, A. J. Klemm, and K. H. Khayat, "Recommendations of RILEM TC 260-RSC for using superabsorbent polymers (SAP) for improving freeze–thaw resistance of cement-based materials," *Mater. Struct.*, vol. 52, no. 4, pp. 1–7, 2019.
[89] S. Laustsen, D. P. Bentz, M. T. Hasholt, and O. M. Jensen, "CT measurement of SAP voids in concrete," in *International RILEM conference on use of superabsorbent polymers and other new additives in concrete*, 2010, pp. 153–162.
[90] B. J. Olawuyi and W. P. Boshoff, "Influence of SAP content and curing age on air void distribution of high performance concrete using 3D volume analysis," *Constr. Build. Mater.*, vol. 135, pp. 580–589, 2017.
[91] Y. Xu, Q. Yuan, X. Dai, and G. Xiang, "Improving the freeze-thaw resistance of mortar by a combined use of superabsorbent polymer and air entraining agent," *J. Build. Eng.*, vol. 52, p. 104471, 2022.
[92] H. Russel, "Concrete crisis: Shortages cracking up B.C. construction," *Journal of commerce*, 2022.
[93] J. S. J. Van Deventer, J. L. Provis, and P. Duxson, "Technical and commercial progress in the adoption of geopolymer cement," *Miner. Eng.*, vol. 29, pp. 89–104, 2012.
[94] J. Zhang *et al.*, "Water absorption behavior of starch: A review of its determination methods, influencing factors, directional modification, and food applications," *Trends Food Sci. Technol.*, vol. 144, p. 104321, 2024, doi: https://doi.org/10.1016/j.tifs.2023.104321.
[95] "Production-Corn."
[96] A. M. Donald, "Plasticization and self assembly in the starch granule," *Cereal Chem.*, vol. 78, no. 3, pp. 307–314, 2001.
[97] W. S. Ratnayake and D. S. Jackson, "Gelatinization and solubility of corn starch during heating in excess water: new insights," *J. Agric. Food Chem.*, vol. 54, no. 10, pp. 3712–3716, 2006.
[98] S. Afzal, K. Shahzada, M. Fahad, S. Saeed, and M. Ashraf, "Assessment of early-age autogenous shrinkage strains in concrete using bentonite clay as internal curing technique," *Constr. Build. Mater.*, vol. 66, pp. 403–409, 2014, doi: https://doi.org/10.1016/j.conbuildmat.2014.05.051.
[99] "ASTM C150 Standard Specification for Portland Cement," 2017. Accessed: Dec. 25, 2021. [Online]. Available: https://www.astm.org/c0150-00.html
[100] "ASTM C494/C494M-08 Standard Specification for Chemical Admixtures for Concrete,"

2017. Accessed: Dec. 26, 2021. [Online]. Available: https://www.astm.org/c0494_c0494m-08.html
[101] C. Tuleu, M. K. Khela, D. F. Evans, B. E. Jones, S. Nagata, and A. W. Basit, "A scintigraphic investigation of the disintegration behaviour of capsules in fasting subjects: A comparison of hypromellose capsules containing carrageenan as a gelling agent and standard gelatin capsules," *Eur. J. Pharm. Sci.*, vol. 30, no. 3–4, pp. 251–255, 2007.
[102] "ASTM C192/C192M-16a Standard Practice for Making and Curing Concrete Test Specimens in the Laboratory," 2019.
[103] V. Mechtcherine, E. Secrieru, and C. Schröfl, "Effect of superabsorbent polymers (SAPs) on rheological properties of fresh cement-based mortars—Development of yield stress and plastic viscosity over time," *Cem. Concr. Res.*, vol. 67, pp. 52–65, 2015.
[104] F. Winnefeld and S. Barlag, "Calorimetric and thermogravimetric study on the influence of calcium sulfate on the hydration of ye'elimite," *J. Therm. Anal. Calorim.*, vol. 101, no. 3, pp. 949–957, 2010.
[105] A. Assmann, "Physical properties of concrete modified with superabsorbent polymers," 2013.
[106] F. Horkay, I. Tasaki, and P. J. Basser, "Osmotic swelling of polyacrylate hydrogels in physiological salt solutions," *Biomacromolecules*, vol. 1, no. 1, pp. 84–90, 2000.
[107] C. Schröfl, V. Mechtcherine, and M. Gorges, "Relation between the molecular structure and the efficiency of superabsorbent polymers (SAP) as concrete admixture to mitigate autogenous shrinkage," *Cem. Concr. Res.*, vol. 42, no. 6, pp. 865–873, 2012, doi: 10.1016/j.cemconres.2012.03.011.
[108] K. Farzanian1a, Y. Wehbe1b, and A. Ghahremaninezhad1c, "The effect of superabsorbent polymers (SAP) on the performance of cementitious materials," 2016.
[109] D. Snoeck, S. Steuperaert, K. Van Tittelboom, P. Dubruel, and N. De Belie, "Visualization of water penetration in cementitious materials with superabsorbent polymers by means of neutron radiography," *Cem. Concr. Res.*, vol. 42, no. 8, pp. 1113–1121, 2012.
[110] S.-H. Kang, S.-G. Hong, and J. Moon, "Absorption kinetics of superabsorbent polymers (SAP) in various cement-based solutions," *Cem. Concr. Res.*, vol. 97, pp. 73–83, 2017.
[111] G. Mailar, B. M. Sreedhara, D. S. Manu, P. Hiremath, and K. Jayakesh, "Investigation of concrete produced using recycled aluminium dross for hot weather concreting conditions," *Resour. Technol.*, vol. 2, no. 2, pp. 68–80, 2016.
[112] S. Dey and M. M. Karthik, "Modelling four-pile cap behaviour using three-dimensional compatibility strut-and-tie method," *Eng. Struct.*, vol. 198, p. 109499, 2019.
[113] V. Mechtcherine *et al.*, "Testing superabsorbent polymer (SAP) sorption properties prior to implementation in concrete: results of a RILEM Round-Robin Test," *Mater. Struct.*, vol. 51, no. 1, pp. 1–16, 2018.
[114] C. Schröfl, V. Mechtcherine, and M. Gorges, "Relation between the molecular structure and the efficiency of superabsorbent polymers (SAP) as concrete admixture to mitigate autogenous shrinkage," *Cem. Concr. Res.*, vol. 42, no. 6, pp. 865–873, 2012.
[115] R. Mahon, Y. Balogun, G. Oluyemi, and J. Njuguna, "Swelling performance of sodium polyacrylate and poly (acrylamide-co-acrylic acid) potassium salt," *SN Appl. Sci.*, vol. 2, no. 1, pp. 1–15, 2020.
[116] K. Van Breugel, "Simulation of hydration and formation of structure in hardening cement-based materials.," 1993.

[117] S. Mindess, J. F. Young, and D. Darwin, “Concrete Prentice-Hall,” *Englewood Cliffs, NJ*, vol. 481, 1981.
[118] P. Chindasiriphan and H. Yokota, “Self-healing ability of concrete made with fly ash and superabsorbent polymer,” in *Proceedings of the 2nd ACF symposium, Chiang Mai, Thailand*, 2017, pp. 23–25.
[119] H. Wang and J. E. Gillott, “Mechanism of alkali-silica reaction and the significance of calcium hydroxide,” *Cem. Concr. Res.*, vol. 21, no. 4, pp. 647–654, 1991.
[120] S. Setunge, N. Nguyen, B. L. Alexander, and L. Dutton, “Leaching of alkali from concrete in contact with waterways,” *Water, Air, Soil Pollut. Focus*, vol. 9, no. 5, pp. 381–391, 2009.
[121] “ASTM C260-10 Standard Specification for Air-Entraining Admixtures for Concrete,” 2010.
[122] A. Danish, M. A. Mosaberpanah, and M. U. Salim, “Robust evaluation of superabsorbent polymers as an internal curing agent in cementitious composites,” *J. Mater. Sci.*, vol. 56, no. 1, pp. 136–172, 2021, doi: 10.1007/s10853-020-05131-2.
[123] M. J. Krafcik and K. A. Erk, “Characterization of superabsorbent poly(sodium-acrylate acrylamide) hydrogels and influence of chemical structure on internally cured mortar,” *Mater. Struct. Constr.*, vol. 49, no. 11, pp. 4765–4778, 2016, doi: 10.1617/s11527-016-0823-7.
[124] A. Jalal and R. Kiran, “Quantifying the water donation potential of commercial and corn starch hydrogels in a cementitious matrix,” *J. Mater. Res. Technol.*, vol. 24, pp. 4336–4352, 2023, doi: https://doi.org/10.1016/j.jmrt.2023.04.031.
[125] J. Siramanont, W. Vichit-Vadakan, and W. Siriwatwechakul, “The impact of SAP structure on the effectiveness of internal curing,” in *International RILEM conference on Use of superabsorbent polymers and other new additives in concrete*, 2010, pp. 243–252.
[126] J. B. Schwartz and J. A. Zelinskie, “The binding and disintegrant properties of the corn starch fractions: amylose and amylopectin,” *Drug Dev. Ind. Pharm.*, vol. 4, no. 5, pp. 463–483, 1978.
[127] S. J. McGrane, C. J. Rix, D. E. Mainwaring, and H. J. Cornell, “The effect of water interactions on the rheological behaviour of amylose, amylopectin, and mixtures from corn,” K. B. T.-H. Nishinari, Ed. Amsterdam: Elsevier Science, 2000, pp. 337–342. doi: https://doi.org/10.1016/B978-044450178-3/50043-3.
[128] Y. Guo, P. Zhang, H. Ding, and C. Le, “Experimental study on the permeability of SAP modified concrete,” *Materials (Basel).*, vol. 13, no. 15, p. 3368, 2020.
[129] G. H. Tattersall, *Workability and quality control of concrete*. CRC Press, 1991.
[130] “ASTM C1437-20 Standard Test Method for Flow of Hydraulic Cement Mortar,” 2020.
[131] “ASTM C109/C109M-20 Standard Test Method for Compressive Strength of Hydraulic Cement Mortars (Using 2-in. or [50-mm] Cube Specimens),” 2020.
[132] G.-F. Peng, Q. Ma, H.-M. Hu, R. Gao, Q.-F. Yao, and Y.-F. Liu, “The effects of air entrainment and pozzolans on frost resistance of 50–60MPa grade concrete,” *Constr. Build. Mater.*, vol. 21, no. 5, pp. 1034–1039, 2007, doi: https://doi.org/10.1016/j.conbuildmat.2006.02.002.
[133] R. Wang, Z. Hu, Y. Li, K. Wang, and H. Zhang, “Review on the deterioration and approaches to enhance the durability of concrete in the freeze–thaw environment,” *Constr. Build. Mater.*, vol. 321, p. 126371, 2022, doi: https://doi.org/10.1016/j.conbuildmat.2022.126371.

[134] D. Cooper, A. Turinsky, C. Sensen, and B. Hallgrimsson, “Effect of Voxel Size on 3D Micro-CT Analysis of Cortical Bone Porosity,” *Calcif. Tissue Int.*, vol. 80, no. 3, pp. 211–219, 2007, doi: 10.1007/s00223-005-0274-6.
[135] “ASTM C125 Standard Terminology Relating to Concrete and Concrete Aggregates,” 2021.
[136] J. Punkki, J. Golaszewski, and O. E. Gjørv, “Workability loss of high-strength concrete,” *ACI Mater. J.*, vol. 93, pp. 427–431, 1996.
[137] M. Grzegorczyk-Frańczak, D. Barnat-Hunek, K. Materak, and G. Łagód, “Influence of Water with Oxygen and Ozone Micro-Nano Bubbles on Concrete Physical Properties,” *Materials*, vol. 15, no. 22. 2022. doi: 10.3390/ma15227938.
[138] F. Fouad, S. Janusz, and W. Stan, “Influence of Superplasticizers on Workability of Concrete,” *J. Mater. Civ. Eng.*, vol. 11, no. 2, pp. 151–157, May 1999, doi: 10.1061/(ASCE)0899-1561(1999)11:2(151).
[139] “ASTM C457/C457M-23a Standard Test Method for Microscopical Determination of Parameters of the Air-Void System in Hardened Concrete,” 2023.
[140] V. Mechtcherine, “Use of superabsorbent polymers (SAP) as concrete additive,” *RILEM Tech. Lett.*, vol. 1, pp. 81–87, 2016.
[141] H. Peidayesh, Z. Ahmadi, H. A. Khonakdar, M. Abdouss, and I. Chodák, “Baked hydrogel from corn starch and chitosan blends cross-linked by citric acid: Preparation and properties,” *Polym. Adv. Technol.*, vol. 31, no. 6, pp. 1256–1269, 2020.
[142] R. D. T. Filho, E. F. Silva, A. N. M. Lopes, V. Mechtcherine, and L. Dudziak, “Effect of Superabsorbent Polymers on the Workability of Concrete and Mortar BT - Application of Super Absorbent Polymers (SAP) in Concrete Construction: State-of-the-Art Report Prepared by Technical Committee 225-SAP,” V. Mechtcherine and H.-W. Reinhardt, Eds. Dordrecht: Springer Netherlands, 2012, pp. 39–50. doi: 10.1007/978-94-007-2733-5_5.
[143] C. E. de Normalisation, “Concrete-Part 1: Specification, performance, production and conformity,” *EN206-1, 22 CEN*, vol. 69, p. 23, 2000.
[144] J. Yuan, Y. Wu, and J. Zhang, “Characterization of air voids and frost resistance of concrete based on industrial computerized tomographical technology,” *Constr. Build. Mater.*, vol. 168, pp. 975–983, 2018.
[145] C.-S. Shon, D. Lee, J.-H. Kim, and C.-W. Chung, “Freezing and thawing resistance of cellular concrete containing binary and ternary cementitious mixtures,” *Constr. Build. Mater.*, vol. 168, pp. 73–81, 2018, doi: https://doi.org/10.1016/j.conbuildmat.2018.02.117.
[146] C.-S. Shon, A. Abdigaliyev, S. Bagitova, C.-W. Chung, and D. Kim, “Determination of air-void system and modified frost resistance number for freeze-thaw resistance evaluation of ternary blended concrete made of ordinary Portland cement/silica fume/class F fly ash,” *Cold Reg. Sci. Technol.*, vol. 155, pp. 127–136, 2018, doi: https://doi.org/10.1016/j.coldregions.2018.08.003.
[147] J. M. Aristoff, T. T. Truscott, A. H. Techet, and J. W. M. Bush, “The water entry of decelerating spheres,” *Phys. Fluids*, vol. 22, no. 3, p. 32102, Mar. 2010, doi: 10.1063/1.3309454.
[148] P. C. Fonseca and G. W. Scherer, “An image analysis procedure to quantify the air void system of mortar and concrete,” *Mater. Struct.*, vol. 48, no. 10, pp. 3087–3098, 2015, doi: 10.1617/s11527-014-0381-9.
[149] H. Wadell, “Volume, Shape, and Roundness of Quartz Particles,” *J. Geol.*, vol. 43, no. 3, pp. 250–280, Apr. 1935, doi: 10.1086/624298.

[150] A. Koenig, “Analysis of air voids in cementitious materials using micro X-ray computed tomography (μXCT),” *Constr. Build. Mater.*, vol. 244, p. 118313, 2020.
[151] K. A. Snyder, “A numerical test of air void spacing equations,” *Adv. Cem. based Mater.*, vol. 8, no. 1, pp. 28–44, 1998.
[152] M. T. Hasholt, “Air void structure and frost resistance: A challenge to Powers’ spacing factor,” *Mater. Struct.*, vol. 47, no. 5, pp. 911–923, 2014.
[153] W. Shi, H. Zhu, Y. Yu, C. Luo, J. Shan, and T. Wang, “Case study of a SAP-CRC bridge deck in Lu-shan County, Henan, China,” *Struct. Concr.*, vol. 22, no. 3, pp. 1523–1533, Jun. 2021, doi: https://doi.org/10.1002/suco.202000655.
[154] J. Liu, N. Farzadnia, C. Shi, and X. Ma, “Effects of superabsorbent polymer on shrinkage properties of ultra-high strength concrete under drying condition,” *Constr. Build. Mater.*, vol. 215, pp. 799–811, 2019, doi: https://doi.org/10.1016/j.conbuildmat.2019.04.237.
[155] “icep_jmacr65_914.”
[156] Y. Chen, Y. Hao, S. Li, Z. Luo, and Q. Gao, “Preparation of hydroxybutyl starch with a high degree of substitution and its application in temperature-sensitive hydrogels,” *Food Chem.*, vol. 355, p. 129472, 2021, doi: https://doi.org/10.1016/j.foodchem.2021.129472.
[157] Z. Deng, H. Cheng, Z. Wang, G. Zhu, and H. Zhong, “Compressive behavior of the cellular concrete utilizing millimeter-size spherical saturated SAP under high strain-rate loading,” *Constr. Build. Mater.*, vol. 119, pp. 96–106, 2016, doi: https://doi.org/10.1016/j.conbuildmat.2016.05.018.
[158] L. P. Esteves, I. Lukošiūtė, and J. Čėsnienė, “Hydration of cement with superabsorbent polymers,” *J. Therm. Anal. Calorim.*, vol. 118, no. 2, pp. 1385–1393, 2014, doi: 10.1007/s10973-014-4133-4.
[159] J. Justs, M. Wyrzykowski, D. Bajare, and P. Lura, “Internal curing by superabsorbent polymers in ultra-high performance concrete,” *Cem. Concr. Res.*, vol. 76, pp. 82–90, 2015, doi: 10.1016/j.cemconres.2015.05.005.
[160] Y.-N. Hwang *et al.*, “Effect of lattice contraction on the Raman shifts of CdSe quantum dots in glass matrices,” *Phys. Rev. B*, vol. 54, no. 21, p. 15120, 1996.
[161] H. Wang *et al.*, “Synergy of hydrophobic surface capping and lattice contraction for stable and high-efficiency inorganic CsPbI2Br perovskite solar cells,” *Sol. RRL*, vol. 2, no. 12, p. 1800216, 2018.
[162] S. C. Devi and R. A. Khan, “Influence of graphene oxide on sulfate attack and carbonation of concrete containing recycled concrete aggregate,” *Constr. Build. Mater.*, vol. 250, p. 118883, 2020.
[163] FHWA, “‘Highway Statistics Publications, Highway Finance Tables SF-4C and LGF-2,’ 1997 to 2005,” 2005.
[164] M. R. GivKashi and M. Tohidloo, “The effect of freeze-thaw cycles and sulfuric acid attack separately on the compressive strength and microstructure of 3D-printed air-entrained concrete,” *Constr. Build. Mater.*, vol. 440, p. 137411, 2024, doi: https://doi.org/10.1016/j.conbuildmat.2024.137411.
[165] J. Kong *et al.*, “The screening effect of coarse aggregate on the air void structure and durability of air-entrained concrete,” *Constr. Build. Mater.*, vol. 451, p. 138786, 2024, doi: https://doi.org/10.1016/j.conbuildmat.2024.138786.
[166] B. Lu *et al.*, “Characteristics of CSH under carbonation and its effects on the hydration and microstructure of cement paste,” *Constr. Build. Mater.*, vol. 364, p. 129952, 2023, doi: https://doi.org/10.1016/j.conbuildmat.2022.129952.

[167] T. Yeşim and Ş. Remzi, “The Physicomechanical Behavior and Microstructure of Air-Entrained 3D Printable Concrete,” *J. Mater. Civ. Eng.*, vol. 36, no. 1, p. 4023489, Jan. 2024, doi: 10.1061/JMCEE7.MTENG-16224.
[168] K. S. Sikora and A. J. Klemm, “Effect of superabsorbent polymers on workability and hydration process in fly ash cementitious composites,” *J. Mater. Civ. Eng.*, vol. 27, no. 5, p. 4014170, 2015.
[169] Z. He *et al.*, “Cement-based materials modified with superabsorbent polymers: A review,” *Constr. Build. Mater.*, vol. 225, pp. 569–590, 2019, doi: 10.1016/j.conbuildmat.2019.07.139.
[170] A. Jalal and R. Kiran, “Sustainable Biobased Hydrogel as an Alternative Air-Entrainment Agent in Cement-Based Materials,” *J. Mater. Civ. Eng.*, vol. 36, no. 11, p. 4024342, 2024.
[171] X. Huang, X. Liu, H. Rong, X. Yang, Y. Duan, and T. Ren, “Effect of Super-Absorbent Polymer (SAP) Incorporation Method on Mechanical and Shrinkage Properties of Internally Cured Concrete,” *Materials*, vol. 15, no. 21. 2022. doi: 10.3390/ma15217854.
[172] Y. Tan, X. Lu, R. He, H. Chen, and Z. Wang, “Influence of superabsorbent polymers (SAPs) type and particle size on the performance of surrounding cement-based materials,” *Constr. Build. Mater.*, vol. 270, p. 121442, 2021.
[173] S. E. Chidiac, S. N. Mihaljevic, S. A. Krachkovskiy, and G. R. Goward, “Efficiency measure of SAP as internal curing for cement using NMR & MRI,” *Constr. Build. Mater.*, vol. 278, p. 122365, 2021.
[174] Z. Wu, C. Shi, P. Gao, D. Wang, and Z. Cao, “Effects of Deicing Salts on the Scaling Resistance of Concrete,” *J. Mater. Civ. Eng.*, vol. 27, no. 5, p. 04014160, 2015, doi: 10.1061/(asce)mt.1943-5533.0001106.
[175] P. Hagan, “Freezing Point Determinations of Safecote Brine Mixtures.”
[176] D. Jana, “Concrete scaling–a critical review,” in *Proceedings of the 29th Conference on Cement Microscopy, Quebec, QC, Canada*, 2007, vol. 20.
[177] K. Wang, D. E. Nelsen, and W. A. Nixon, “Damaging effects of deicing chemicals on concrete materials,” *Cem. Concr. Compos.*, vol. 28, no. 2, pp. 173–188, 2006, doi: 10.1016/j.cemconcomp.2005.07.006.
[178] M. F. Green, L. A. Bisby, Y. Beaudoin, and P. Labossière, “Effect of freeze-thaw cycles on the bond durability between fibre reinforced polymer plate reinforcement and concrete,” *Can. J. Civ. Eng.*, vol. 27, no. 5, pp. 949–959, Oct. 2000, doi: 10.1139/l00-031.
[179] H. U. Sajid, A. Jalal, R. Kiran, and A. Al-Rahim, “A survey on the effects of deicing materials on properties of Cement-based materials,” *Constr. Build. Mater.*, vol. 319, p. 126062, 2022.
[180] V. Baroghel-Bouny, P. Belin, M. Maultzsch, and D. Henry, “AgNO 3 spray tests: Advantages, weaknesses, and various applications to quantify chloride ingress into concrete. Part 1: Non-steady-state diffusion tests and exposure to natural conditions,” *Mater. Struct.*, vol. 40, pp. 759–781, 2007.
[181] K. Amini, P. Vosoughi, H. Ceylan, and P. Taylor, “Linking air-void system and mechanical properties to salt-scaling resistance of concrete containing slag cement,” *Cem. Concr. Compos.*, vol. 104, p. 103364, 2019, doi: https://doi.org/10.1016/j.cemconcomp.2019.103364.
[182] “ASTM C672 / C672M - 12 Standard Test Method for Scaling Resistance of Concrete Surfaces Exposed to Deicing Chemicals,” 2021. Accessed: Oct. 28, 2021. [Online]. Available: https://www.astm.org/Standards/C672.htm

[183] A. Mesbah, C. Cau-dit-Coumes, G. Renaudin, F. Frizon, and F. Leroux, “Uptake of chloride and carbonate ions by calcium monosulfoaluminate hydrate,” *Cem. Concr. Res.*, vol. 42, no. 8, pp. 1157–1165, 2012.
[184] Y. Li, C. Zhang, T. Li, and G. Sun, “Exploring the role of SAP chemical composition in the internal curing of high-performance cementitious materials,” *Constr. Build. Mater.*, vol. 451, p. 138784, 2024.
[185] J. Liu, N. Farzadnia, K. H. Khayat, and C. Shi, “Effects of SAP characteristics on internal curing of UHPC matrix,” *Constr. Build. Mater.*, vol. 280, p. 122530, 2021.
[186] H. Yang, L. Wu, J. Liu, and W. Wang, “The re-swelling mechanism of superabsorbent polymers (SAP) in the SAP voids of cement-based materials,” *Cem. Concr. Compos.*, vol. 130, p. 104561, 2022.
[187] Q. Deng, Z. Wang, S. Li, and Q. Yu, “Salt scaling resistance of pre-cracked ultra-high performance concrete with the coupling of salt freeze-thaw and wet-dry cycles,” *Cem. Concr. Compos.*, vol. 146, p. 105396, 2024.
[188] Z. Liu, “Frost deterioration in concrete due to deicing salt exposure: Mechanism, mitigation and conceptual surface scaling model.” University of Michigan, 2014.
[189] M. C. Santagata and M. Collepardi, “The effect of CMA deicers on concrete properties,” *Cem. Concr. Res.*, vol. 30, no. 9, pp. 1389–1394, 2000, doi: https://doi.org/10.1016/S0008-8846(00)00334-3.
[190] D. J. HANNANT, “4.11 - Cement-based Composites,” A. Kelly and C. B. T.-C. C. M. Zweben, Eds. Oxford: Pergamon, 2000, pp. 323–362. doi: https://doi.org/10.1016/B0-08-042993-9/00098-X.
[191] T. C. Powers, “A discussion of cement hydration in relation to the curing of concrete,” 1947.
[192] H. U. Sajid, R. Kiran, and D. S. Bajwa, “Effect of agro-derived corrosion inhibitors on the properties of Portland cement mortar,” *Constr. Build. Mater.*, vol. 310, p. 125236, 2021.
[193] L. Bai, J. Xie, J. Liu, and Y. Xie, “Effect of salt on hygroscopic properties of cement mortar,” *Constr. Build. Mater.*, vol. 305, p. 124746, 2021.
[194] F. Autelitano, M. Rinaldi, and F. Giuliani, “Winter highway maintenance strategies: Are all the sodium chloride salts the same?,” *Constr. Build. Mater.*, vol. 226, pp. 945–952, 2019.
[195] J. Jain, J. Olek, A. Janusz, and D. Jozwiak-Niedzwiedzka, “Effects of Deicing Salt Solutions on Physical Properties of Pavement Concretes,” *Transp. Res. Rec.*, vol. 2290, no. 1, pp. 69–75, Jan. 2012, doi: 10.3141/2290-09.
[196] S. Sim *et al.*, “Gypsum-Dependent Effect of NaCl on Strength Enhancement of CaO-Activated Slag Binders,” *Applied Sciences*, vol. 8, no. 12. 2018. doi: 10.3390/app8122515.
[197] R. Wang, Q. Zhang, and Y. Li, “Deterioration of concrete under the coupling effects of freeze–thaw cycles and other actions: A review,” *Constr. Build. Mater.*, vol. 319, p. 126045, 2022.
[198] S. Subash and S. Subash, “Scaling in Concrete–Causes, Prevention, and Repair,” *Ind. Scale Inhib. Princ. Des. Appl.*, p. 341, 2024.
[199] F. P. Browne, *Deicer scaling mechanisms in concrete*. The Pennsylvania State University, 1972.
[200] S. Popovics, “Effect of Porosity on the Strength of Concrete,” *J. Mater.*, 1969.
[201] B. J. Olawuyi, A. J. Babafemi, and W. P. Boshoff, “Early-age and long-term strength development of high-performance concrete with SAP,” *Constr. Build. Mater.*, vol. 267, p.

121798, 2021.
[202] M. T. Hasholt, M. H. S. Jespersen, and O. M. Jensen, “Mechanical properties of concrete with SAP. Part I: Development of compressive strength,” in *International RILEM conference on use of superabsorbent polymers and other new additives in concrete*, 2010, pp. 117–126.
[203] A. Hossain and M. Islam, *EFFECTS OF DEICING SALTS ON STRENGTH PROPERTIES OF CONCRETE*. 2019.
[204] H. E. Cutler, K. Wang, V. R. Schaefer, and J. T. Kevern, “Resistance of Portland cement pervious concrete to deicing chemicals,” *Transp. Res. Rec.*, vol. 2164, no. 1, pp. 98–104, 2010.
[205] Y. Huamei, H. Zhen, S. Yixin, and L. Lei, “Improving Freeze-Thaw Resistance and Strength Gain of Roller Compacted Fly Ash Concretes with Modified Absorbent Polymer,” *J. Mater. Civ. Eng.*, vol. 30, no. 3, p. 4018010, Mar. 2018, doi: 10.1061/(ASCE)MT.1943-5533.0002159.
[206] B. Craeye, G. Cockaerts, and P. Kara De Maeijer, “Improving Freeze–Thaw Resistance of Concrete Road Infrastructure by Means of Superabsorbent Polymers,” *Infrastructures*, vol. 3, no. 1. 2018. doi: 10.3390/infrastructures3010004.
[207] X. Kong and Z. Zhang, “Effect of super-absorbent polymer on pore structure of hardened cement paste in high-strength concrete,” *J. Chinese Ceram. Soc.*, vol. 41, no. 11, pp. 1474–1480, 2013.
[208] X. Ma, J. Liu, Z. Wu, and C. Shi, “Effects of SAP on the properties and pore structure of high performance cement-based materials,” *Constr. Build. Mater.*, vol. 131, pp. 476–484, 2017.
[209] X. Liu, K. S. Chia, and M.-H. Zhang, “Water absorption, permeability, and resistance to chloride-ion penetration of lightweight aggregate concrete,” *Constr. Build. Mater.*, vol. 25, no. 1, pp. 335–343, 2011.
[210] F. Zhu, Z. Ma, and T. Zhao, “Influence of Freeze-Thaw Damage on the Steel Corrosion and Bond-Slip Behavior in the Reinforced Concrete,” *Adv. Mater. Sci. Eng.*, vol. 2016, no. 1, p. 9710678, 2016.